RENEWAL EQUATIONS APPLIED TO EVALUATION OF INTERVENTIONS FOR THE CONTROL AND PREVENTION OF INFECTIOUS DISEASES

MAHNAZ ALAVINEJAD

A DISSERTATION SUBMITTED TO
THE FACULTY OF GRADUATE STUDIES
IN PARTIAL FULFILLMENT OF THE REQUIREMENTS
FOR THE DEGREE OF
DOCTOR OF PHILOSOPHY

GRADUATE PROGRAM IN MATHEMATICS AND STATISTICS
YORK UNIVERSITY
TORONTO, ONTARIO

February 2021

Abstract

Control and prevention of infectious disease prevalence have been a priority to reduce the burden (mortality and morbidity) of the diseases. Mathematical modeling has been used to study the direct and indirect effect of Infection Prevention and Control (IPC) measures on the disease transmission dynamics and to estimate the cost effectiveness of immunization programs including vaccine production and immunization program design and implementation. However, for more efficient programs regarding IPC priority policies and in order to optimize the limited available resources for the control of infectious diseases, more rigorous mathematical models and analyses are required. This dissertation is dedicated to the development of a mathematical framework using delay systems (delay/functional differential equations and Volterra integral equations of second type) to examine the effectiveness of control and prevention interventions for infectious diseases. The framework enables us to formulate and derive mathematical and epidemiological analyses of a wide range of compartmental models that have been traditionally studied using ordinary, partial and delay differential equations. We specifically use this framework to address heterogeneity in the population and to better understand the disease dynamics and the burden of the disease with and without interventions. We also use this framework to study vertical transmission and vector-borne diseases.

I dedicate this to my parents

Acknowledgements

I would like to express my gratitude to Professor Jianhong Wu for his supervision and guidance in the research and also for his support in every challenge during my journey as a PhD student. I would also like to thank my supervisory committee, Professor Neal Madras and Professor Jane Heffernan, for their insightful comments and constructive input. And finally, I would like to express my gratitude to the Department of Mathematics and Statistics, Faculty of Science and the Faculty of Graduate Studies for supporting my education and research at York University.

Table of Contents

List of Figures

List of Tables

1 | Introduction

The control and prevention of the emerging and reemerging infectious diseases have always been challenging to public health decision makers. There are many control and prevention strategies that can be applied prior to and during an infectious disease outbreak. The effectiveness of control strategies depends on many factors such as transmission probabilities and severity of the disease outcomes (morbidity and mortality). Evaluation of the effectiveness of the control and prevention strategies, for both the policies that have been implemented in the past for various diseases and novel methods suggested for emerging diseases, is a crucial part in the process of establishing effective control measures. Significant components of control and prevention strategies include identifying risk groups, immunization methods and timeline (e.g., vaccine availability and their efficacy), timely implementation of a combination of other effective control strategies (e.g., different forms of quarantine) and effective communication of prevention programs to the public and health care personnel, prior to and during epidemics and pandemics. The reliability and quality of surveillance systems are essential for better estimation of the disease burden, and therefore better control of the disease.

Numerous statistical and mathematical models have been developed to study the dynamics of the infectious diseases in the presence of control measures and to understand the impact of these measures on reducing the health and economic burden of the disease. The purpose of this dissertation is to develop a mathematical framework using delay systems in which a group of compartmental models for different types of diseases can be studied.

1.1 Review of the Mathematical Tools and their Applications

Delay equations (differential and integral) as described by Diekmann [39], are “rules for extending a function of time towards the future on the basis of the assumed to be known past". Among different types of delay equations Volterra integral equations of second kind[1], also known as *renewal equations* (RE), have arisen in many applications. Renewal equations (linear and non-

[1]For the Volterra integral equations of the first kind, the unknown function $x(t)$ only appears as a part of integrand: $f(t) = \int_{t_0}^{t} g(x(t-\tau))\mathcal{K}(\tau)d\tau$.

linear) of the form:

$$x(t) = f(t) + \int_{t_0}^{t} g(x(t-\tau))\mathcal{K}(\tau)d\tau, \tag{1.1}$$

where g, f and $\mathcal{K}$ are known functions, have been used to describe dynamics of different phenomena in various fields such as biology, epidemiology and economics. Here, $g : \mathbb{R}^n_+ \to \mathbb{R}^n_+$ is a (linear or) non-linear function and the *forcing function* f and the *kernel* $\mathcal{K}$ are defined on $\mathbb{R}_+$. As an example, the population growth (structured by age and in an environment where the growth rate does not directly depend on the environmental conditions) can be described by the linear renewal equation

$$b(t) = \int_0^{\infty} b(t-a)\beta(a)\mathcal{F}(a)da, \tag{1.2}$$

where $b(t)$ is the birth rate, $\mathcal{F}(a)$ is the age dependent survival probability and $\beta(a)$ is the age dependent fertility. Such equations have been used to study different phenomena in population dynamics such as birth process, cannibalism and physiologically structured populations ([14, 33, 34, 47, 46, 72, 87, 121]).

The 1927 epidemic model of Kermack and McKendrick [71], was also formulated using renewal equations. In a closed population, let $S(t)$ denote the density of susceptible individuals, $F(t)$ be the force of infection (the probability per unit of time a susceptible becomes infected) and $A(\tau)$ denote the *expected contribution to the force of infection by an individual who was infected τ units of time ago* [18]. Then the force of infection can be described by the following integral equation

$$F(t) = \int_0^{\infty} S(t-\tau)F(t-\tau)A(\tau)d\tau. \tag{1.3}$$

This formulation was further studied by Diekmann [38] and Brauer [15], extended to a heterogeneous population, consisting of two sub-populations, in [16] and to endemic case and waning of immunity in [18]. This approach has been recently used to study continuous vaccination strategies [90] and to evaluate the effect of contact tracing on epidemic control [106].

Many epidemiological models using ordinary and delay differential equations are indeed simplifications of the renewal equations by making a certain assumption about the kernel function. For example, ODE model arises naturally if we take an exponential function, and DDE model arises

with delta kernel function. It is well known, for example, as pointed out in the book of Wu and Zhang [129] (pp 53-54), that these simplifications lead to over- or under-estimation of the infection risk in comparison with the kernel. For instance, in the HIV/AIDS modelling, the infectivity varies as the age since infection changes, and the kernel function can have double peak, with a lower peak in the early stage, and a higher peak in the late stage leading to AIDS).

Specific forms of $A(\tau)$ may lead to different compartmental models [45], described by systems of ordinary differential equations, and therefore the results from analyzing this equation can be applied to various compartmental models. For some ODE models $A(\tau)$ is as follows

- SIR model: $A(\tau) = \beta e^{-\alpha\tau}$
- $SEIR$ model: $A(\tau) = \beta\frac{\gamma}{\gamma-\alpha}(e^{-\alpha\tau} - e^{-\gamma\tau})$

The cumulative force of infection, defined by $y(t) = \int_{-\infty}^{t} F(\sigma)d\sigma$, satisfies the following renewal equation

$$y(t) = \int_0^\infty S(-\infty)(1 - e^{-y(t-\tau)})A(\tau)d\tau. \tag{1.4}$$

When $t \to \infty$, $y(t) \to y(\infty)$ with

$$y(\infty) = \int_0^\infty S(-\infty)(1 - e^{-y(\infty)})A(\tau)d\tau.$$

There exists a positive solution for $y(\infty)$ (total cumulative force of infection) if the basic reproduction number $\mathcal{R}_0 = \int_0^\infty S(-\infty)A(\tau)d\tau > 1$ and the final size of the epidemic is given by the following relation

$$(1 - \frac{S(\infty)}{S(-\infty)}) = y(\infty)/\mathcal{R}_0. \tag{1.5}$$

The dynamics of the disease in the population is then given by the following:

If $\mathcal{R}_0 > 1$, then the introduction of an infective agent leads to an outbreak. The final size of the outbreak is given by the above equation.

If $\mathcal{R}_0 \leq 1$, then the introduction of an infective agent leads to an outbreak with the final size close to zero.

In an age-structured population with a constant birth B and a general survival function $\mathcal{F}(a)$, the dynamics of the susceptible population in the presence of an infectious disease can be described by the following PDE

$$\begin{aligned}(\frac{\partial}{\partial t}+\frac{\partial}{\partial a})S(t,a) &= -(\mu(a)+F(t))S(t,a)\\ S(t,0) &= B\end{aligned} \tag{1.6}$$

where $\mathcal{F}(a)=e^{-\int_0^a \mu(s)ds}$. Equivalently we have

$$S(t,a)=B\mathcal{F}(a)e^{-\int_0^a F(t-a+\sigma)d\sigma}.$$

The force of infection is described by the following equation

$$F(t)=\int_0^\infty F(t-\tau)\int_0^\infty S(t-\tau,a)\frac{\mathcal{F}(a+\tau)}{\mathcal{F}(a)}daA(\tau)d\tau \tag{1.7}$$

A positive solution $\bar{F}$ exists if $\mathcal{R}_0=B\int_0^\infty\int_0^\infty \mathcal{F}(a+\tau)A(\tau)dad\tau>1$. In the special case of exponential survival function the following result is given in [18]:

If $\mathcal{R}_0\leq 1$, then the disease free equilibrium $\bar{F}=0$ is locally asymptotically stable.

If $\mathcal{R}_0>1$, then $\bar{F}=0$ is unstable, there exists a positive equilibrium and is locally asymptotically stable.

The basic reproduction number, defined as the number of secondary cases from an infected individual during his/her infectious period in an entirely susceptible population, is a fundamental concept in epidemiology. A number of methods have been developed to calculate this quantity for different types of models: the next generation matrix method, the next generation operator method, the survival function method [64, 118]. The next generation matrix and next generation operator methods are described in [48, 51]. The survival function method, describes $\mathcal{R}_0$ based on the infection survival probability at the age of infection a, denoted by $\mathfrak{F}(a)$, and the average number of secondary infections by an infectious individual of age of infection a per unit of time,

denoted by $b(a)$:

$$\mathcal{R}_0 = \int_0^\infty \mathfrak{F}(a)b(a)da.$$

Comparing this definition to the definition of $\mathcal{R}_0$ in [18], we can see that the product $\mathfrak{F}(a)b(a)$, with age of infection a, is equivalent to $A(\tau)$, with age of infection τ. We note that based on [18] the infectivity function $A(\tau)$ has two main components: the contact intensity and the probability of transmission, given a contact with a susceptible.

The fundamental theory and long-term dynamics of equations of the form (1.1) have been extensively studied in [31, 42, 40, 47, 41, 43, 44, 49, 61, 83, 116]. Numerical methods for bifurcation and stability analysis of periodic solutions of delay systems have been developed via reduction of the infinite dimensional problem to finite dimensional cases using the method of pseudospectral discretization [3, 20, 21, 22, 19, 23, 24, 50, 58, 62].

1.2 Structure of the Dissertation

We aim to develop mathematical models using renewal equations to better understand the dynamics of infectious diseases and the effect of control and prevention strategies. In the second chapter, the framework developed in [18] is extended here to incorporate a variable level of immunity to a certain disease in the population. A mathematical model is developed using renewal equations with a general function describing the changes in the susceptibility of individuals as well as a general function for the contribution of infected individuals with a certain level of immunity, before contracting the disease, to the force of infection. In this model, a continuous time-varying variable is used to describe individuals' level of immunity to an infectious disease, defined as the probability of not contracting the disease if exposed, denoted by $\mathfrak{m}$ with $0 \leq \mathfrak{m} \leq 1$. Dynamics of the susceptible population at time t with immunity $\mathfrak{m}$ is given by a PDE. A generalization of the Equation (1.4) is used to describe the force of infection received by individuals of immunity $\mathfrak{m}$, where $\mathfrak{m}$ is assumed to remain unchanged for every individual during the epidemic. A special case of this model is studied in full detail in a population with a finite number of sub-populations where individuals in each sub-population have a fixed value of immunity. The sub-populations are

assumed to be fully connected, i.e., the between-sub-population transmission matrix is supposed to be positive. The results can be applied to study disease dynamics in a population stratified based on different factors, such as age. Major parts of this chapter are published in a paper in the journal of Canadian Mathematical Bulletin [2].

The third chapter is devoted to understanding of the disease dynamics in the presence of vertical transmission (from infected mother to her newborns) in an age-structured population, with a constant birth B and a general survival function $\mathcal{F}(a)$, where the probability of producing an infected offspring depends on the time since infection. The force of infection ($F(t)$) and the birth rate of infected newborn ($b(t)$) are formulated as the following coupled system of renewal equation

$$\begin{aligned} F(t) &= \int_0^\infty \Big(F(t-\tau) \int_0^\infty B(1-b(t-\tau-a)) e^{-\int_0^a F(t-\tau-a+\sigma)d\sigma} \mathcal{F}(a+\tau) da A(\tau) \Big) d\tau \\ &\quad + \int_0^\infty B b(t-\tau) \mathcal{F}(\tau) \tilde{A}(\tau) d\tau \end{aligned}$$

$$\begin{aligned} b(t) &= \int_0^\infty b(t-a)\beta(a)\mathcal{F}(a)P(a)da \\ &\quad + \int_0^\infty (1-b(t-a))\beta(a)\mathcal{F}(a) \int_0^a F(t-a+\sigma) e^{-\int_{t-a}^{t-a+\sigma} F(u)du} P(a-\sigma) d\sigma da. \end{aligned} \tag{1.8}$$

Here, $\beta(a)$ is the age-dependent fertility of individuals and $P(\tau)$ is the probability of producing an infected offspring by an infected mother. The existence and uniqueness of a positive equilibrium is discussed and the local stability of the disease-free equilibrium is given. Numerical analysis is performed to study the dependence of the positive equilibrium and the basic reproduction number on the two major components, $P(\tau)$ and $\int_0^\infty e^{-\mu\tau} A(\tau) d\tau$ (when $\mathcal{F}(a) = e^{-\mu a}$) . This chapter is contained in a manuscript that is in preparation for submission.

The first section of chapter 4 is devoted to the dynamics of vector-borne diseases using renewal equations. In the first part, both the vector and host populations have no demographics. The models here are special cases of the model in chapter 2, where the sub-populations are not fully connected, i.e., the transmission probability matrix is non-negative (some entries can be zero). Several scenarios are considered here: one vector population and one host population with and

without host-to-host transmission; one vector population and several host populations without host-to-host transmission. In the second part of this section, both the vector and host populations have demographics with constant birth and general survival functions. Existence and uniqueness of a positive equilibrium and the local stability analysis are given. In the next section of this chapter, a delay differential system is developed for the population dynamics of black legged ticks, also known as deer ticks, which are responsible for transmission of Lyme pathogen in the tick-host natural cycle, and for the Lyme disease in humans and other animal species, to study the impact of host resistance that has been observed in different types of hosts. The results of this section are published in a paper in the journal of Mathematics in Applied Sciences and Engineering [1].

The last chapter features the control measures of respiratory diseases, in particular influenza and COVID-19 among specific age groups. The focus of this chapter is to evaluate the control measures to protect the senior population with a higher probability of experiencing severe adverse events resulting from respiratory diseases. This chapter also presents some motivation for studying the epidemiological models involving different age groups, and hence the need of further research using the renewal equation framework. Major parts of this chapter are being submitted for publication.

1.3 Author contribution for the published and submitted papers

Chapters of this thesis are based on the following publications and pre-prints:

- Alavinejad, M., & Wu, J. (2020). Coupled systems of renewal equations for forces of infection through a contact network.Canadian Mathematical Bulletin,63(3), 624-632.

  Author contribution: J.W. originated the research idea. The model formulation and mathematical analysis was carried out by M.A. and J.W. The writing of the manuscript was completed by M.A.

- Alavinejad, M., Sadiku, J., & Wu, J. (2020). Modeling the impact of host resistance on structured tick population dynamics. Mathematics in Applied Sciences and Engineering ,1(1), 65-84.

Author contribution: The research idea was originated by J.S. The model formulation was carried out by M.A and J.S. The mathematical and stability analyses were completed by M.A. Numerical simulations were performed by M.A. and J.S. LHS-PRCC was performed by J.S. The writing of the manuscript was completed by M.A. and J.S. The project was supervised by J.W.

- Alavinejad, M., Tosato, M., Bragazzi, N. L., McCarthy, Z., Wu, J. & Bourouiba, L. Markers of community outbreak and facility type for mitigation of COVID-19 in long-term care homes in Ontario, Canada: insights and implications from a time-series analysis. In Preparation.

  Author contribution L.B. and J. W. originated the research idea presented. Z.M. provided the data. M.A. performed both statistical analysis and data analysis and visualizations. M.T. performed data clustering analysis. M.A. and M.T. carried out the numerical simulations. N.B. performed literature review. All authors provided critical feedback and helped shape the research, analysis and manuscript. M.A. took the lead in writing the manuscript, together with M.T. and N.B. J.W. and L.B. supervised the project.

2 | Dynamics of Infectious Diseases in a Population Structured by Immunity

It is well-known that the immunity to an infectious disease differs by individuals and there are different factors that affect the level of immunity to a particular disease, such as: age, presence of chronic diseases, temporary clinical conditions and vaccination status. The human immune system and its response to a pathogen is in particular complicated depending on age and clinical conditions. Also for some diseases where the vaccine does not give perfect immunity, the efficacy of vaccine and the level of immunity induced by vaccine varies significantly with age. Mathematical models have been used widely to study the dynamics of infectious diseases and to inform policy makers regarding the control and prevention of the diseases. Modelers have tried to include as many factors as possible to get the most comprehensive model that can describe the dynamics of the disease spread and determine factors that contribute the most in order to better control the diseases. Based on the characteristics of diseases, mathematical models have been developed to study the impact of factors such as age, vaccine induced immunity, infection acquired immunity, time since last infection, time since vaccination, time dependent contact rates, time dependent infectivity.

Disease transmission dynamics models for a population structured by immunity have been studied in [134, 8, 7], focusing on the waning and boosting of the immunity after recovering from infection. Here we develop a mathematical model in a population stratified based on the level of immunity to a disease.

2.1 The general formulation

Consider a closed population. Suppose individuals' level of immunity to an infectious disease is a continuous time-varying variable, defined as the probability of not contracting the disease if exposed, denoted by $\mathfrak{m}$ ($0 \leq \mathfrak{m} \leq 1$) with $\mathfrak{m} = 0$ corresponding to fully susceptible individuals and $\mathfrak{m} = 1$ corresponding to fully immune individuals (e.g., immunity with vaccination or infection-acquired immunity). Here the immunity is referred to as the immunity against transmission. The

immunity level can vary based on age, presence of chronic diseases, temporary clinical conditions, vaccination status, time since vaccination and time since last infection. The density of the susceptible (partially immune) population at time t and with immunity $\mathfrak{m}$ is denoted by $S(t, \mathfrak{m})$.

Assume the force of infection from infected individuals depends on their immunity status before being infected. Let $F(t, \mathfrak{m})$ denote the force of infection imposed on individuals with immunity $\mathfrak{m}$. Dynamics of the susceptible population can be described by the following partial differential equation:

$$\begin{gathered}(\frac{\partial}{\partial t} + \frac{\partial}{\partial \mathfrak{m}}.g(\mathfrak{m}))S(t, \mathfrak{m}) = -\epsilon(\mathfrak{m})F(t, \mathfrak{m})S(t, \mathfrak{m}), \quad S(0, \mathfrak{m}) = S_0(\mathfrak{m}) \\ \frac{\partial \mathfrak{m}}{\partial t} = g(\mathfrak{m}), \quad g(0) = \mathfrak{m}_0\end{gathered} \tag{2.1}$$

subject to a certain boundary condition, where the function g determines how the immunity of individuals changes with time and $\epsilon(\mathfrak{m})$ is the corresponding susceptibility. Note that the incidence for individuals with immunity $\mathfrak{m}$ is given by

$$\text{incidence} = \epsilon(\mathfrak{m})F(t, \mathfrak{m})S(t, \mathfrak{m}). \tag{2.2}$$

Let $A(\tau, \mathfrak{u}, \mathfrak{m})$ be the contribution to the force of infection by an infected individual with immunity $\mathfrak{u}$ imposed on individuals with immunity $\mathfrak{m}$. In a special case we can assume that the immunity does not change during the epidemic, i.e., $g = 0$, except by infection and recovery. The force of infection can be then described by the following renewal equation

$$F(t, \mathfrak{m}) = \int_0^\infty \int_0^1 \epsilon(\mathfrak{u})F(t - \tau, \mathfrak{u})S(t - \tau, \mathfrak{u})A(\tau, \mathfrak{u}, \mathfrak{m})d\mathfrak{u}d\tau. \tag{2.3}$$

Determining the immunity of individuals to the transmission of a disease can be a challenging task, however, some information can be used to estimate these numbers. For instance, the protection imposed by vaccination depends highly on the age of individuals in case of influenza and on the time since vaccination in case of pertussis.

As a special case we assume the population is divided into n sub-populations $S_1, \cdots, S_n$ with a

fixed level of immunity. In each sub-population $m_{i-1} \leq \mathfrak{m}_i \leq m_i$, where $0 = m_0 \leq m_1 \leq \cdots < m_n = 1$. The number of sub-populations n and the values $m_1, \cdots, m_{n-1}$ can be determined based on the characteristics of the susceptible individuals such as age, clinical conditions, and vaccination status. In this formulation, we consider a wide class of compartmental models in a multi-group susceptible population. A special case would be an n-sub-population SIR model with transmission probabilities β_{ij}, when we allow various contact rates and infectivities for different sub-populations.

2.2 Coupled systems of renewal equations for forces of infection through a contact network

In this section, we formulate a coupled system of renewal equations for the forces of infection in a population consisting of multiple sub-populations. Due to different between-sub-population contact patterns and sub-populations' infectiousness (resulted from such factors as age, immunization practices and social distance), we allow the forces of infection from an infected subgroup imposed on a susceptible subgroup to be non-symmetric for both the contact rate and the infectiousness. We apply the theory of sub-homogeneous and order preserving discrete dynamical systems to establish the existence and uniqueness of a positive total cumulative force of infection perceived by each sub-population. We obtain the basic reproduction number and a final size relation of the epidemic, and illustrate our general results by a SIR model for a population with multiple sub-populations.

2.2.1 Epidemic in a closed Population Consisting of Sub-Populations

Consider a closed population, i.e., no birth, death and migration. Suppose the population is divided into sub-populations (e.g., age groups). Let $S_1, \cdots, S_n$ denote sub-populations of susceptible individuals and $S_i(-\infty)$, $i = 1, \cdots, n$, be the initial density of susceptibles. Suppose $S_i(-\infty) > 0$, for all $i = 1, \cdots, n$.

Recall that the *force of infection* in epidemiology is referred to the rate at which susceptible individuals become infected (or the probability that a susceptible individual gets infected).

Let $F_{ij}(t)$ be the force of infection from the i-th infected group to the j-th susceptible group (through direct interaction), and $A_{ij}(\tau)$ be the *"expected contribution to the force of infection F_{ij} by an infected individual in i-th group, who was infected τ units of time ago"*[18].

We assume the functions $A_{ij}(\tau)$ have the following properties

- $A_{ij} : [0, \infty) \to [0, \infty)$;
- A_{ij} is integrable, i.e., $\int_0^\infty A_{ij}(\tau)d\tau < \infty$.

First we note that the incidence in i-th subgroup is given by

$$\text{incidence} = S_i(t) \sum_k F_{ki}(t).$$

Also, we assume that recovered individuals have permanent immunity. Therefore,

$$S_i'(t) = -S_i(t) \sum_k F_{ki}(t). \tag{2.4}$$

Solving this equation results in the following

$$S_i(t) = S_i(-\infty) e^{-\int_{-\infty}^t \sum_k F_{ki}(\sigma)d\sigma}. \tag{2.5}$$

The forces of infection can be described by a nonlinear system of renewal equations

$$F_{ij}(t) = \int_0^\infty S_i(t-\tau) \sum_k F_{ki}(t-\tau) A_{ij}(\tau) d\tau.$$

Note that the properties of A_{ij} ensure that F_{ij} are well-defined and non-negative.

We introduce the notation $F_{\cdot i}(t) = \sum_k F_{ki}(t)$ so that

$$F_{ij}(t) = \int_0^\infty S_i(t-\tau) F_{\cdot i}(t-\tau) A_{ij}(\tau) d\tau.$$

Therefore, the force of infection perceived by group j is as follows

$$F_{\cdot j}(t) = \int_0^\infty \sum_i S_i(t-\tau)F_{\cdot i}(t-\tau)A_{ij}(\tau)d\tau$$

Next, we derive the cumulative force of infection defined by

$$y_{\cdot j}(t) = \int_{-\infty}^t F_{\cdot j}(\sigma)d\sigma. \tag{2.6}$$

Therefore

$$\begin{aligned} y_{\cdot j}(t) &= \sum_i \int_0^\infty \int_{-\infty}^t S_i(\sigma-\tau)F_{\cdot i}(\sigma-\tau)d\sigma A_{ij}(\tau)d\tau \\ &= \sum_i \int_0^\infty S_i(-\infty)(1-e^{-y_{\cdot i}(t-\tau)})A_{ij}(\tau)d\tau. \end{aligned}$$

We use (2.4) and (2.5) to get

$$\begin{aligned} \int_{-\infty}^t S_i(\sigma-\tau)F_{\cdot i}(\sigma-\tau)d\sigma &= \int_{-\infty}^t -S_i'(\sigma-\tau)d\sigma \\ &= S_i(-\infty) - S_i(t-\tau) \\ &= S_i(-\infty)(1-e^{-\int_{-\infty}^{t-\tau} F_{\cdot i}(\sigma)d\sigma}) \\ &= S_i(-\infty)(1-e^{-y_{\cdot i}(t-\tau)}) \end{aligned}$$

so that

$$y_{\cdot j}(t) = \sum_i \int_0^\infty S_i(-\infty)(1-e^{-y_{\cdot i}(t-\tau)})A_{ij}(\tau)d\tau, \quad j = 1, \cdots, n. \tag{2.7}$$

System (2.7) is a system of renewal equations of convolution type for $Y(t) = (y_{\cdot 1}(t), \cdots, y_{\cdot n}(t))$. The solution to this equation exists and is positive [61]. Also, since $0 \leq 1 - e^{-y_{\cdot j}(t)} \leq 1$, $y_{\cdot j}(t)$ are increasing and bounded on $(0, \infty)$, therefore $Y(\infty) = lim_{t\to\infty} Y(t)$ exists.

Let $t \to \infty$ in (2.7), then

$$y_{\cdot j}(\infty) = \sum_i \int_0^\infty S_i(-\infty)(1-e^{-y_{\cdot i}(\infty)})A_{ij}(\tau)d\tau. \tag{2.8}$$

Let $X_j = y_{\cdot j}(\infty)$, $f(X_j) = 1 - e^{-X_j}$, $\mathbf{B} = (b_{ij})$, where $b_{ij} = S_i(-\infty)\int_0^\infty A_{ij}(\tau)d\tau \geq 0$. Then

System (2.8) can be expressed as follows:

$$X = \mathbf{B}^T G(X), \tag{2.9}$$

where $\mathbf{B}^T$ is the transpose matrix, and

$$G(X) = \begin{pmatrix} f(X_1) \\ f(X_2) \\ \vdots \\ f(X_n) \end{pmatrix}.$$

Remark. Let $\hat{A}_{ij} = \int_0^\infty A_{ij}(\tau)d\tau$, $\hat{A} = (\hat{A}_{ij})_{1\le i,j\le n}$ and $D_s = diag(S_i(-\infty))$. Then $\mathbf{B} = D_s\hat{A}$.

In the following we let $H(X) = \mathbf{B}^T G(X)$. We have the following result about the existence of a positive solution of System (2.9).

Theorem 2.1. *Suppose* $\mathbf{B}$ *is positive (*$b_{ij} > 0$*,* $i, j = 1, \cdots, n$*). System* (2.9) *has a unique positive solution if* $\rho(\mathbf{B})$*, the spectral radius of* $\mathbf{B}$*, is greater than one.*

In order to prove this theorem, we need to introduce some concepts relevant to discrete dynamical systems. We follow the notations in [135] and let E be a Banach space and $P \subseteq E$ be a positive cone. A partial order on E induced by P is defined by the following relation: $x \ge y \Leftrightarrow x - y \in P$; $x > y \Leftrightarrow x - y \in P \setminus \{0\}$; $x \gg y \Leftrightarrow x - y \in int(P)$. With the partial order defined on E, for $a < b$ the intervals in E are defined by $[a, b]_E = \{x \in E : a \le x \le b\}$ and $[[a, b]]_E = \{x \in E : a \ll x \ll b\}$.

Let $U \subset P$ be a nonempty, closed and order convex subset, i.e., $[u, v]_E \subset U$ for all $u, v \in U$ with $u < v$.

Definition 2.2. A map $f : U \to U$ is said to be *monotone* if $f(x) \ge f(y)$ for all $x \ge y$, *strongly monotone* if $f(x) \gg f(y)$ for all $x > y$.

Definition 2.3. A map $f : U \to U$ is said to be *sub-homogeneous* if $f(tx) \ge tf(x)$ for all $x \in U$

and $t \in [0,1]$; strictly sub-homogeneous if $f(tx) > tf(x)$ for all $x \gg 0$ and $t \in (0,1)$; strongly sub-homogeneous if $f(tx) \gg tf(x)$ for all $x \gg 0$ and $t \in (0,1)$.

Definition 2.4. A linear map L on E is said to be positive if $L(x) \in P$ for all $x \in P$ and *strongly positive* if $L(x) \in int(P)$ for all $x \in P \setminus \{0\}$.

Definition 2.5. A continuous mapping $f : E \to E$ is said to be *asymptotically smooth* if for any nonempty closed bounded set $U \subset E$ with $f(U) \subset U$, there is a compact set $J \subset U$ such that J attracts U.

Theorem 2.6. *Let either $V = [0,b]_E$ with $b \gg 0$ or $V = P$. Assume that*

(H1) $f : V \to V$ is monotone and strongly sub-homogeneous;

(H2) $f : V \to V$ is asymptotically smooth, and every positive orbit of f in V is bounded;

(H3) $f(0) = 0$ and $Df(0)$ is compact and strongly positive.

Then there exists threshold dynamics described below:

(a) *If $\rho(Df(0)) \leq 1$, then every positive orbit in V converges to 0;*

(b) *If $\rho(Df(0)) > 1$, then there exists a unique fixed point $u^* \gg 0$ in V such that every positive orbit in $V \setminus \{0\}$ converges to u^*.*

In the following let $E = \mathbb{R}^n$ and $P = \mathbb{R}^n_{\geq 0}$. For $X, Y \in P$, we define $X \geq Y \Leftrightarrow X_i \geq Y_i, \quad \text{for all} \quad i = 1, \cdots, n; X > Y \Leftrightarrow X \geq Y, \quad X_i \neq Y_i, \quad \text{for some} \quad i = 1, \cdots, n; \; X \gg Y \Leftrightarrow X_i > Y_i, \quad \text{for all} \quad i = 1, \cdots, n.$ We note that a linear map on $\mathbb{R}^n$ is strongly positive if and only if the corresponding matrix is positive.

We can now give a proof of Theorem 2.1 by showing that the map $H : P \to P$ satisfies conditions of Theorem 2.6.

(H1) H is monotone and strongly sub-homogeneous: Let $X, Y \in P$ with $X \gg Y$, then $X_k > Y_k$ for $k = 1, \cdots, n$. Since $f(X_k) > f(Y_k)$ and B is positive, we have

$$H_j(X) = \sum_k b_{kj} f(X_k) > \sum_k b_{kj} f(y_k) = H_j(Y), \quad j = 1, \cdots, n.$$

Therefore, $H(X) \gg H(Y)$. Let $0 < t < 1$. We show that $H(tX) \gg tH(X)$. First we note that $f(x) = 1 - e^{-x}$ is strongly sub-homogeneous. Let $X \in P$, $X \gg 0$. Then

$$H_j(tX) = \sum_k b_{kj} f(tX_k) > \sum_k b_{kj} t f(X_k) = tH_j(X), \quad j = 1, \cdots, n.$$

Thus H is strongly sub-homogeneous.

(H2) Since $f(x) < 1$ for all $x \geq 0$, we have

$$H_j(X) = \sum_k b_{kj} f(X_k) < \sum_k b_{kj} = c_j,$$

So $|H(X)| < |(c_j)| = c$. Thus every positive orbit is bounded. Also, every continuous transformation on a finite dimensional vector space is asymptotically smooth [63].

(H3) $H(0) = 0$ and $DH(0) = \mathbf{B}^T$ which is a compact operator. Also $\mathbf{B}^T$ is strongly positive since it is positive. This completes the proof.

It is worth mentioning that the positivity assumption of $\mathbf{B}$ is equivalent to assuming that $\int_0^\infty A_{ij}(\tau)d\tau > 0$, for all $i, j = 1 \cdots, n$.

2.2.2 Final size of the epidemic

From (2.5) and (2.6) we have

$$S_i(t) = S_i(-\infty)e^{-y_{\cdot i}(t)}, \tag{2.10}$$

and therefore

$$1 - e^{-y_{\cdot i}(\infty)} = 1 - \frac{S_i(\infty)}{S_i(-\infty)}.$$

Substituting this in (2.8) we get

$$y_{\cdot j}(\infty) = \sum_i \big(1 - \frac{S_i(\infty)}{S_i(-\infty)}\big) S_i(-\infty) \int_0^\infty A_{ij}(\tau)d\tau. \tag{2.11}$$

Let $u^* = (y_{\cdot j}(\infty))$ be the unique, strongly positive solution of (2.8). Then (2.11) can be expressed

as

$$u^* = \mathbf{B}^T S^*,$$

where

$$S^* = (s_i^*), \quad s_i^* = 1 - \frac{S_i(\infty)}{S_i(-\infty)}.$$

Let $\mathcal{R}_0 = \rho(\mathbf{B}^T)$. Since $\mathbf{B}^T$ is irreducible and nonnegative, by Perron-Frobenius Theorem [65], there exists a left eigenvector $V \gg 0$ of $\mathbf{B}^T$ corresponding to $\mathcal{R}_0$

$$V^T \mathbf{B}^T = \mathcal{R}_0 V^T.$$

The final size is related to $\mathcal{R}_0$ by equation

$$V^T u^* = \mathcal{R}_0 V^T S^*.$$

Remark. Note that $u_i^* = \ln \frac{S_i(-\infty)}{S_i(\infty)}$. Also, the basic reproduction number of each subgroup in isolation from the rest of the population is given by

$$\mathcal{R}_{0i} = S_i(-\infty) \int_0^\infty A_{ii}(\tau) d\tau.$$

The matrix $\mathbf{B}$ can be expressed as $\mathbf{B} = diag(\mathcal{R}_{0i})P$, where $P = (p_{ij})_{1 \le i,j \le n}$ with $p_{ij} = \hat{A}_{ij}/\hat{A}_{ii}$. Therefore the basic reproduction number for a fully connected network of sub-populations is related to the basic reproduction numbers of sub-populations, when isolated from the rest of the population, by the equation

$$\mathcal{R}_0 = \rho\big(diag(\mathcal{R}_{0i})P\big).$$

With the above expression for $\mathbf{B}$, the final size relation (2.11) is as follows

$$\ln \frac{S_i(-\infty)}{S_i(\infty)} = \sum_{j=1}^{n} \mathcal{R}_{0j} p_{ji} \Big(1 - \frac{S_j(\infty)}{S_j(-\infty)}\Big), \tag{2.12}$$

which relates the final size of sub-populations to the basic reproduction numbers of sub-populations

in isolation.

If we have information on the basic reproduction numbers within subgroups, for a particular disease, Equation (2.12) can be used to calculate the basic reproduction number and final sizes of the disease in the total population and also to estimate some parameters such as contact rates and transmission probabilities between the subgroups.

Theorem 2.7. *We have the following cases:*

- *If $\mathcal{R}_0 > 1$, then introduction of an infected individual will result in an outbreak and the final size is given by the equation* (2.11)
- *If $\mathcal{R}_0 \leq 1$, then there is a minor outbreak and the final size is close to 0.*

Proof. From Theorem 2.1, a strongly positive solution exists for the total cumulative force of infection when $\mathcal{R}_0 > 1$, which in turn results in the final size relation (2.12). This proves the first part of the result.

In the second part of the result above, System (2.8) has only the zero solution when $\mathcal{R}_0 < 1$ and the final size being close to 0 can be justified in a similar way for a single population as in [18]. Also, initially, a positive fraction of the population is assumed to be infected.

2.2.3 Special Case: The SIR Model

In this section, we illustrate our general results with an example of the SIR model in a population of multiple sub-populations. Assume in each subgroup we have three compartments of susceptible, infected and recovered individuals with permanent immunity.

Exponentially distributed infectious period

Suppose the infectious period in the SIR model is exponentially distributed. Then the infectivity rates are given by $A_{ij}(\tau) = \beta_{ij}e^{-\alpha_i\tau}$, $i, j = 1, \cdots, n$, where β_{ij} denotes the transmission rate between the i-th infected group and the j-th susceptible group, and α_i is the recovery rate in the

i-th subgroup. In this case, System (2.8) has the following form

$$y_{.j}(\infty) = \sum_i S_i(-\infty)\frac{\beta_{ij}}{\alpha_i}(1 - e^{-y_{.i}(\infty)}). \tag{2.13}$$

Let $\mathbf{B_1}$ be the matrix given in Section 2.2.1

$$\mathbf{B_1} = \begin{pmatrix} S_1(-\infty)\frac{\beta_{11}}{\alpha_1} & \cdots & S_1(-\infty)\frac{\beta_{1n}}{\alpha_1} \\ \vdots & & \\ S_n(-\infty)\frac{\beta_{n1}}{\alpha_n} & \cdots & S_n(-\infty)\frac{\beta_{nn}}{\alpha_n} \end{pmatrix}.$$

The basic reproduction number is $\mathcal{R}_0 = \rho(\mathbf{B_1})$. Note that by Remark 2.2.1

$$\hat{A} = \begin{pmatrix} \frac{\beta_{11}}{\alpha_1} & \cdots & \frac{\beta_{1n}}{\alpha_1} \\ \vdots & & \\ \frac{\beta_{11}}{\alpha_1} & \cdots & \frac{\beta_{1n}}{\alpha_1} \end{pmatrix},$$

and by Remark 2.2.2 matrix $\mathbf{B_1}$ can be expressed as

$$\mathbf{B_1} = \begin{pmatrix} \mathcal{R}_{01}\frac{\beta_{11}}{\beta_{11}} & \cdots & \mathcal{R}_{01}\frac{\beta_{1n}}{\beta_{11}} \\ \vdots & & \\ \mathcal{R}_{0n}\frac{\beta_{n1}}{\beta_{nn}} & \cdots & \mathcal{R}_{0n}\frac{\beta_{nn}}{\beta_{nn}} \end{pmatrix},$$

equivalently, $\mathbf{B_1} = diag(\mathcal{R}_{0i})P$, where $\mathcal{R}_{0i} = S_i(-\infty)\frac{\beta_{ii}}{\alpha_i}$, $i = 1, \cdots, n$ and $p_{ij} = \frac{\beta_{ij}}{\beta_{ii}}$, $i, j = 1, \cdots, n$. The final size relation is given by

$$\begin{cases} \ln\frac{S_1(-\infty)}{S_1(\infty)} & = S_1(-\infty)\frac{\beta_{11}}{\alpha_1}\left(1 - \frac{S_1(\infty)}{S_1(-\infty)}\right) + \cdots + S_n(-\infty)\frac{\beta_{n1}}{\alpha_n}\left(1 - \frac{S_n(\infty)}{S_n(-\infty)}\right), \\ & \vdots \\ \ln\frac{S_n(-\infty)}{S_n(\infty)} & = S_1(-\infty)\frac{\beta_{1n}}{\alpha_1}\left(1 - \frac{S_1(\infty)}{S_1(-\infty)}\right) + \cdots + S_n(-\infty)\frac{\beta_{nn}}{\alpha_n}\left(1 - \frac{S_n(\infty)}{S_n(-\infty)}\right). \end{cases}$$

which is equivalent to

$$\begin{cases} \ln \frac{S_1(-\infty)}{S_1(\infty)} & = \mathcal{R}_{01}p_{11}\Big(1-\frac{S_1(\infty)}{S_1(-\infty)}\Big)+\cdots+\mathcal{R}_{0n}p_{n1}\Big(1-\frac{S_n(\infty)}{S_n(-\infty)}\Big), \\ & \vdots \\ \ln \frac{S_n(-\infty)}{S_n(\infty)} & = \mathcal{R}_{01}p_{1n}\Big(1-\frac{S_1(\infty)}{S_1(-\infty)}\Big)+\cdots+\mathcal{R}_{0n}p_{nn}\Big(1-\frac{S_n(\infty)}{S_n(-\infty)}\Big). \end{cases}$$

If additionally we assume that $\alpha_i = \alpha$ and $\beta_{ij} = a_i b_i c_{ij}$, where b_i is the probability of becoming infected for an individual in subgroup i, a_i is the contact rate and c_{ij} is the proportion of contacts between an individual in sub-group i with individuals in sub-group j with $\sum_i c_{ij} = 1$, then the matrix $\mathbf{B_1}$ and the above final size relation are the same as the matrix K and the relation (14) given in [32]. proportion of the ith sub-group's contacts that is with members of the jth group

Non-exponentially distributed infectious period

Here we consider a SIR model where the infectious period has Gamma distribution with the rate α_i and shape κ_i for each sub-population. The probability density function and survival function are given by:

$$g_i(t;\kappa_i,\alpha_i) = \frac{\alpha_i^{\kappa_i}}{\Gamma(\kappa_i)} t^{\kappa_i-1}e^{-\alpha_i t},$$
$$K_i(t;\kappa_i,\alpha_i) = 1 - \frac{\alpha_i^{\kappa_i}}{\Gamma(\kappa_i)}\int_0^t s^{\kappa_i-1}e^{-\alpha_i s}ds.$$

Let $\kappa_i = 2$, then $g_i(t;\alpha_i,2) = \alpha_i^2 t e^{-\alpha_i t}$ and the survival function is given by $K_i(t;\alpha_i,2) = (\alpha_i t+1)e^{-\alpha_i t}$. First we note that the corresponding infectivity rates $A_{ij}(\tau)$ can be defined as the product of two components: transmission probability and probability of being infectious after τ units of time. Therefore

$$A_{ij}(\tau) = \beta_{ij}(\alpha_i\tau+1)e^{-\alpha_i\tau}$$

Next we calculate $\int_0^\infty A_{ij}(\tau)d\tau$

$$\begin{aligned}\int_0^\infty A_{ij}(\tau)d\tau &= \beta_{ij}\int_0^\infty (\alpha_i\tau+1)e^{-\alpha_i\tau}d\tau \\ &= \frac{2\beta_{ij}}{\alpha_i}.\end{aligned}$$

Let $\mathbf{B_2}$ denote the matrix from section 2.2.1, then

$$\mathbf{B_2} = \begin{pmatrix} S_1(-\infty)\frac{2\beta_{11}}{\alpha_1} & \cdots & S_1(-\infty)\frac{2\beta_{1n}}{\alpha_1} \\ \vdots & & \\ S_n(-\infty)\frac{2\beta_{n1}}{\alpha_n} & \cdots & S_n(-\infty)\frac{2\beta_{nn}}{\alpha_n} \end{pmatrix}.$$

The basic reproduction number is $\mathcal{R}_0 = \rho(\mathbf{B_2})$. We note that, in the literature using a Gamma distribution for the latent and infectious period with the shape parameter κ_i, the rate parameter is normally taken as α_i, since the entire latent/infectious period is distributed into κ_i stages [73, 77]. Therefore, the basic reproduction number in a SIR model with Gamma distribution for the infectious period, with shape $\kappa_i = 2$ and rate $2\alpha_i$, is the same the basic reproduction number when the infectious period is exponentially distributed with rate α_i.

2.3 Conclusions

In this chapter, a general model was formulated to describe the transmission dynamics of infectious diseases in a closed population stratified based on individuals' level of immunity using: 1) a system of partial differential equations to describe the dynamics of the susceptible population and the variation of immunity in the population; 2) renewal equations for the forces of infection. In this general formulation, the time-varying immunity is described by an ODE. The key idea is understanding the underlying factors contributing to the immunity of individuals, such as age, clinical conditions and vaccination status, and therefore to identify risk groups in the population. The general model has an advanced level of complexity and requires further studies in terms of mathematical and numerical analyses.

A special case with a finite number of fixed values of immunity for individuals in the population is studied in full detail in this chapter. The population is divided into n sub-populations and a system of renewal equations for the forces of infection between sub-populations is used to describe the disease dynamics. The threshold value for a disease outbreak in all sub-populations is derived. Using the threshold theory for sub-homogeneous monotone discrete dynamical systems, the criteria for the existence and uniqueness of a positive final size in all subgroups are given. The

relation between basic reproduction number of the total population and the basic reproduction numbers of sub-populations in isolation as well as a final size relation for the sub-populations is given. The theory is then illustrated through a SIR model. A comparison of the results for SIR model with exponentially distributed infectious period and a SIR model considering a Gamma distribution for the infectious period is given.

2.4 A remark

Major components of this chapter have been published in the paper in the Canadian Mathematical Bulletin [2]. I am grateful to Professor Neal Madras for his valuable suggestions and helpful comments on the presentation of this chapter and to two reviewers for their constructive comments. The research of this Chapter has been partially supported by the Natural Sciences and Engineering Research Council of Canada (NSERC), the Canada Research Chair Program and the NSERC-Sanofi Industrial Research Chair Program in Vaccine Mathematics, Modeling and Manufacturing.

3 | Dynamics of Vertically Transmitted Diseases Described by Renewal Equations

Many diseases can be transmitted from an infected mother to a newborn, known as vertically transmitted diseases. Pathogens transmitted during human pregnancy include: Zika virus, Toxoplasma gondii, Listeria monocytogenes, Treponema pallidium, parvovirus, HIV, HCV, varicella zoster virus, Rubella, and Herpesviruses [6]. Based on WHO's report [124], the rates of mother-to-child transmission of HIV, in the absence of any treatment, vary between 15%-45% (during pregnancy, delivery and breastfeeding). However, the mother-to-child transmission can be reduced to 1% and even be eliminated if both mother and baby receive antiretroviral (AVR) treatment. Some countries are validated for the elimination of mother-to-child transmission of HIV such as Anguilla, Antigua and Barbuda, Armenia, Belarus, Bermuda, Cayman Islands, Cuba, Malaysia, Maldives, Montserrat, Saint Kitts and Nevis, and Thailand.

Mathematical models, using partial, ordinary and functional differential equations, have been developed widely to study the dynamics of vertically transmitted diseases [28, 9, 113, 122]. Here, we consider a single population with constant birth rate and a general survival function and study the dynamics of vertically transmitted diseases, i.e., a fraction of the offspring of infected individuals are infected, described by a coupled system of renewal equations for the force of infection and the birth function for the fraction of infected newborn. Local stability of the disease-free equilibrium and existence and uniqueness of the positive equilibrium point are given.

Consider an age-structured population with the population level birth rate $B(t)$ and survival function $\mathcal{F}(a)$. Let N be the total population and assume it is constant. The birth rate is given by $B(t) = \int_0^\infty B(t-a)\beta(a)\mathcal{F}(a)da$ where $\beta(a)$ is *"the probability per unit of time, for a female, to produce an offspring at age a"*. We normalize $\beta(a)$ so that $\int_0^\infty \beta(a)\mathcal{F}(a)da = 1$ (this is the basic reproduction ratio and the equality means that the population is at equilibrium). We also assume a constant birth rate B so we have $N = B\int_0^\infty \mathcal{F}(a)da$. Note that $-\int_0^\infty a\mathcal{F}(da)$ is the average lifetime of individuals. Here we assume $\beta(a)$ is a piecewise continuous nonnegative bounded function.

First we consider the model formulated in [18], without vertical transmission. Let $S(t,a)$ be the density of susceptible population at time t and age a and $\tilde{S}(t) := \int_0^\infty S(t,a)da$ denote the total susceptible population. In the absence of an infectious disease the density of the (susceptible) population is given by

$$S(t,a) = B\mathcal{F}(a). \tag{3.1}$$

Suppose there is a disease circulating in the population with the force of infection $F(t)$, defined as the probability per unit of time a susceptible individual becomes infected [18]. Then the density of the susceptible population is given by

$$S(t,a) = B\mathcal{F}(a)e^{-\int_0^a F(t-a+\sigma)d\sigma} \tag{3.2}$$

and the dynamics of the disease can be described by the following renewal equation for the force of infection:

$$F(t) = \int_0^\infty \underbrace{F(t-\tau)\int_0^\infty S(t-\tau,a)\frac{\mathcal{F}(a+\tau)}{\mathcal{F}(a)}da}_{\text{incidence in total susceptible population}} A(\tau)d\tau.$$

The force of infection imposed on the susceptible population is generated by infectious individuals, of all ages, who were susceptible and came in contact with infected individuals at previous times. The incidence, i.e., the number of new infections as a result of contact between susceptible and infected individuals, at time t is as follows

$$\text{incidence} = F(t)\tilde{S}(t).$$

3.1 Model Formulation

We now formulate a general age of infection model in a population where there is also vertical transmission. Let $b(t)$ denote the proportion of the newborn that are, at time t, born infected, then

$$S(t,a) = B(1-b(t-a))\mathcal{F}(a)e^{-\int_0^a F(t-a+\sigma)d\sigma}.$$

In order to derive the equations for $b(t)$ and $F(t)$ we introduce the following. Let $K(a,\tau)$ be the probability per unit of time that an infected individual of chronological age a, and infection age τ produces an infected offspring.

The function $K(a,\tau)$ has two components: the age-dependent fertility of individuals, denoted by $\beta(a)$, and "the probability an offspring produced by an infected mother of age of infection τ is infected", which we assume does not depend on the age of mother and denote by $P(\tau)$. We can assume $P(\tau) = A(\tau)/(c + A(\tau))$ for some positive parameter c. Then, there is no vertical transmission if $c \to \infty$, and for $c \to 0$, we have the following cases:

$$\begin{cases} P(\tau) &= 1, \quad A(\tau) > 0, \\ P(\tau) &= 0, \quad A(\tau) = 0. \end{cases}$$

Here we consider a two-sex population with a 1-1 ratio, and the population being constant means that a reproducing female has two offspring on average with one male and one female. When we count for the individuals infected at birth, first we count the number of infected females at previous times (only females can reproduce) and therefore divide by 2, and then we count number of infected newborn of both sexes and multiply by 2.

With the above notation we have the following for $b(t)$

$$\begin{aligned} b(t) = \int_0^\infty \Big(& b(t-a)\beta(a)\mathcal{F}(a)P(a) + (1 - b(t-a))\beta(a)\mathcal{F}(a) \\ & \int_0^a F(t-a+\sigma) e^{-\int_{t-a}^{t-a+\sigma} F(u)du} P(a-\sigma) d\sigma \Big) da. \end{aligned} \tag{3.3}$$

One can derive this equation directly from the interpretation. We note that individuals infected at birth come from two sources:

- from individuals who were born infected at time $t - a$, survive until time t and produce an infected offspring at time t (at the age of a) with probability per unit of time $K(a,a) = \beta(a)P(a)$;
- from individuals who were born susceptible at time $t - a$, survive until time t, became

infected at time $t-a+\sigma$ (at the age of σ, $0 \leq \sigma \leq a$) and produce an infected offspring at time t (at the age of a and infection age $a-\sigma$) with probability per unit of time $K(a, a-\sigma) = \beta(a)P(a-\sigma)$.

The renewal equation for the force of infection has now the following form

$$F(t) = \int_0^\infty \Big(F(t-\tau) \int_0^\infty B(1-b(t-\tau-a)) e^{-\int_0^a F(t-\tau-a+\sigma)d\sigma} \mathcal{F}(a+\tau) da A(\tau) \Big) d\tau + \int_0^\infty B b(t-\tau) \mathcal{F}(\tau) \tilde{A}(\tau) d\tau,$$

where the age of infection and the chronological age are identical in the second part. Here $\tilde{A}(\tau)$ is the contribution to the force of infection at age of τ of an individual infected at birth. We may assume that $\tilde{A}(\tau) = A(\tau)$, however, this needs not be the case.

Finally, the coupled system is as follows

$$\begin{cases} F(t) &= \int_0^\infty \Big(F(t-\tau) \int_0^\infty B(1-b(t-\tau-a)) e^{-\int_0^a F(t-\tau-a+\sigma)d\sigma} \mathcal{F}(a+\tau) da A(\tau) \Big) d\tau + \int_0^\infty B b(t-\tau) \mathcal{F}(\tau) \tilde{A}(\tau) d\tau \\ \\ b(t) &= \int_0^\infty \Big(b(t-a)\beta(a)\mathcal{F}(a)P(a) + (1-b(t-a))\beta(a)\mathcal{F}(a) \int_0^a F(t-a+\sigma) e^{-\int_{t-a}^{t-a+\sigma} F(u)du} P(a-\sigma) d\sigma \Big) da. \end{cases} \tag{3.4}$$

We make the following assumptions on $A(\tau)$, $\tilde{A}(\tau)$, $P(a)$ and $\beta(a)$.

(i) $A(\tau)$, $\tilde{A}(\tau)$, $P(\tau)$ and $\beta(a)$ are all non-negative integrable functions;

(ii) none of these functions are equal to zero on their entire domain $[0, \infty)$.

3.2 Steady states and their stability

In this section we study the local stability of the disease-free equilibrium $(0,0)$ and existence and uniqueness of a positive steady state of the system (3.4). Let $(\bar{F},\bar{b})$ denote the steady state, then

$$\begin{cases} \bar{F} &= \int_0^\infty \bar{F}B(1-\bar{b})\int_0^\infty e^{-\bar{F}a}\mathcal{F}(a+\tau)daA(\tau)d\tau + \int_0^\infty B\bar{b}\mathcal{F}(\tau)\tilde{A}(\tau)d\tau \\ \\ \bar{b} &= \int_0^\infty \bar{b}\beta(a)\mathcal{F}(a)P(a)da + \int_0^\infty (1-\bar{b})\beta(a)\mathcal{F}(a)\bar{F}\int_0^a e^{-\bar{F}\sigma}P(a-\sigma)d\sigma da. \end{cases} \tag{3.5}$$

Clearly $(0,0)$ is an equilibrium. We can also see that $\bar{F}=0$ corresponds to the disease-free equilibrium which results in $\bar{b}=0$, i.e., if there are no infected individuals, then there are no infection at birth. On the other hand, if $\bar{F}\neq 0$, then $\bar{b}=0$ means $b(t)=0$ for all $t\geq 0$ and therefore there is no vertical transmission.

First we study the existence and uniqueness of the positive equilibrium. Let $X=(\bar{F},\bar{b})$, and $f(X)$ be the right hand side of (3.5), then (3.5) can be written as $X=f(X)$. Here the theory of order-preserving and sub-homogeneous discrete dynamical systems is used to prove the existence and uniqueness of the positive fixed point of $f(X)$ [135].

It is straightforward to show that f satisfies the conditions of Theorem 2.6. The derivative $Df(0)$ is given by the following matrix:

$$Df(0)=\begin{pmatrix} B\int_0^\infty\int_0^\infty \mathcal{F}(a+\tau)daA(\tau)d\tau & B\int_0^\infty \mathcal{F}(\tau)\tilde{A}(\tau)d\tau \\ \\ \int_0^\infty \beta(a)\mathcal{F}(a)\int_0^a P(a-\sigma)d\sigma da & \int_0^\infty \beta(a)\mathcal{F}(a)P(a)da \end{pmatrix},$$

By theorem 2.6, there exists a unique positive equilibrium $(\bar{F},\bar{b})$ if $\mathcal{R}_0=\rho(Df(0))>1$.

To study the stability of the equilibria, we linearize System (3.4) about a given equilibrium.

$$\begin{cases} u(t) & = B\int_0^\infty v(t-\tau)\mathcal{F}(\tau)\tilde{A}(\tau)d\tau - B\int_0^\infty \bar{F}\int_0^\infty v(t-\tau-a)e^{-\bar{F}a}\mathcal{F}(a+\tau)daA(\tau)d\tau \\ & +B\int_0^\infty u(t-\tau)\int_0^\infty B(1-\bar{b})e^{-\bar{F}a}\mathcal{F}(a+\tau)daA(\tau)d\tau \\ & -B\int_0^\infty \bar{F}(1-\bar{b})\int_0^\infty\int_0^a u(t-\tau-a+\sigma)d\sigma\mathcal{F}(a+\tau)daA(\tau)d\tau \\ \\ v(t) & = \int_0^\infty v(t-a)\beta(a)\mathcal{F}(a)P(a)da - \int_0^\infty v(t-a)\beta(a)\mathcal{F}(a)\int_0^a \bar{F}e^{-\bar{F}\sigma}P(a-\sigma)d\sigma da \\ & +\int_0^\infty(1-\bar{b})\beta(a)\mathcal{F}(a)\int_0^a u(t-a+\sigma)e^{-\bar{F}\sigma}P(a-\sigma)d\sigma da \\ & -\int_0^\infty(1-\bar{b})\beta(a)\mathcal{F}(a)\int_0^a \bar{F}e^{-\bar{F}\sigma}\int_{t-a}^{t-a+\sigma} u(s)dsP(a-\sigma)d\sigma da. \end{cases} \tag{3.6}$$

Looking for solutions of exponential form, $u(t) = c_1e^{\lambda t}$, $v(t) = c_2e^{\lambda t}$, yields the following system

$$\begin{cases} c_1 & = \Bigg(B\int_0^\infty e^{-\lambda\tau}\int_0^\infty(1-\bar{b})e^{-\bar{F}a}\mathcal{F}(a+\tau)daA(\tau)d\tau \\ & -B\int_0^\infty \bar{F}(1-\bar{b})\int_0^\infty\int_0^a e^{-\lambda(\tau+a)}e^{\lambda\sigma}d\sigma\mathcal{F}(a+\tau)daA(\tau)d\tau\Bigg)c_1 \\ & +\Bigg(B\int_0^\infty e^{-\lambda\tau}\mathcal{F}(\tau)\tilde{A}(\tau)d\tau - B\int_0^\infty \bar{F}\int_0^\infty e^{-\lambda(\tau+a)}e^{-\bar{F}a}\mathcal{F}(a+\tau)daA(\tau)d\tau\Bigg)c_2 \\ \\ c_2 & = \Bigg(\int_0^\infty(1-\bar{b})\beta(a)\mathcal{F}(a)\int_0^a e^{-\lambda a}e^{\lambda\sigma}e^{-\bar{F}\sigma}P(a-\sigma)d\sigma da \\ & -\int_0^\infty(1-\bar{b})\beta(a)\mathcal{F}(a)\int_0^a \frac{\bar{F}}{\lambda}e^{-\bar{F}\sigma}\Big(e^{-\lambda(a-\sigma)}-e^{-\lambda a}\Big)P(a-\sigma)d\sigma da\Bigg)c_1 \\ & +\Bigg(\int_0^\infty e^{-\lambda a}\beta(a)\mathcal{F}(a)P(a)da - \int_0^\infty e^{-\lambda a}\beta(a)\mathcal{F}(a)\int_0^a \bar{F}e^{-\bar{F}\sigma}P(a-\sigma)d\sigma\Bigg)c_2 \end{cases}$$

This system can be written as $\Phi(\lambda)C = C$ where $C = (c_1, c_2)^T$ and $\Phi(\lambda)$ is given by

$$\Phi(\lambda) = \begin{pmatrix} \phi_{11}(\lambda) & \phi_{12}(\lambda) \\ \phi_{12}(\lambda) & \phi_{22}(\lambda) \end{pmatrix}$$

with

$$\begin{aligned}
\phi_{11}(\lambda) &= B\int_0^\infty e^{-\lambda\tau}\int_0^\infty (1-\bar{b})e^{-\bar{F}a}\mathcal{F}(a+\tau)daA(\tau)d\tau \\
&\quad - B\int_0^\infty \bar{F}(1-\bar{b})\int_0^\infty\int_0^a e^{-\lambda(\tau+a)}e^{\lambda\sigma}d\sigma\mathcal{F}(a+\tau)daA(\tau)d\tau \\
\phi_{12}(\lambda) &= B\int_0^\infty e^{-\lambda\tau}\mathcal{F}(\tau)\tilde{A}(\tau)d\tau - B\int_0^\infty \bar{F}\int_0^\infty e^{-\lambda(\tau+a)}e^{-\bar{F}a}\mathcal{F}(a+\tau)daA(\tau)d\tau \\
\phi_{21}(\lambda) &= \int_0^\infty (1-\bar{b})\beta(a)\mathcal{F}(a)\int_0^a e^{-\lambda a}e^{\lambda\sigma}e^{-\bar{F}\sigma}P(a-\sigma)d\sigma da \\
&\quad - \int_0^\infty (1-\bar{b})\beta(a)\mathcal{F}(a)\int_0^a \frac{\bar{F}}{\lambda}e^{-\bar{F}\sigma}\Big(e^{-\lambda(a-\sigma)} - e^{-\lambda a}\Big)P(a-\sigma)d\sigma da \\
\phi_{22}(\lambda) &= \int_0^\infty e^{-\lambda a}\beta(a)\mathcal{F}(a)P(a)da - \int_0^\infty e^{-\lambda a}\beta(a)\mathcal{F}(a)\int_0^a \bar{F}e^{-\bar{F}\sigma}P(a-\sigma)d\sigma
\end{aligned} \tag{3.7}$$

The characteristic equation is given by $\det(\Phi(\lambda) - I) = 0$, which in turn results in the following equation

$$
\begin{aligned}
&\left(B\int_0^\infty e^{-\lambda\tau}\int_0^\infty (1-\bar{b})e^{-\bar{F}a}\mathcal{F}(a+\tau)daA(\tau)d\tau \right.\\
&\left. - B\int_0^\infty \bar{F}(1-\bar{b})\int_0^\infty\int_0^a e^{-\lambda(\tau+a)}e^{\lambda\sigma}d\sigma\mathcal{F}(a+\tau)daA(\tau)d\tau - 1\right)\\
&\left(\int_0^\infty e^{-\lambda a}\beta(a)\mathcal{F}(a)P(a)da - \int_0^\infty e^{-\lambda a}\beta(a)\mathcal{F}(a)\int_0^a \bar{F}e^{-\bar{F}\sigma}P(a-\sigma)d\sigma - 1\right)\\
-&\left(B\int_0^\infty e^{-\lambda\tau}\mathcal{F}(\tau)\tilde{A}(\tau)d\tau - B\int_0^\infty \bar{F}\int_0^\infty e^{-\lambda(\tau+a)}e^{-\bar{F}a}\mathcal{F}(a+\tau)daA(\tau)d\tau\right)\\
&\left(\int_0^\infty (1-\bar{b})\beta(a)\mathcal{F}(a)\int_0^a e^{-\lambda a}e^{\lambda\sigma}e^{-\bar{F}\sigma}P(a-\sigma)d\sigma da\right.\\
&\left. - \int_0^\infty (1-\bar{b})\beta(a)\mathcal{F}(a)\int_0^a \frac{\bar{F}}{\lambda}e^{-\bar{F}\sigma}\Big(e^{-\lambda(a-\sigma)}-e^{-\lambda a}\Big)P(a-\sigma)d\sigma da\right) = 0
\end{aligned}
\tag{3.8}
$$

Equivalently

$$
\begin{aligned}
&\left(B\int_0^\infty e^{-\lambda\tau}\int_0^\infty (1-\bar{b})e^{-\bar{F}a}\mathcal{F}(a+\tau)daA(\tau)d\tau \right.\\
&\left. - B\int_0^\infty \bar{F}(1-\bar{b})\int_0^\infty\int_0^a e^{-\lambda(\tau+a)}e^{\lambda\sigma}d\sigma\mathcal{F}(a+\tau)daA(\tau)d\tau \right)\\
&+\left(\int_0^\infty e^{-\lambda a}\beta(a)\mathcal{F}(a)P(a)da - \int_0^\infty e^{-\lambda a}\beta(a)\mathcal{F}(a)\int_0^a \bar{F}e^{-\bar{F}\sigma}P(a-\sigma)d\sigma \right)\\
&-\left(B\int_0^\infty e^{-\lambda\tau}\int_0^\infty (1-\bar{b})e^{-\bar{F}a}\mathcal{F}(a+\tau)daA(\tau)d\tau \right.\\
&\left. - B\int_0^\infty \bar{F}(1-\bar{b})\int_0^\infty\int_0^a e^{-\lambda(\tau+a)}e^{\lambda\sigma}d\sigma\mathcal{F}(a+\tau)daA(\tau)d\tau \right) \qquad (3.9)\\
&\left(\int_0^\infty e^{-\lambda a}\beta(a)\mathcal{F}(a)P(a)da - \int_0^\infty e^{-\lambda a}\beta(a)\mathcal{F}(a)\int_0^a \bar{F}e^{-\bar{F}\sigma}P(a-\sigma)d\sigma \right)\\
&+\left(B\int_0^\infty e^{-\lambda\tau}\mathcal{F}(\tau)\tilde{A}(\tau)d\tau - B\int_0^\infty \bar{F}\int_0^\infty e^{-\lambda(\tau+a)}e^{-\bar{F}a}\mathcal{F}(a+\tau)daA(\tau)d\tau \right)\\
&\left(\int_0^\infty (1-\bar{b})\beta(a)\mathcal{F}(a)\int_0^a e^{-\lambda a}e^{\lambda\sigma}e^{-\bar{F}\sigma}P(a-\sigma)d\sigma da \right.\\
&\left. - \int_0^\infty (1-\bar{b})\beta(a)\mathcal{F}(a)\int_0^a \frac{\bar{F}}{\lambda}e^{-\bar{F}\sigma}\Big(e^{-\lambda(a-\sigma)}-e^{-\lambda a}\Big)P(a-\sigma)d\sigma da \right) = 1
\end{aligned}
$$

Here we study the (local) stability of the disease-free equilibrium.

Theorem 3.1. *Let $X(t) = (x_1(t), \cdots, x_n(t))^T$ be a vector-function, $X : \mathbb{R} \to \mathbb{R}^n$, and $K(s) = (k_{ij}(s))$, $i, j = 1, \cdots, n$ be a matrix-function, $K : \mathbb{R}_{\geq 0} \to \mathbb{R}^n$ (the kernel). Consider the system of linear renewal equations*

$$X(t) = \int_0^\infty K(\tau)X(t-\tau)d\tau.$$

Suppose, additionally, that K is positive and (piecewise) continuous, with compact support. Let $\bar{K}(z)$ denote the Laplace transform of the matrix-function K. Then the equilibrium $X^* = 0$ is locally asymptotically stable if $\rho(\bar{K}(0)) < 1$ and unstable if $\rho(\bar{K}(0)) > 1$.

This theorem can be obtained from an equivalent form in [61].

For the disease-free equilibrium (of the System (3.4)), the matrix $\bar{K}(0)$ of the above theorem is given by $\Phi(\lambda)$ at $\lambda = 0$ which is also equal to the matrix $Df(0)$ given in previous section. Theorem 3.1 implies that the disease-free equilibrium is locally asymptotically stable for $\mathcal{R}_0 < 1$, and unstable for $\mathcal{R}_0 > 1$.

3.3 Sensitivity Analysis

In this section, we study the dependence of the positive equilibrium $(\bar{F}, \bar{b})$ on the probability of producing an infected offspring $P(\tau)$. In order to numerically solve the System (3.5), we consider a special case where the survival probability has an exponential distribution, i.e., $\mathcal{F}(a) = e^{-\mu a}$. First we consider a constant value for both $\beta(a) = \beta^*$ and $P(\tau) = p^*$. In this case, System (3.5) is equivalent to

$$\begin{cases} \bar{F} &= B(1-\bar{b})\frac{\bar{F}}{\bar{F}+\mu}\int_0^\infty e^{-\mu\tau}A(\tau)d\tau + B\bar{b}\int_0^\infty e^{-\mu\tau}\tilde{A}(\tau)d\tau \\ \bar{b} &= \frac{\beta^* p^*}{\mu}\bar{b} + (1-\bar{b})\frac{\beta^* p^*}{\mu}\frac{\bar{F}}{\bar{F}+\mu}. \end{cases} \tag{3.10}$$

Without specifying the functions $A(\tau)$ and $\tilde{A}(\tau)$, we suppose the values for $A_1 = \int_0^\infty e^{-\mu\tau}A(\tau)d\tau$ and $A_2 = \int_0^\infty e^{-\mu\tau}\tilde{A}(\tau)d\tau$ are given. The parameter values are chosen in a reasonable range for a vertically transmitted disease such as HIV.

Figure 3.1a shows how the value of $\bar{b}$ increases as the probability p^* increases, while the value of $\bar{F}$ remains almost unchanged. The change of the equilibrium value with changing B and β^* is similar to p^*. The value of the equilibrium changes from 0 to a positive value as A_1 increases in 3.1b, showing that the basic reproduction number increases from below 1 to above 1 by increasing the value of A_1.

Figure 3.2 shows the sensitivity of the positive equilibrium $\bar{b}$ and $\mathcal{R}_0$ to the values of p^* and A_1. We observe in 3.2a that the values of $\bar{b}$ increase significantly by changing both p^* and A_1. On the other hand, 3.2b shows that the values of $\mathcal{R}_0$ are more sensitive to the variation of A_1, which means that the initial growth rate of the disease is not affected by the transmission probabilities from infected mothers to the newborn.

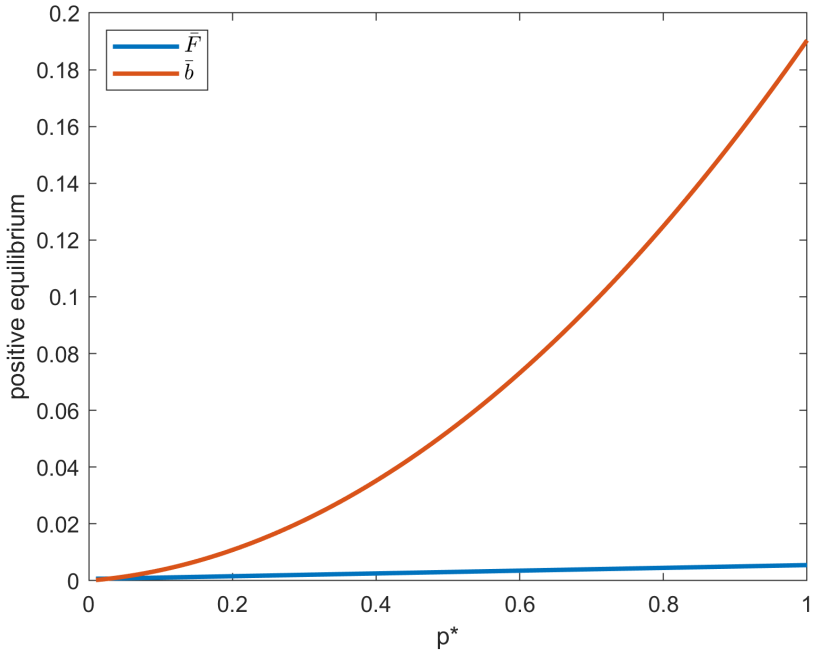

(a)

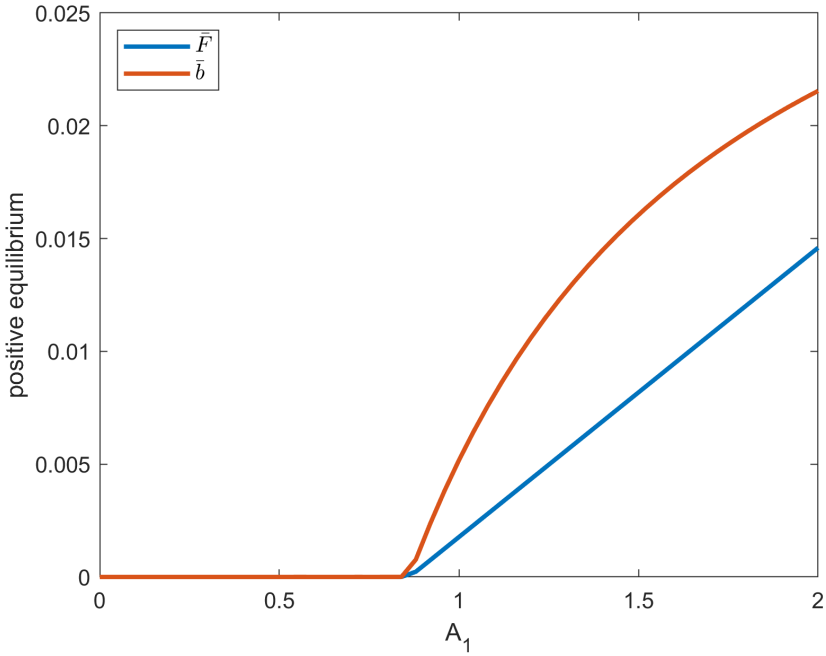

(b)

Figure 3.1: The numerical solution of the equilibrium point $(\bar{F}, \bar{b})$ for different values of: (a) p^* and (b) A_1, while the other parameter values are fixed.

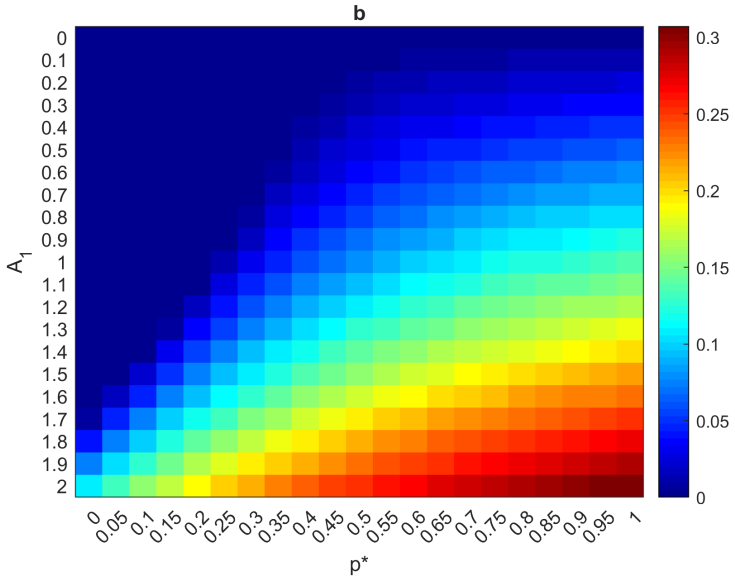

(a)

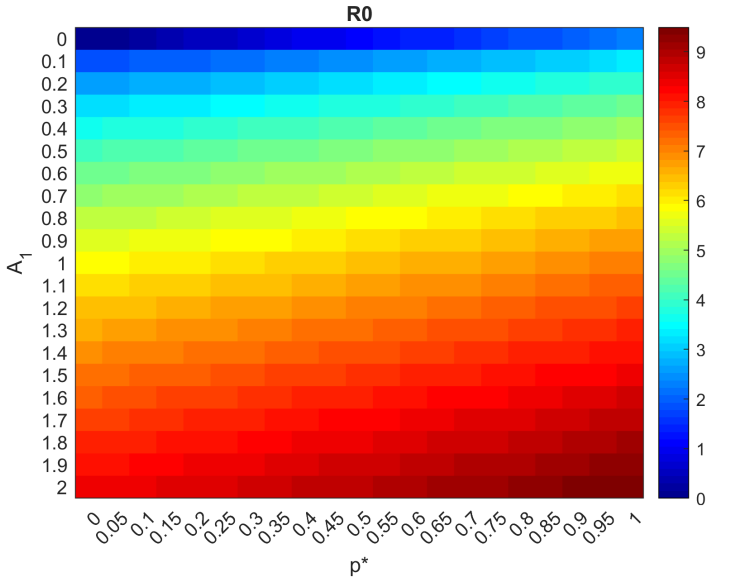

(b)

Figure 3.2: (a) Dependence of the positive equilibrium for the birth rate of infected newborn on the value of p^* and the values of $A_1 = \int_0^\infty e^{-\mu\tau} A(\tau) d\tau$, which reflects the contact rates and the infectivity of individuals in the population. (b) Dependence of the basic reproduction number on the value of p^* and the values of A_1.

Table 3.1: Definition of parameters and their values

Symbol	Description	Value (unit)	Reference
N	Total population	$[16 \times 10^6, 29 \times 10^6]$*	[126]
B	Birth rate	[0.01,0.02] (year^{-1})	[4]
μ	Death rate	[0.01,0.02] (year^{-1})	[4]
β^*	constant fertility rate	[0.01,0.02] (year^{-1})	Assumed
p^*	probability of producing infected offspring	[0,1]	Assumed
A_1		[0,2]	Assumed
A_2		[0,2]	Assumed

*Population of Malaysia between 1986-2011 based on [4].

3.4 Conclusions

The formulation of the vertically transmitted diseases using renewal equations with the general survival function, infectivity, and transmission probability from infected mothers to newborns, allows us to study and examine the dynamical behaviour of such diseases both analytically and numerically. A system of renewal equations for the force of infection and the fraction of infected newborns was developed in this chapter. The criteria for the existence and uniqueness of an endemic equilibrium was derived and the stability of the disease-free equilibrium was studied. A sensitivity analysis was performed for the special case with exponential survival function and constant values for the fertility function and the probability of producing of an infected newborn by an infected individual.

Further mathematical and numerical analyses are required to explore and evaluate the prevention and control approaches aiming at reducing the mother to child transmission, considering a more realistic function for $\beta(a)$ and $P(\tau)$ which can also include information on the effect of treatment on this probability.

3.5 A remark

The model in this chapter was formulated and studied in consultation with Professor Odo Diekmann and revised by Professor Jianhong Wu and Professor Neal Madras. This work was also

supported by the Fields-CQAM Laboratory of Mathematics for Public Health.

4 | Epidemic Dynamics of Vector-Transmitted Diseases and Vector Population Dynamics

Arthropods such as mosquitoes, sand flies, lice, and ticks are agents for the transmission of pathogens in many deadly diseases, known as vector-borne diseases. Malaria, for instance, causes more than 219 million cases and $400,000$ deaths every year [125]. These diseases can be controlled using different methods. Vector control has been used as a principle method using insecticides or some novel methods such as gene drive, Wolbachia, Spatial repellents and Eave tubes [128]. Understanding the long-term trends of vector-host interactions and vector population dynamics is crucial in the risk assessment of vector-borne diseases for humans and other hosts.

In this chapter, first we focus on the development of general models describing the dynamics of vector-borne diseases. We study a class of models for vector-transmitted diseases by analyzing the forces of infection formulated as a coupled system of renewal equations. We derive the basic reproduction number and a final size relation for closed vector and host populations. We extend the model to the case where both vector and host populations have demographic dynamics and derive the positive equilibrium and its local stability. The second part of this chapter is devoted to a stage-structured dynamical model of ticks responsible for a wide range of tick-borne diseases including Lyme diseases and tick-borne encephalitis.

4.1 Dynamics of vector-transmitted diseases

Suppose both host and vector populations are closed and there is no vertical transmission. Consider three cases: there is only one type of host with no host-to-host transmission; one host population with host-to-host transmission; and there are multiple host populations.

4.1.1 Epidemics: One type of host without host-to-host transmission

Let S_H and S_V denote the susceptible host and vector population, respectively. Let F_H be the force of infection imposed by the infected vectors on the susceptible hosts and F_V be the force

of infection imposed by infected hosts on the susceptible vectors and $A_H(\tau)$/$A_V(\tau)$ be the contribution to the force of infection by an infected vector/host ($F_H = F_{vh}$, $F_V = F_{hv}$, $A_H = A_{vh}$, $A_V = A_{hv}$).

The incidence in the host and vector populations are as follows

$$\begin{aligned} S'_H(t) &= -F_H(t)S_H(t) \\ S'_V(t) &= -F_V(t)S_V(t), \end{aligned} \tag{4.1}$$

and the forces of infection are given by the following coupled system of renewal equations:

$$\begin{aligned} F_H(t) &= \int_0^\infty S_V(t-\tau)F_V(t-\tau)A_H(\tau)d\tau \\ F_V(t) &= \int_0^\infty S_H(t-\tau)F_H(t-\tau)A_V(\tau)d\tau. \end{aligned} \tag{4.2}$$

The above system is a system of non-linear renewal equations for $F(t) = (F_H, F_v)^T$. Now we define the cumulative force of infection for F by $Y(t) = (y_H(t), y_V(t))^T = \int_{-\infty}^t F(\sigma)d\sigma$, and we get

$$\begin{aligned} y_H(t) &= \int_{-\infty}^t F_H(\sigma)d\sigma = \int_0^\infty S_V(-\infty)(1-e^{-y_V(t-\tau)})A_H(\tau)d\tau \\ y_V(t) &= \int_{-\infty}^t F_V(\sigma)d\sigma = \int_0^\infty S_H(-\infty)(1-e^{-y_H(t-\tau)})A_V(\tau)d\tau. \end{aligned}$$

Let $t \to \infty$, then

$$\begin{aligned} y_H(\infty) &= \int_0^\infty S_V(-\infty)(1-e^{-y_V(\infty)})A_H(\tau)d\tau \\ y_V(\infty) &= \int_0^\infty S_H(-\infty)(1-e^{-y_H(\infty)})A_V(\tau)d\tau. \end{aligned} \tag{4.3}$$

This system can be reduced to the following equation for $y_H(\infty)$

$$y_H(\infty) = S_V(-\infty)\int_0^\infty A_H(\tau)d\tau\Big(1-e^{-S_H(-\infty)\int_0^\infty A_V(\tau)d\tau(1-e^{-y_H(\infty)})}\Big)$$

equivalently $y_H(\infty) = g(y_H(\infty))$, where g is the right hand side of the above equation. The function g is monotone-increasing, sub-homogeneous, bounded function with $g(0) = 0$. There-

fore there exists a unique positive solution for $x = g(x)$, if and only if $g'(0) > 1$, i.e., if

$$\mathcal{R}_0 := S_V(-\infty) \int_0^\infty A_H(\tau) d\tau S_H(-\infty) \int_0^\infty A_V(\tau) d\tau > 1.$$

Note that solving System (4.4) gives the following equations

$$S_H(t) = S_H(-\infty) e^{-y_H(t)}$$
$$S_V(t) = S_V(-\infty) e^{-y_V(t)}$$

therefore, the existence of a unique positive steady state for $Y(\infty) = (y_H(\infty), y_V(\infty))^T$ for $\mathcal{R}_0 > 1$ means that there is an epidemic in the host and vector populations and the final sizes of the epidemic are given by the following relations:

$$\begin{cases} \ln \frac{S_H(-\infty)}{S_H(\infty)} & = S_V(-\infty) \int_0^\infty A_H(\tau) d\tau \big(1 - \frac{S_V(\infty)}{S_V(-\infty)}\big) \\ \\ \ln \frac{S_V(-\infty)}{S_V(\infty)} & = S_H(-\infty) \int_0^\infty A_V(\tau) d\tau \big(1 - \frac{S_H(\infty)}{S_H(-\infty)}\big) \end{cases}$$

Note that in most vector-borne diseases, the infected vectors do not recover (e.g., SI/SEI model). However, in a closed vector population, the function $A_H(\tau)$ for models without recovery is not integrable, i.e., $\int_0^\infty A_H(\tau) d\tau = \infty$ and therefore $\mathcal{R}_0 = \infty$, which yields that the disease free equilibrium is always unstable.

4.1.2 One type of host with host-to-host transmission

In this section F_H denotes the force of infection imposed by both infected vectors and hosts on the susceptible host population and F_V is same as before. Let $A_{vh}(\tau)$/$A_{hv}(\tau)$/A_{hh} be the contribution to the force of infection by an infected vector/host ($F_H = F_{vh} + F_{hh}$, $F_V = F_{hv}$). We assume there is no vector-to-vector transmission.

The incidence in the host and vector populations are as follows

$$\begin{aligned} S'_H(t) &= -F_H(t)S_H(t) \\ S'_V(t) &= -F_V(t)S_V(t), \end{aligned} \tag{4.4}$$

and the forces of infection are given by the following coupled system of renewal equations:

$$\begin{aligned} F_H(t) &= \int_0^\infty S_V(t-\tau)F_V(t-\tau)A_{vh}(\tau)d\tau + \int_0^\infty S_H(t-\tau)F_H(t-\tau)A_{hh}(\tau)d\tau \\ F_V(t) &= \int_0^\infty S_H(t-\tau)F_H(t-\tau)A_{hv}(\tau)d\tau. \end{aligned} \tag{4.5}$$

The the cumulative force of infection for F is therefore given by

$$\begin{aligned} y_H(t) &= \int_0^\infty S_V(-\infty)(1-e^{-y_V(t-\tau)})A_{vh}(\tau)d\tau + \int_0^\infty S_H(-\infty)(1-e^{-y_H(t-\tau)})A_{hh}(\tau)d\tau \\ y_V(t) &= \int_0^\infty S_H(-\infty)(1-e^{-y_H(t-\tau)})A_{hv}(\tau)d\tau. \end{aligned}$$

When $t \to \infty$ we have

$$\begin{aligned} y_H(\infty) &= S_V(-\infty)(1-e^{-y_V(\infty)})\int_0^\infty A_{vh}(\tau)d\tau + S_H(-\infty)(1-e^{-y_H(\infty)})\int_0^\infty A_{hh}(\tau)d\tau \\ y_V(\infty) &= S_H(-\infty)(1-e^{-y_H(\infty)})\int_0^\infty A_{hv}(\tau)d\tau. \end{aligned}$$

which is equivalent to

$$\begin{aligned} y_H(\infty) = S_V(-\infty)&\int_0^\infty A_{vh}(\tau)d\tau\Big(1-e^{-S_H(-\infty)\int_0^\infty A_{hv}(\tau)d\tau(1-e^{-y_H(\infty)})}\Big) \\ &+ S_H(-\infty)\int_0^\infty A_{hh}(\tau)d\tau\Big(1-e^{-y_H(\infty)}\Big). \end{aligned}$$

Let G denote the right hand side function. It can be shown that G is also a monotone-increasing, sub-homogeneous, bounded function with $G(0) = 0$. Therefore there exists a unique positive solution for $x = G(x)$, if and only if $G'(0) > 1$, which gives the basic reproduction number as

follows

$$\mathcal{R}_0 := S_V(-\infty)\int_0^\infty A_{vh}(\tau)d\tau S_H(-\infty)\int_0^\infty A_{hv}(\tau)d\tau + S_H(-\infty)\int_0^\infty A_{hh}(\tau)d\tau.$$

Using the same method given in the previous section we get the following final size relations

$$\begin{cases} \ln\frac{S_H(-\infty)}{S_H(\infty)} & = S_V(-\infty)\int_0^\infty A_{vh}(\tau)d\tau\big(1-\frac{S_V(\infty)}{S_V(-\infty)}\big) + S_H(-\infty)\int_0^\infty A_{hh}(\tau)d\tau\big(1-\frac{S_H(\infty)}{S_H(-\infty)}\big) \\ \ln\frac{S_V(-\infty)}{S_V(\infty)} & = S_H(-\infty)\int_0^\infty A_{hv}(\tau)d\tau\big(1-\frac{S_H(\infty)}{S_H(-\infty)}\big) \end{cases}$$

4.1.3 Multiple hosts without host-to-host transmission

Let $S_1, \cdots, S_n$ denote n types of host for a vector-borne disease (e.g., humans, mice and deer for tick-borne diseases) with one type of vector. Then the following system of renewal equations describe the forces of infection $F_1, \cdots, F_n$ for hosts and F_V for the vector

$$\begin{aligned} F_i(t) &= \int_0^\infty S_V(t-\tau)F_V(t-\tau)A_{vi}(\tau)d\tau, \quad i = 1, \cdots, n \\ F_V(t) &= \sum_{i=1}^n \int_0^\infty S_i(t-\tau)F_i(t-\tau)A_{iv}(\tau)d\tau, \end{aligned}$$

and the cumulative forces of infection satisfy

$$\begin{aligned} y_i(t) &= \int_0^\infty S_V(-\infty)(1-e^{-y_V(t-\tau)})A_{vi}(\tau)d\tau, \quad i = 1, \cdots, n \\ y_V(t) &= \sum_{i=1}^n \int_0^\infty S_i(-\infty)(1-e^{-y_i(t-\tau)})A_{iv}(\tau)d\tau. \end{aligned}$$

Let $t \to \infty$, then

$$\begin{aligned} y_i(\infty) &= S_V(-\infty)(1-e^{-y_V(\infty)})\int_0^\infty A_{vi}(\tau)d\tau, \quad i = 1, \cdots, n \\ y_V(\infty) &= \sum_{i=1}^n S_i(-\infty)(1-e^{-y_i(\infty)})\int_0^\infty A_{iv}(\tau)d\tau. \end{aligned}$$

Equivalently

$$y_V(\infty) = \sum_{i=1}^{n} S_i(-\infty)\Big(1 - e^{-S_V(-\infty)(1-e^{-y_V(\infty)})\int_0^\infty A_{vi}(\tau)d\tau}\Big)\int_0^\infty A_{iv}(\tau)d\tau.$$

Let $g(x)$ be the right hand side function in the above equation. It can be shown that g is a monotone increasing, sub-homogeneous and bounded function with $g(0) = 0$ and therefore the equation has a unique positive solution iff $g'(0) > 1$. Thus the basic reproduction number is as follows

$$\mathcal{R}_0 = \sum_{i=1}^{n} S_i(-\infty)\int_0^\infty A_{iv}(\tau)d\tau S_V(-\infty)\int_0^\infty A_{vi}(\tau)d\tau.$$

4.1.4 Endemic Vector-Transmitted Diseases

In this section, we assume that both host and vector populations have demographic dynamics without migration and vertical transmission. Suppose constant birth rates B_H and B_V and general survival functions $\mathcal{F}_H(a)$ and $\mathcal{F}_H(a)$ for the host and vector populations. Using the notations from the previous section for forces of infection we have the following system of equations

$$\begin{aligned} F_H(t) &= \int_0^\infty F_V(t-\tau)B_V\int_0^\infty e^{-\int_0^a F_V(t-\tau-a+\sigma)d\sigma}\mathcal{F}_V(a+\tau)daA_H(\tau)d\tau \\ F_V(t) &= \int_0^\infty F_H(t-\tau)B_H\int_0^\infty e^{-\int_0^a F_H(t-\tau-a+\sigma)d\sigma}\mathcal{F}_H(a+\tau)daA_V(\tau)d\tau \end{aligned} \tag{4.6}$$

It is clear that $F_H = 0$ and $F_V = 0$ is a solution to the above system. Let $\bar{F}_H$ and $\bar{F}_V$ be the positive equilibrium for F_H and F_V, respectively. Then

$$\begin{aligned} \bar{F}_H &= B_V\bar{F}_V\int_0^\infty\int_0^\infty e^{-\bar{F}_V a}\mathcal{F}_V(a+\tau)daA_H(\tau)d\tau \\ \bar{F}_V &= B_H\bar{F}_H\int_0^\infty\int_0^\infty e^{-\bar{F}_H a}\mathcal{F}_H(a+\tau)daA_V(\tau)d\tau \end{aligned}$$

Substituting $\bar{F}_H$ from the first equation in the second we get the following equation for $\bar{F}_V$:

$$\begin{aligned} 1 =& B_H B_V \int_0^\infty \int_0^\infty e^{-\bar{F}_V s} \mathcal{F}_V(s+u) ds A_H(u) du \\ & \int_0^\infty \int_0^\infty e^{-\left(B_V \bar{F}_V \int_0^\infty \int_0^\infty e^{-\bar{F}_V s} \mathcal{F}_V(s+u) ds A_H(u) du\right) a} \mathcal{F}_H(a+\tau) da A_V(\tau) d\tau \end{aligned} \tag{4.7}$$

Note that the the right hand side function is a monotonically decreasing function of $\bar{F}_V$, since all integrands are positive. Therefore, there is a positive solution to the above equation if and only if

$$\mathcal{R}_0 := B_H B_V \int_0^\infty \int_0^\infty \mathcal{F}_V(a+\tau) da A_H(\tau) d\tau \int_0^\infty \int_0^\infty \mathcal{F}_H(a+\tau) da A_V(\tau) d\tau > 1. \tag{4.8}$$

This expression of $\mathcal{R}_0$ can be interpreted as the number of vectors that become infected by a an infected host during the infectious period multiplied by the number of infected hosts by an infected vector. Also, the transmission in vector-borne diseases can be considered as two generations, i.e., from host to vector to host, as well as one generation [17]. The above formula for the basic reproduction number considers the transmission as one generation. If we consider two generations, i.e., consider the number of infected hosts as a result of host to vector and then vector to host transmission, then the basic reproduction number would be the square root of the left hand side in (4.8).

The basic reproduction of vector-borne diseases, as described in [64], can be given by $\int_0^\infty b(a)\mathfrak{F}(a)da$, where a denotes the age of infection and b and $\mathfrak{F}$ are as defined in Chapter 1. In this case, $b(a)$ would be the average number of hosts infected by an infected vector of age of infection a, and $\mathfrak{F}(a)$ can be defined as follows

$$\begin{aligned} \mathfrak{F}(a) = \int_0^a & \text{ Probability (host infected at time 0 exists at time s)} \\ & \times \text{ Probability (host infected for total time s infects vectors)} \\ & \times \text{ Probability (infected vector lives to be age a-s)} dt \end{aligned} \tag{4.9}$$

This will yield the basic reproduction number as the average number of newly infected hosts as opposed to the basic reproduction umber defined by (4.8).

Stability of the positive equilibrium

In this part, we provide the stability analysis of the positive equilibrium $(\bar{F}_H, \bar{F}_V)$ using the linearization principal for system of renewal equations. First we linearize the system (4.6) for the general survival functions. Then we consider the special case of exponential survival function for both host and vector populations with constant death rates μ_H and μ_V, respectively.

The linearized system is as follows

$$\begin{aligned} u(t) &= B_V \int_0^\infty v(t-\tau) \int_0^\infty e^{-\bar{F}_V a} \mathcal{F}_V(a+\tau) da A_H(\tau) d\tau \\ &\quad - B_V \bar{F}_V \int_0^\infty \int_0^\infty e^{-\bar{F}_V a} \mathcal{F}_V(a+\tau) \int_0^a v(t-\tau-a+\sigma) d\sigma da A_H(\tau) d\tau \\ v(t) &= B_H \int_0^\infty u(t-\tau) \int_0^\infty e^{-\bar{F}_H a} \mathcal{F}_H(a+\tau) da A_V(\tau) d\tau \\ &\quad - B_H \bar{F}_H \int_0^\infty \int_0^\infty e^{-\bar{F}_H a} \mathcal{F}_H(a+\tau) \int_0^a u(t-\tau-a+\sigma) d\sigma da A_V(\tau) d\tau \end{aligned} \tag{4.10}$$

Suppose the solutions of the linear System (4.10) are of the exponential form $u(t) = c_u e^{\lambda t}$ and $v(t) = c_v e^{\lambda t}$, then (c_u, c_v) satisfy the following system of equations

$$\begin{aligned} c_u &= \Big(B_V \int_0^\infty e^{-\lambda\tau} \int_0^\infty e^{-\bar{F}_V a} \mathcal{F}_V(a+\tau) da A_H(\tau) d\tau \\ &\quad - B_V \bar{F}_V \int_0^\infty \int_0^\infty e^{-\bar{F}_V a} \mathcal{F}_V(a+\tau) \int_0^a e^{-\lambda\tau} e^{-\lambda a} e^{\lambda\sigma} d\sigma da A_H(\tau) d\tau \Big) c_v \end{aligned}$$

$$\begin{aligned} c_v &= \Big(B_H \int_0^\infty e^{-\lambda\tau} \int_0^\infty e^{-\bar{F}_H a} \mathcal{F}_H(a+\tau) da A_H(\tau) d\tau \\ &\quad - B_H \bar{F}_H \int_0^\infty \int_0^\infty e^{-\bar{F}_H a} \mathcal{F}_H(a+\tau) \int_0^a e^{-\lambda\tau} e^{-\lambda a} e^{\lambda\sigma} d\sigma da A_V(\tau) d\tau \Big) c_u \end{aligned}$$

This system has a unique, nontrivial solution for (c_u, c_v) iff λ satisfies the following characteristic

equation

$$
\begin{aligned}
B_H B_V \Big(& \int_0^\infty e^{-\lambda\tau} \int_0^\infty e^{-\bar{F}_V a} \mathcal{F}_V(a+\tau) da A_H(\tau) d\tau \\
& - \bar{F}_V \int_0^\infty \int_0^\infty e^{-\bar{F}_V a} \mathcal{F}_V(a+\tau) e^{-\lambda(a+\tau)} \frac{(e^{\lambda a}-1)}{\lambda} da A_H(\tau) d\tau \Big) \\
& \Big(\int_0^\infty e^{-\lambda\tau} \int_0^\infty e^{-\bar{F}_H a} \mathcal{F}_H(a+\tau) da A_H(\tau) d\tau \\
& - \bar{F}_H \int_0^\infty \int_0^\infty e^{-\bar{F}_H a} \mathcal{F}_H(a+\tau) \int_0^a e^{-\lambda(a+\tau)} \frac{(e^{\lambda a}-1)}{\lambda} da A_V(\tau) d\tau \Big) = 1.
\end{aligned}
\tag{4.11}
$$

Substituting $\mathcal{F}_H(a) = e^{-\mu_H a}$ and $\mathcal{F}_V(a) = e^{-\mu_V a}$, and using the Laplace transform of a function A, defined by $\bar{A}(z) = \int_0^\infty e^{-zu} A(u) du$ the above equation takes the following form:

$$
\begin{aligned}
B_H B_V & \left(\frac{\bar{A}_H(\lambda+\mu_V)}{\bar{F}_V+\mu_V} - \frac{\bar{F}_V \bar{A}_H(\lambda+\mu_V)}{\lambda} \big(\frac{1}{\bar{F}_V+\mu_V} - \frac{1}{\bar{F}_V+\mu_V+\lambda} \big) \right) \\
& \left(\frac{\bar{A}_V(\lambda+\mu_H)}{\bar{F}_H+\mu_H} - \frac{\bar{F}_H \bar{A}_V(\lambda+\mu_H)}{\lambda} \big(\frac{1}{\bar{F}_H+\mu_H} - \frac{1}{\bar{F}_H+\mu_H+\lambda} \big) \right) = 1
\end{aligned}
\tag{4.12}
$$

Note that in this case the basic reproduction number is

$$
\mathcal{R}_0 = \frac{B_H B_V}{\mu_H \mu_V} \bar{A}_H(\mu_V) \bar{A}_V(\mu_H)
$$

and the equilibrium point $(\bar{F}_H, \bar{F}_V)$ is as follows

$$
\bar{F}_H = \frac{B_V \bar{F}_V}{\bar{F}_V+\mu_V} \bar{A}_H(\mu_V), \quad \bar{F}_V = \frac{B_H B_V \bar{A}_H(\mu_V) \bar{A}_V(\mu_H) - \mu_H \mu_V}{B_V \bar{A}_H(\mu_V) + \mu_H}. \tag{4.13}
$$

Theorem 4.1. *Consider System* (4.6)*. If* $\mathcal{R}_0 > 1$*, then the positive equilibrium given by* (4.13) *is locally asymptotically stable.*

Proof. Suppose $\mathcal{R}_0 > 1$. We show that all roots of the characteristic equation (4.12) have negative real part. Let λ be a characteristic root with $\mathfrak{Re}(\lambda) \geq 0$. Then

$$|\bar{A}_H(\lambda+\mu_V)| \leq \bar{A}_H(\mathfrak{Re}(\lambda)+\mu_V) \leq \bar{A}_H(\mu_V),$$
$$|\bar{A}_V(\lambda+\mu_H)| \leq \bar{A}V(\mathfrak{Re}(\lambda)+\mu_H) \leq \bar{A}_V(\mu_H).$$

We can rewrite (4.13) to get the following

$$\bar{F}_H = \frac{(\mathcal{R}_0-1)\mu_H\mu_V}{B_H\bar{A}_V(\mu_H)+\mu_V}, \quad \bar{F}_V = \frac{(\mathcal{R}_0-1)\mu_H\mu_V}{B_V\bar{A}_H(\mu_V)+\mu_H}. \tag{4.14}$$

Now we can show that absolute value of the left hand side of (4.12) is strictly less than 1. First note that the left hand side of (4.12) can be written as follows

$$B_HB_V\left(\frac{\bar{A}_H(\lambda+\mu_V)(\mu_V+\lambda)}{(\bar{F}_V+\mu_V)(\bar{F}_V+\mu_V+\lambda)}\right)\left(\frac{\bar{A}_V(\lambda+\mu_H)(\mu_H+\lambda)}{(\bar{F}_H+\mu_H)(\bar{F}_H+\mu_H+\lambda)}\right) \tag{4.15}$$

Substituting $\bar{F}_H$ and $\bar{F}_V$ from (4.14) we have

$$|\frac{\mu_V+\lambda}{\bar{F}_V+\mu_V+\lambda}| = \frac{\sqrt{(\mu_V+\mathfrak{Re}(\lambda))^2+\mathfrak{Im}(\lambda)^2}}{\sqrt{(\mu_V\frac{\mathcal{R}_0\mu_H+B_V\bar{A}_H(\mu_V)}{\mu_H+B_V\bar{A}_H(\mu_V)}+\mathfrak{Re}(\lambda))^2+\mathfrak{Im}(\lambda)^2}} < 1,$$

$$|\frac{\mu_H+\lambda}{\bar{F}_H+\mu_H+\lambda}| = \frac{\sqrt{(\mu_H+\mathfrak{Re}(\lambda))^2+\mathfrak{Im}(\lambda)^2}}{\sqrt{(\mu_H\frac{\mathcal{R}_0\mu_V+B_H\bar{A}_V(\mu_H)}{\mu_V+B_H\bar{A}_V(\mu_H)}+\mathfrak{Re}(\lambda))^2+\mathfrak{Im}(\lambda)^2}} < 1$$

since $\mathcal{R}_0 > 1$. We can also show that

$$|B_H\frac{\bar{A}_H(\lambda+\mu_V)}{\bar{F}_V+\mu_V}| < 1 \quad \text{and} \quad |B_V\frac{\bar{A}_V(\lambda+\mu_H)}{\bar{F}_H+\mu_H}| < 1.$$

This completes the proof.

4.1.5 Discussion

The results of this section can be applied to many vector-transmitted diseases: 1) the host population has stabilized at an equilibrium and the disease dynamics is faster than the vector population

dynamics; 2) both host and vector populations have a constant birth rate and a negative exponential survival probability. In the second case, vertical transmission can be incorporated for the host and vector. A stage-structured population model of the vector will be required for a more rigorous study of the impact of vector-host interactions during different stages of vector life cycle, on the disease dynamics. The next section focuses on some of these vector-host interactions, in the absence of a disease, and their impact on the vector population dynamics.

4.2 Modeling the Impact of Host Resistance on Structured Tick Population Dynamics

Background and Motivation

Lyme Disease is the most reported athropod-borne illness and it was first recognized in 1976 in Lyme, Connecticut, USA [111]. *Borrelia burgdorferi* is a tick-borne spirochete responsible for Lyme disease which is found in nymphal *Ixodes dammini* and has the highest chance to be transmitted to the host if the infected tick feeds for a duration of 72 hours or more [99, 112, 69]. Once an infected tick bites the host, a skin lesion called erythema migrans (EM) starts emerging and more than 95% of those patients diagnosed with Lyme disease have EM on the tick biting site [52, 111]. Once the bacterium enters the body it starts spreading in many organs and tissues through the lymph system and blood [52]. As time progresses the patient will experience headache, neck pain, fever, fatigue, and migratory musculoskeletal pain [112, 69, 52]. The government of Canada has data representing an increase from 144 cases in 2009 to 2025 cases in 2017 [91]. The *I.scopularis* also known as a black-legged tick is the main carrier of *B. burgdorferi* and has a life cycle of nearly two years [111]. The tick population undergoes three main stages: L-larvae, N-nymph, A-adult and to move from one stage to the other ticks will quest (i.e., search for hosts to attach to), feed and molt [82, 130, 101, 102]. Larvae and nymph feed on small rodents such as mice while adult ticks are more selective when it comes to their host since their body is larger compared to larvae and nymph and therefore the host must be a large mammal such as a deer. For ticks to move from one stage to the next it requires three hosts per stage and often the

tick may use the same host for all three blood meals [82, 130, 101, 102]. Female ticks lay eggs in the spring and larvae hatch during late summer. The larvae that feeds during the late summer starts molting to nymph during winter. The nymph then starts feeding in the spring of the following year and molts into adult on the same year. Adult ticks die shortly right after they lay their eggs in the early spring [130, 101].

When a tick bites a host the expression of immunity varies depending on different hosts and tick species.The effects on ticks can vary from a simple rejection of the tick to interfering with the duration of feeding, inhibition of egg laying, also decreasing their viability to death of the tick while feeding. In addition, studies reveal that when female ticks feed on immune cattle their body of fully engorged tick was reduced by 30% [80, 119, 13]. According to Brown [67] hosts with resistance respond to tick bites with an intensified *grooming behaviour* and the attachment site is marked by serous exudes which could engulf the tick. In an experiment conducted on resistant guinea pigs bitten by Dermacentor andersoni, basophilia is present on the biting site. The attachment of a tick on a tick-sensitized host is characterized by packs of basophils located in the intraepidermal vesicles. When ticks' extracts are injected into tick-sensitized host it causes a skin reaction and the plasma of the host expresses anti-tick antibodies which suggests a present mediated immune response. In case of unbitten animals, the reaction starts with neutrophils and the feeding site is characterized by an hemorrhage as feeding progresses. Basophils start to also accumulate to the feeding site, however little degranulation occurs. In an experiment to study the effect of resistance of guinea pigs to ticks, basophil degranulation at tick feeding sites, resulted in tick rejection after tick-attachment: 29% after 6 hours, 18% after 12 hours, 22% after 24 hours, 37% after 48 hours and 7.3% after 72 and 96 hours. This shows that ticks are most susceptible to the resistance at 6, 12, 24 and 48 hours after attachment which are corresponding to the attachment time and rapid feeding period [26].

There have been intensive studies modelling the dynamics of tick-host interaction and the transmission of various pathogens. Different aspects have also been included such as: seasonality , environmental changes, geographical heterogeneity and so on. On the other hand, few models incorporate delays in the development of tick from each life stage to the next [54, 120, 131].

Jennings et al. [68] studied the effect of host resistance on tick population dynamics. They developed a mathematical model, described by a system of ordinary differential equations, focusing on tick-host interaction where the tick's life cycle was divided into two main stages, adult and juvenile, and the host was subdivided into host with no immunity and host with immunity. Their focus is to show how immunity affects the extinction or persistence of tick dynamics. However, their model does not include all biological stages (and sub-stages) of ticks and the possibility of different immunological response for each stage is ignored.

Here, we consider a stage-structured model that involves the full biological dynamics of tick and the emphasis is on the grooming behaviour of the host, and its impact on tick population dynamics. We analyze the grooming behaviour in the mathematical model as a reduction in the successful attachment rates of ticks on the host i.e., the host-finding rates are reduced by a fraction for the host that shows resistance to tick bites. The model includes three main stages of tick's life cycle in which the ticks interact with hosts during questing-feeding-molting process. There is one more stage that we consider between Adult and Egg which is egg laying female. The host is divided into two compartments: host with resistance (host has been bitten by ticks before) and host with no resistance (host that has not been exposed to ticks). We observe that the basic reproduction number does not change with the resistance factor, however, numerical simulations show that the value of the positive equilibrium for different stages of tick population, and the dynamical behaviour of the solutions change with varying the resistance factor. Also, the sensitivity analysis demonstrates the dependence of the solutions on different parameters.

4.2.1 The Model Formulation

We start the model aiming to focus on the grooming behaviour. We model the three stages of larvae, nymph, and adult. The larvae and nymph populations are subdivided into questing, feeding and molting. On the other hand, for the adult population we consider adult egg laying female A_{elf}, adult questing (A_q) and feeding (A_f). Since a single female tick lays several thousands eggs the birth rate is the entry into population which is represented by Ricker function, $\gamma(A) = pAe^{-qA}$ [104, 95]. Tick dynamics are regulated by insufficient resources for blood meal and this is illustrated in parameter q.

Table 4.1: Definition of Variables and their initial values

Symbol	Meaning	Initial value
L_q	Number of questing larvae	$L_{q_0} = 1 \times 10^6$
L_f	Number of feeding larvae	$L_{f_0}(\theta) = 0, -\tau_{(E,L)} \leq \theta \leq 0$
L_m	Number of molting larvae	
N_q	Number of questing nymph	$N_{q_0} = 0$
N_f	Number of feeding nymph	$N_{f_0}(\theta) = 0, -\tau_{(L,N)} \leq \theta \leq 0$
N_m	Number of molting nymph	
A_q	Number of questing adult	$A_{q_0} = 0$
A_f	Number of feeding adult	$A_{f_0} = 0$
A_{elf}	Number of egg laying female adult	$A_{elf_0}(\theta) = 0, -\tau_{(N,A)} \leq \theta \leq 0$
E	Number of eggs	
H	Number of hosts	
H_{r+}	Number of hosts with resistance	$H_{r+} = 0$
H_{r-}	Number of host with no resistance	

Table 4.2: Definition of parameters and their values

Symbol	Meaning	Value	Reference
d^{L_q}	Per capita mortality rate of L_q	0.6×10^{-2} per day	[95]
d^{L_m}	Per capita mortality rate of L_m	0.3×10^{-2} per day	[95]
d^{N_q}	Per capita mortality rate of N_q	0.6×10^{-2} per day	[95]
d^{N_m}	Per capita mortality rate of N_m	0.2×10^{-2} per day	[95]
d^{A_q}	Per capita mortality rate of A_q	0.6×10^{-2} per day	[95]
$d^{A_{elf}}$	Per capita mortality rate of A_{elf}	1 per day	[132]
d^{E}	Per capita mortality rate of E	0.2×10^{-2} per day	[95]
β_L	Successful attachment rate of questing larva to host	0.6×10^{-3} per day per host	[79]
β_N	Successful attachment rate of questing nymph to host	0.6×10^{-3} per day per host	[79]
β_A	Successful attachment rate of questing adult to host	0.2×10^{-2} per day per host	[79]
β_L^*	Rate of developing resistance to larva	$\kappa \times \beta_L$ per day per tick	Calculated
β_N^*	Rate of developing resistance to nymph	$\kappa \times \beta_N$ per day per tick	Calculated
β_A^*	Rate of developing resistance to adult	$\kappa \times \beta_A$ per day per tick	Calculated
δ	Detachment rate	0.01 per day	[103]
α_L	Host grooming effect for larva	0.4, $[0, 1]$ unitless	Assumed
α_N	Host grooming effect for nymph	0.6, $[0, 1]$ unitless	Assumed
α_A	Host grooming effect for adult	0.5, $[0, 1]$ unitless	Assumed
ϵ	Female proportion	0.5 unitless	[57]
$\tau_{(E,L)}$	The delay of development form egg to larvae	21 days	[95]
$\tau_{(L,N)}$	The delay of development form larvae to nymph	$101.18 \times Temp^{-2.25}$, 200 days	[95]
$\tau_{(N,A)}$	The delay of development form nymph to adult	$1596 \times Temp^{-1.21}$, 61 days	[95]
b	Birth rate of the host	0.66×10^{-3} per day	[120]
μ	Death rate of the host	0.33×10^{-3} per day	[120]
c	Crowding	3.5×10^{-4} per day	Calculated
K	Carrying Capacity of deers	20	[95]
p	Maximum number of eggs per female adult tick	3000	[95]
q	The strength of density dependence	0.001 unitless	[104]
κ	Constant factor for resistance development	0.0001 unitless	Assumed

Table 4.3: Modified parameter values to get different values for $\mathcal{R}_0$

Symbol	Modified Value	Comments
d^E	$1.2 \times 0.2 \times 10^{-2}$	p+20%p
d^{L_q}	$1.2 \times 0.6 \times 10^{-2}$	p+20%p
d^{L_m}	$1.2 \times 0.3 \times 10^{-2}$	p+20%p
d^{N_q}	$1.2 \times 0.6 \times 10^{-2}$	p+20%p
d^{N_m}	$1.2 \times 0.2 \times 10^{-2}$	p+20%p
d^{A_q}	$1.2 \times 0.6 \times 10^{-2}$	p+20%p
β_L	$0.1 \times 0.6 \times 10^{-3}$, $0.2 \times 0.6 \times 10^{-3}$	$10\%p, 20\%p$
β_N	$0.3 \times 0.6 \times 10^{-3}$, $0.5 \times 0.6 \times 10^{-3}$	$30\%p, 50\%p$
β_A	$0.5 \times 0.2 \times 10^{-2}$	50%p fixed
β_L^*	$\kappa \times \beta_L$	changed by changing β_L
β_N^*	$\kappa \times \beta_N$	changed by changing β_N
β_A^*	$\kappa \times \beta_A$	changed by changing β_A
α_L	0.4	varied in $[0, 1]$
α_N	0.6	varied in $[0, 1]$
α_A	0.5	varied in $[0, 1]$
c	$1.2 \times 3.5 \times 10^{-4}$	$p + 20\%p$ fixed
q	0.001	not changed

The delay functions, demonstrating the time delays of ticks molting from one stage to another, are constants. In the model, $\tau_{(E,L)}$, $\tau_{(L,N)}$, $\tau_{(N,A)}$ represent the time it takes for ticks to molt from egg to larvae, larvae to nymph and nymph to adult, respectively. The host population is divided into two compartments: H_{r+} represents the bitten host compartment that have developed with immunity; H_{r-} represents the compartment of hosts that have never been bitten before and therefore without immunity. H is the total host population with a birth rate b and a mortality rate μ. The density-dependent regulations of the host population is described by K, c, and $b - \mu$. The variables and parameters and their meaning are given in Tables 4.1 and 4.2. We suppose the successful attachment rates are reduced by a fraction α_L for larvea, α_N for nymph and α_A for adult ticks. Based on the results from [26] we can assume that α is in the range $[0.6, 0.95]$, however we will study the effect of α values in $[0, 1]$. We also assume the hosts with no resistance develop resistance to ticks at a rate, denoted by κ, that depends on the tick densities, tick attachment rates and the immune system response.

In order to make the model comprehensible we neglect few biological factors of tick dynamics. There are multiple blood meals that take place during molting procedures however in our model we consider only a homogeneous molting process, that is, ticks feed once, drop and molt with a constant time delay. The death rate depends on the stage of the tick (egg, larvae, nymph, adult) and also on whether the tick is questing or feeding. However, we consider a constant mortality rate. Impact of climate change on development of ticks having a nonlinear relationship with increasing ambient temperature has not also been modelled. In addition, the ticks' attachment rate is considered constant, even though it decreases as the temperatures and the day light decreases.

The model is described by the following system of delay differential equations:

$$\begin{aligned}
\frac{dL_q}{dt} &= e^{-d^E\tau_{(E,L)}}\gamma(A_{elf}(t-\tau_{(E,L)})) - \beta_L L_q(t)(\alpha_L H_{r+}(t) + H_{r-}(t)) - d^{L_q}L_q(t)\\
\frac{dL_f}{dt} &= \beta_L L_q(t)(\alpha_L H_{r+}(t) + H_{r-}(t)) - \delta L_f(t)\\
\frac{dL_m}{dt} &= \delta L_f(t) - d^{L_m}L_m(t) - \delta\psi e^{-d^{L_m}\tau_{(L,N)}}L_f(t-\tau_{(L,N)})\\
\frac{dN_q}{dt} &= \delta\psi e^{-d^{L_m}\tau_{(L,N)}}L_f(t-\tau_{(L,N)}) - \beta_N N_q(t)(\alpha_N H_{r+}(t) + H_{r-}(t)) - d^{N_q}N_q(t)\\
\frac{dN_f}{dt} &= \beta_N N_q(t)(\alpha_N H_{r+}(t) + H_{r-}(t)) - \delta N_f(t)\\
\frac{dN_m}{dt} &= \delta N_f(t) - d^{N_m}N_m(t) - \delta\psi e^{-d^{N_m}\tau_{(N,A)}}N_f(t-\tau_{(N,A)})\\
\frac{dA_q}{dt} &= \delta\psi e^{-d^{N_m}\tau_{(N,A)}}N_f(t-\tau_{(N,A)}) - \beta_A A_q(t)(\alpha_A H_{r+}(t) + H_{r-}(t)) - d^{A_q}A_q(t)\\
\frac{dA_f}{dt} &= \beta_A A_q(t)(\alpha_A H_{r+}(t) + H_{r-}(t)) - \delta A_f(t)\\
\frac{dA_{elf}}{dt} &= \varepsilon\delta A_f(t) - d^{A_{elf}}A_{elf}(t)\\
\frac{dE}{dt} &= \gamma(A_{elf}(t)) - d^E E(t) - e^{-d^E\tau_{(E,L)}}\gamma(A_{elf}(t-\tau_{(E,L)}))\\
\frac{dH_{r-}}{dt} &= bH(t) - \mu H_{r-}(t) - \frac{c}{K}H(t)H_{r-}(t) - (\beta_L^* L_q(t) + \beta_N^* N_q(t) + \beta_A^* A_q(t))H_{r-}(t)\\
\frac{dH_{r+}}{dt} &= -\mu H_{r+}(t) - \frac{c}{K}H(t)H_{r+}(t) + (\beta_L^* L_q(t) + \beta_N^* N_q(t) + \beta_A^* A_q(t))H_{r-}(t)
\end{aligned} \tag{4.16}$$

where $\gamma(A) = pAe^{-qA}$ is the birth function. Here, we use the following equation for the host population dynamics

$$\frac{dH(t)}{dt} = (b-\mu)H(t) - \frac{c}{K}(H(t))^2 \tag{4.17}$$

where $H(t) = H_{r-}(t) + H_{r+}(t)$. Note that the positive equilibrium of this equation is given by $\bar{H} = \frac{(b-\mu)}{c}K$. Interpreting K as an environmental constraint, and in order to have $\bar{H} \leq K$ we assume $c \geq (b-\mu)$, with $\bar{H} = K$ when the equality holds.

From System (4.16) we can get the following integral equations for $L_m(t)$, $N_m(t)$ and $E(t)$

$$\begin{aligned}
L_m(t) &= L_m(0) - \int_{-\tau_{(L,N)}}^{0} e^{-d^{L_m}(-s)}\delta L_f(s)ds + \int_{t-\tau_{(L,N)}}^{t} e^{-d^{L_m}(t-s)}\delta L_f(s)ds \\
N_m(t) &= N_m(0) - \int_{-\tau_{(N,A)}}^{0} e^{-d^{N_m}(-s)}\delta N_f(s)ds + \int_{t-\tau_{(N,A)}}^{t} e^{-d^{N_m}(t-s)}\delta N_f(s)ds \\
E(t) &= E(0) - \int_{-\tau_{(E,L)}}^{0} e^{-d^{E}(-s)}\gamma(A_{elf}(s))ds + \int_{t-\tau_{(E,L)}}^{t} e^{-d^{E}(t-s)}\gamma(A_{elf}(s))ds
\end{aligned} \tag{4.18}$$

Therefore System (4.16) is equivalent to the following

$$\begin{aligned}
\frac{dL_q}{dt} &= e^{-d^E\tau_{(E,L)}}\gamma(A_{elf}(t-\tau_{(E,L)})) - \beta_L L_q(t)(\alpha_L H_{r+}(t) + H_{r-}(t)) - d^{L_q}L_q(t) \\
\frac{dL_f}{dt} &= \beta_L L_q(t)(\alpha_L H_{r+}(t) + H_{r-}(t)) - \delta L_f(t) \\
\frac{dN_q}{dt} &= \delta\psi e^{-d^{L_m}\tau_{(L,N)}}L_f(t-\tau_{(L,N)}) - \beta_N N_q(t)(\alpha_N H_{r+}(t) + H_{r-}(t)) - d^{N_q}N_q(t) \\
\frac{dN_f}{dt} &= \beta_N N_q(t)(\alpha_N H_{r+}(t) + H_{r-}(t)) - \delta N_f(t) \\
\frac{dA_q}{dt} &= \delta\psi e^{-d^{N_m}\tau_{(N,A)}}N_f(t-\tau_{(N,A)}) - \beta_A A_q(t)(\alpha_A H_{r+}(t) + H_{r-}(t)) - d^{A_q}A_q(t) \\
\frac{dA_f}{dt} &= \beta_A A_q(t)(\alpha_A H_{r+}(t) + H_{r-}(t)) - \delta A_f(t) \\
\frac{dA_{elf}}{dt} &= \varepsilon\delta A_f(t) - d^{A_{elf}}A_{elf}(t) \\
\frac{dH_{r-}}{dt} &= bH(t) - \mu H_{r-}(t) - \frac{c}{K}H(t)H_{r-}(t) - (\beta_L^* L_q(t) + \beta_N^* N_q(t) + \beta_A^* A_q(t))H_{r-}(t) \\
\frac{dH_{r+}}{dt} &= -\mu H_{r+}(t) - \frac{c}{K}H(t)H_{r+}(t) + (\beta_L^* L_q(t) + \beta_N^* N_q(t) + \beta_A^* A_q(t))H_{r-}(t)
\end{aligned} \tag{4.19}$$

together with (4.18).

For further analyses of this model we use the theory of monotone dynamical systems [109]. Let $\tau = (\tau_1, \cdots, \tau_{12})$ where $\tau_i \geq 0$, $\tau_2 = \tau_{(L,N)}$, $\tau_5 = \tau_{(N,A)}$), $\tau_9 = \tau_{(E,L)}$ are non zero and $\tau_i = 0$ for $i \neq 2, 5, 9$. Assume $|\tau| = \max\{\tau_i\}$.

Let C_τ be the product of Banach spaces $C_{\tau_i} = C([-\tau_i, 0], \mathbb{R})$, i.e.,

$$C_\tau = \prod_{i=1}^{12} C([-\tau_i, 0], \mathbb{R}).$$

Let $X_t = (X_t^1, \cdots, X_t^{12}) \in C_\tau$ be given by

$$X_t^i(\theta) = X^i(t+\theta), \quad i = 1, \cdots, 12.$$

where

$$X(t) = (X^1(t), \cdots, X^{12}(t)) = (L_q, L_f, L_m, N_q, N_f, N_m, A_q, A_f, A_{elf}, E, H_{r-}, H_{r+}).$$

Then the right hand side of the Equation (4.16) is given by

$$X'(t) = f(X_t). \tag{4.20}$$

We assume the initial data is non-negative. So we will assume the initial data X_0 is in the Banach space C_τ^+ defined below

$$C_\tau^+ = \{\phi \in C_\tau : \phi_i(\theta) \geq 0, -\tau_i \leq \theta \leq 0\}.$$

Also, for the initial data to be continuous and positive we assume:

$$\begin{aligned} L_m(0) &\geq \int_{-\tau_{(L,N)}}^0 e^{-d^{L_m}(-s)} \delta L_f(s) ds \\ N_m(0) &\geq \int_{-\tau_{(N,A)}}^0 e^{-d^{N_m}(-s)} \delta N_f(s) ds \\ E(0) &\geq \int_{-\tau_{(E,L)}}^0 e^{-d^E(-s)} \gamma(A_{elf}(s)) ds. \end{aligned} \tag{4.21}$$

The fundamental theory of functional differential equations implies that the solutions exist and are unique for all $t \geq 0$. We now show that the solutions will be positive and remain bounded.

Theorem 4.2. *Let $X^i(0) > 0$ and $X^i(\theta) \geq 0$ for $-\tau_i \leq \theta < 0$, for $i = 1, \cdots, 12$. Then the solutions to the System* (4.19) *are positive and bounded for all $t \geq 0$.*

Proof. Consider the first equation in (4.19). First we look at the solution on $[0, \tau]$: if there exists

$t_1 \in (0, \tau)$ such that $L_q(t_1) = 0$, then the derivative $dL_q(t)/dt$ at t_1 is

$$\left.\frac{dL_q(t)}{dt}\right|_{t_1} = e^{-d^E \tau_{(E,L)}} \gamma(A_{elf}(t_1 - \tau_{(E,L)})). \tag{4.22}$$

Since initial data for A_{elf} on $[-\tau, 0]$ is positive, the derivative of L_q at t_1 is positive and therefore $L_q(t)$ is increasing, so it cannot be negative. The same argument can be applied for $[\tau, 2\tau]$. This proves that $L_q(t) \geq 0$ for all $t \geq 0$. If there exists t_2 such that $L_f(t_2) = 0$, then the derivative of L_f at t_2 is given by

$$\left.\frac{dL_f(t)}{dt}\right|_{t_2} = \beta_L L_q(t)(\alpha_L H_{r+}(t) + H_{r-}(t)) \tag{4.23}$$

which is positive since $L_q(t_2)$, $H_{r+}(t_2)$ and $H_{r-}(t)$ are positive. Thus L_f is increasing at t_2 so it cannot be negative. The same argument applies for other equations. Therefore the solutions are positive.

From Equation (4.17) it is clear that $H(t)$ is positive and bounded by the carrying capacity K. Also the above discussion shows that H_{r-} and H_{r+} are positive for all $t \geq 0$. We show the boundedness of the tick population as follows. Let $T > 0$ and $\tau = \max\{\tau_{(E,L)}, \tau_{(L,N)}, \tau_{(N,A)}\}$. We integrate the first equation in the original system (2.1)

$$\begin{aligned} L_q(t) = e^{-d^{L_q} t - \beta_L \int_0^t (\alpha_L H_{r+}(u) + H_{r-}(u))du} \int_0^t e^{d^{L_q} s + \beta_L \int_0^s (\alpha_L H_{r+}(u) + H_{r-}(u))du} \\ \Big(e^{-d^E \tau_{(E,L)}} \gamma(A_{elf}(s - \tau_{(E,L)}))\Big) ds + e^{-d^{L_q} t - \beta_L \int_0^t (\alpha_L H_{r+}(u) + H_{r-}(u))du} L_q(0) \end{aligned}$$

therefore

$$\sup_{-\tau \leq t \leq T} L_q(t) \leq L_q(0) + \frac{e^{-d^E \tau_{(E,L)}}}{d^{L_q}} \sup_{-\tau \leq t \leq T} \gamma(A_{elf}(t))$$

using

$$\sup_{-\tau \leq t \leq T} e^{-\beta_L \int_s^t (\alpha_L H_{r+}(u) + H_{r-}(u))du} = 1$$

and

$$\int_0^t e^{-d^{L_q}(t-s)} ds < 1/d^{L_q}.$$

Using the fact that $\gamma(A_{elf}(t)) \leq p/qe$ for all $t \geq 0$, we see that

$$\sup_{-\tau \leq t \leq T} L_q(t) \leq C$$

where $C = L_q(0) + pe^{-d^E \tau_{(E,L)}}/qed^{L_q}$ is independent of T. Therefore $L_q(t) \leq C$ for all $-\tau \leq t < \infty$.

Integrating the remaining equations and taking the supremum we have:

$$\begin{aligned}
\sup_{-\tau \leq t \leq T} L_f(t) &\leq \sup_{-\tau \leq t \leq 0} L_{f_0}(t) + \frac{\beta_L K}{\delta} \sup_{-\tau \leq t \leq T} L_q(t) \\
\sup_{-\tau \leq t \leq T} N_q(t) &\leq N_q(0) + \frac{e^{-d^{L_m} \tau_{(L,N)}}}{d^{N_q}} \sup_{-\tau \leq t \leq T} L_f(t) \\
\sup_{-\tau \leq t \leq T} N_f(t) &\leq \sup_{-\tau \leq t \leq 0} N_{f_0}(t) + \frac{\beta_N K}{\delta} \sup_{-\tau \leq t \leq T} N_q(t) \\
\sup_{-\tau \leq t \leq T} A_q(t) &\leq A_q(0) + \frac{e^{-d^{N_m} \tau_{(N,A)}}}{d^{A_q}} \sup_{-\tau \leq t \leq T} N_f(t) \\
\sup_{-\tau \leq t \leq T} A_f(t) &\leq A_f(0) + \frac{\beta_A K}{\delta} \sup_{-\tau \leq t \leq T} A_q(t) \\
\sup_{-\tau \leq t \leq T} A_{elf}(t) &\leq \sup_{-\tau \leq t \leq 0} A_{elf_0}(t) + \frac{\epsilon \delta}{d^{A_{elf}}} \sup_{-\tau \leq t \leq T} A_f(t).
\end{aligned}$$

Combining the above inequalities and assuming that the initial data are bounded we can see that these tick stages are bounded on $-\tau \leq t < \infty$. We can get similar inequalities from System (4.18). This proves that all tick stages are bounded.

Since the host population stabilizes quickly at $\bar{H} = (b-\mu)K/c$, the limiting system is as follows

$$\begin{aligned}
\frac{dL_q}{dt} &= e^{-d^E \tau_{(E,L)}} \gamma(A_{elf}(t-\tau_{(E,L)})) + \beta_L(1-\alpha_L)L_q(t)H_{r+}(t) - (\beta_L \bar{H} + d^{L_q})L_q(t) \\
\frac{dL_f}{dt} &= -\beta_L(1-\alpha_L)L_q(t)H_{r+}(t) + \beta_L \bar{H} L_q(t) - \delta L_f(t) \\
\frac{dN_q}{dt} &= \delta\psi e^{-d^{L_m}\tau_{(L,N)}} L_f(t-\tau_{(L,N)}) + \beta_N(1-\alpha_N)N_q(t)H_{r+}(t) - (\beta_N \bar{H} + d^{N_q})N_q(t) \\
\frac{dN_f}{dt} &= -\beta_N(1-\alpha_N)N_q(t)H_{r+}(t) + \beta_N \bar{H} N_q(t) - \delta N_f(t) \\
\frac{dA_q}{dt} &= \delta\psi e^{-d^{N_m}\tau_{(N,A)}} N_f(t-\tau_{(N,A)}) + \beta_A(1-\alpha_A)A_q(t)H_{r+}(t) - (\beta_A \bar{H} + d^{A_q})A_q(t) \\
\frac{dA_f}{dt} &= -\beta_A A_q(t)(1-\alpha_A)H_{r+}(t) + \beta_A \bar{H} A_q(t) - \delta A_f(t) \\
\frac{dA_{elf}}{dt} &= \varepsilon\delta A_f(t) - d^{A_{elf}} A_{elf}(t) \\
\frac{dH_{r+}}{dt} &= -\mu H_{r+}(t) - \frac{c}{K}\bar{H} H_{r+}(t) + (\beta_L^* L_q(t) + \beta_N^* N_q(t) + \beta_A^* A_q(t))(\bar{H} - H_{r+}(t))
\end{aligned} \tag{4.24}$$

From now on we refer to this system as the main system of our model unless otherwise stated.

4.2.2 Analyses

In this section we give a necessary condition for the existence and uniqueness of a positive equilibrium and sufficient conditions for local stability of the tick free equilibrium.

Equilibria

Let X^* denote the vector $(L_q, L_f, N_q, N_f, A_q, A_f, A_{elf}, H_{r+})$ in $\mathbb{R}^8$, and let $f(X)$ be the right hand side of (4.24). In order to find all equilibria we need to solve the system $f(X) = 0$:

$$
\begin{aligned}
0 &= e^{-d^E \tau_{(E,L)}} \gamma(A_{elf}(t - \tau_{(E,L)})) + \beta_L(1-\alpha_L)L_q(t)H_{r+}(t) - (\beta_L \bar{H} + d^{L_q})L_q(t) \\
0 &= -\beta_L(1-\alpha_L)L_q(t)H_{r+}(t) + \beta_L \bar{H} L_q(t) - \delta L_f(t) \\
0 &= \delta\psi e^{-d^{L_m}\tau_{(L,N)}} L_f(t - \tau_{(L,N)}) + \beta_N(1-\alpha_N)N_q(t)H_{r+}(t) - (\beta_N \bar{H} + d^{N_q})N_q(t) \\
0 &= -\beta_N(1-\alpha_N)N_q(t)H_{r+}(t) + \beta_N \bar{H} N_q(t) - \delta N_f(t) \\
0 &= \delta\psi e^{-d^{N_m}\tau_{(N,A)}} N_f(t - \tau_{(N,A)}) + \beta_A(1-\alpha_A)A_q(t)H_{r+}(t) - (\beta_A \bar{H} + d^{A_q})A_q(t) \\
0 &= -\beta_A A_q(t)(1-\alpha_A)H_{r+}(t) + \beta_A \bar{H} A_q(t) - \delta A_f(t) \\
0 &= \varepsilon\delta A_f(t) - d^{A_{elf}} A_{elf}(t) \\
0 &= -\mu H_{r+}(t) - \frac{c}{K}\bar{H} H_{r+}(t) + (\beta_L^* L_q(t) + \beta_N^* N_q(t) + \beta_A^* A_q(t))(\bar{H} - H_{r+}(t))
\end{aligned}
\tag{4.25}
$$

At the tick-free equilibrium, where all tick stages are equal to zero, we have $H_{r+} = 0$. Let $H_{r+} \neq \bar{H}$ so that $(\bar{H} - (1-\alpha_L)H_{r+}), (\bar{H} - (1-\alpha_N)H_{r+}), (\bar{H} - (1-\alpha_A)H_{r+}) > 0$. We want to derive conditions for existence and uniqueness of a (strongly) positive equilibrium point

($X_i > 0$ for all $i = 1, \cdots, n$). From the equations in (4.25) we get the following

$$
\begin{aligned}
L_q &= \frac{d^{A_{elf}}(\beta_N(\bar{H} - (1-\alpha_N)H_{r+}) + d^{N_q})(\beta_A(\bar{H} - (1-\alpha_A)H_{r+}) + d^{A_q})}{s_2 s_3 \epsilon \beta_L \beta_N \beta_L (\bar{H} - (1-\alpha_L)H_{r+})(\bar{H} - (1-\alpha_N)H_{r+})(\bar{H} - (1-\alpha_A)H_{r+})} A_{elf} \\
L_f &= \frac{d^{A_{elf}}(\beta_N(\bar{H} - (1-\alpha_N)H_{r+}) + d^{N_q})(\beta_A(\bar{H} - (1-\alpha_A)H_{r+}) + d^{A_q})}{s_2 s_3 \delta \epsilon \beta_N \beta_A (\bar{H} - (1-\alpha_N)H_{r+})(\bar{H} - (1-\alpha_A)H_{r+})} A_{elf} \\
N_q &= \frac{d^{A_{elf}}(\beta_A(\bar{H} - (1-\alpha_A)H_{r+}) + d^{A_q})}{s_3 \epsilon \beta_N \beta_A (\bar{H} - (1-\alpha_N)H_{r+})(\bar{H} - (1-\alpha_A)H_{r+})} A_{elf} \\
N_f &= \frac{d^{A_{elf}}(\beta_A(\bar{H} - (1-\alpha_A)H_{r+}) + d^{A_q})}{s_3 \delta \epsilon \beta_A (\bar{H} - (1-\alpha_A)H_{r+})} A_{elf} \\
A_q &= \frac{d^{A_{elf}}}{\epsilon \beta_A (\bar{H} - (1-\alpha_A)H_{r+})} A_{elf} \\
A_f &= \frac{d^{A_{elf}}}{\epsilon \delta} A_{elf}
\end{aligned}
\tag{4.26}
$$

where $s_1 = e^{-d^E \tau_{(E,L)}}$, $s_2 = \psi e^{-d^{Lm} \tau_{(L,N)}}$ and $s_3 = \psi e^{-d^{Nm} \tau_{(N,A)}}$. From the first equation in the system (4.25) we get

$$
L_q = \frac{s_1 \gamma(A_{elf})}{(\beta_L(\bar{H} - (1-\alpha_L)H_{r+}) + d^{L_q})} \tag{4.27}
$$

and therefore

$$
\gamma(A_{elf}) = \frac{d^{A_{elf}}(\beta_L(\bar{H} - (1-\alpha_L)H_{r+}) + d^{L_q})(\beta_N(\bar{H} - (1-\alpha_N)H_{r+}) + d^{N_q})(\beta_A(\bar{H} - (1-\alpha_A)H_{r+}) + d^{A_q})}{s_1 s_2 s_3 \epsilon \beta_L \beta_N \beta_A (\bar{H} - (1-\alpha_L)H_{r+})(\bar{H} - (1-\alpha_N)H_{r+})(\bar{H} - (1-\alpha_A)H_{r+})} A_{elf}. \tag{4.28}
$$

Since $\gamma(A_{elf}) = pA_{elf}e^{-qA_{elf}}$ we have the following cases: $A_{elf} = 0$ or

$$pe^{-qA_{elf}} = \frac{d^{A_{elf}}(\beta_L(\bar{H}-(1-\alpha_L)H_{r+})+d^{Lq})(\beta_N(\bar{H}-(1-\alpha_N)H_{r+})+d^{Nq})(\beta_A(\bar{H}-(1-\alpha_A)H_{r+})+d^{Aq})}{s_1s_2s_3\epsilon\beta_L\beta_N\beta_A(\bar{H}-(1-\alpha_L)H_{r+})(\bar{H}-(1-\alpha_N)H_{r+})(\bar{H}-(1-\alpha_A)H_{r+})} \tag{4.29}$$

Finally, we reduce the system (4.25) to the following system

$$0 = \Gamma(H_{r+}) - pe^{-qA_{elf}} \tag{4.30a}$$

$$0 = -bH_{r+} + \Omega(H_{r+})(\bar{H} - H_{r+})A_{elf} \tag{4.30b}$$

where

$$\Gamma(H_{r+}) = \frac{d^{A_{elf}}(\beta_L(\bar{H} - (1-\alpha_L)H_{r+}) + d^{Lq})(\beta_N(\bar{H} - (1-\alpha_N)H_{r+}) + d^{Nq})(\beta_A(\bar{H} - (1-\alpha_A)H_{r+}) + d^{Aq})}{s_1s_2s_3\epsilon\beta_L\beta_N\beta_A(\bar{H} - (1-\alpha_L)H_{r+})(\bar{H} - (1-\alpha_N)H_{r+})(\bar{H} - (1-\alpha_A)H_{r+})}$$

$$\begin{aligned}\Omega(H_{r+}) = {} & \beta_L^* \frac{d^{A_{elf}}(\beta_N(\bar{H} - (1-\alpha_N)H_{r+}) + d^{Nq})(\beta_A(\bar{H} - (1-\alpha_A)H_{r+}) + d^{Aq})}{s_2s_3\epsilon\beta_L\beta_N\beta_A(\bar{H} - (1-\alpha_L)H_{r+})(\bar{H} - (1-\alpha_N)H_{r+})(\bar{H} - (1-\alpha_A)H_{r+})} \\ & + \beta_N^* \frac{d^{A_{elf}}(\beta_A(\bar{H} - (1-\alpha_L)H_{r+}) + d^{Aq})}{s_3\epsilon\beta_N\beta_A(\bar{H} - (1-\alpha_N)H_{r+})(\bar{H} - (1-\alpha_A)H_{r+})} + \beta_A^* \frac{d^{A_{elf}}}{\epsilon\beta_A(\bar{H} - (1-\alpha_A)H_{r+})}\end{aligned}$$

From (4.30b) we have

$$A_{elf} = \frac{bH_{r+}}{\Omega(H_{r+})(\bar{H} - H_{r+})}$$

given that $H_{r+} \neq \bar{H}$ and $\Omega(H_{r+}) \neq 0$ (it can be proved that this holds). Substituting this in the equation (4.30a) we get the following

$$\Gamma(H_{r+}) = pe^{-q\frac{bH_{r+}}{\Omega(H_{r+})(\bar{H}-H_{r+}).}} \tag{4.31}$$

This is a nonlinear equation for $H_{r+}$and we need to determine under what conditions this equation has a unique positive solution. Let $G(H_{r+})$ be the right hand side of Equation (4.31). The functions Γ and G have the following properties:

(i) Γ is a rational function and is strictly increasing for $0 < H_{r+} < \bar{H}$;

(ii) $\Gamma(0) > 0$ is given by

$$\frac{d^{A_{elf}}(\beta_L\bar{H} + d^{L_q})(\beta_A\bar{H} + d^{A_q})(\beta_N\bar{H} + d^{N_q})}{s_1 s_2 s_3 \epsilon \beta_L \beta_N \beta_A \bar{H}^3};$$

(iii) G is a negative exponential function and it approaches zero (exponentially) as H_{r+} approaches $\bar{H}$;

(iv) $G(0) = p$.

From these properties we can see that the equation (4.31) has at least one solution $0 < H_{r+} < \bar{H}$, if and only if $G(0) > \Gamma(0)$, i.e.,

$$p > \frac{d^{A_{elf}}(\beta_L\bar{H} + d^{L_q})(\beta_A\bar{H} + d^{A_q})(\beta_N\bar{H} + d^{N_q})}{s_1 s_2 s_3 \epsilon \beta_L \beta_N \beta_A \bar{H}^3}.$$

This solution is unique if $G(H_{r+})$ is monotonically decreasing, and this holds if and only if

$$\frac{d}{dH_{r+}}\Big(\frac{H_{r+}}{\Omega(H_{r+})(\bar{H} - H_{r+})}\Big) > 0$$

for all $H_{r+} \in (0, \bar{H})$.

Theorem 4.3. *Let*

$$\mathcal{R}_0^v = \frac{p s_1 s_2 s_3 \epsilon \beta_L \beta_N \beta_A \bar{H}^3}{d^{A_{elf}}(\beta_L\bar{H} + d^{L_q})(\beta_A\bar{H} + d^{A_q})(\beta_N\bar{H} + d^{N_q})}.$$

If $\mathcal{R}_0^v > 1$, then system (4.24) *has a positive equilibrium point. If additionally*

$$\frac{d}{dH_{r+}}\Big(\frac{H_{r+}}{\Omega(H_{r+})(\bar{H} - H_{r+})}\Big) > 0$$

holds, then the positive equilibrium is unique.

Stability of the tick-free Equilibrium

First we linearize System (4.24) about a given equilibrium point using the Fréchet derivative of the function $F(X)$, given by the right hand side of the System (4.24):

$$DF(X^*)X = \lim_{h\to 0}\Big(\frac{F(X^*+hX)-F(X^*)}{h}\Big)$$

The linearized system is given by

$$\begin{aligned}
Df_1(X^*)X &= pe^{-d^E\tau_{(E,L)}}A_{elf}(t-\tau_{(E,L)})e^{-qA^*_{elf}(t-\tau_{(E,L)})}\\
&\quad - pqe^{-d^E\tau_{(E,L)}}A_{elf}(t-\tau_{(E,L)})A^*_{elf}(t-\tau_{(E,L)})e^{-qA^*_{elf}(t-\tau_{(E,L)})}\\
&\quad + (1-\alpha_L)\beta_L(L^*_q(t)H_{r+}(t)+L_q(t)H^*_{r+}(t)) - (\beta_L\bar{H}+d^{L_q})L_q(t)\\
Df_2(X^*)X &= -(1-\alpha_L)\beta_L(L^*_q(t)H_{r+}(t)+L_q(t)H^*_{r+}(t)) + \beta_L\bar{H}L_q(t) - \delta L_f(t)\\
Df_4(X^*)X &= \delta\psi e^{-d^{L_m}\tau_{(L,N)}}L_f(t-\tau_{(L,N)})\\
&\quad + (1-\alpha_N)\beta_N(N^*_q(t)H_{r+}(t)+N_q(t)H^*_{r+}(t)) - (\beta_N\bar{H}+d^{N_q})N_q(t)\\
Df_5(X^*)X &= -(1-\alpha_N)\beta_N(N^*_q(t)H_{r+}(t)+N_q(t)H^*_{r+}(t)) + \beta_N\bar{H}N_q(t) - \delta N_f(t)\\
Df_7(X^*)X &= \delta\psi e^{-d^{N_m}\tau_{(N,A)}}N_f(t-\tau_{(N,A)})\\
&\quad + (1-\alpha_A)\beta_A(A^*_q(t)H_{r+}(t)+A_q(t)H^*_{r+}(t)) - (\beta_A\bar{H}+d^{A_q})A_q(t)\\
Df_8(X^*)X &= -(1-\alpha_A)\beta_A(A^*_q(t)H_{r+}(t)+A_q(t)H^*_{r+}(t)) + \beta_A\bar{H}A_q(t) - \delta A_f(t)\\
Df_9(X^*)X &= \varepsilon\delta A_f(t) - d^{A_{elf}}A_{elf}(t)\\
Df_{12}(X^*)X &= -(\mu+\frac{c}{K}\bar{H})H_{r+}(t) + \bar{H}(\beta^*_L L^*_q(t)+\beta^*_N N^*_q(t)+\beta^*_A A^*_q(t))\\
&\quad - \Big((\beta^*_L L_q(t)+\beta^*_N N_q(t)+\beta^*_A A_q(t))H^*_{r+}(t) + (\beta^*_L L^*_q(t)+\beta^*_N N^*_q(t)+\beta^*_A A^*_q(t))H_{r+}(t)\Big)
\end{aligned} \tag{4.32}$$

The linearized system about the tick-free equilibrium point is as follows:

$$\begin{aligned}
Df_1(X^*)X &= ps_1 A_{elf}(t-\tau_{(E,L)}) - (\beta_L \bar{H} + d^{L_q})L_q(t) \\
Df_2(X^*)X &= \beta_L \bar{H} L_q(t) - \delta L_f(t) \\
Df_4(X^*)X &= \delta s_2 L_f(t-\tau_{(L,N)}) - (\beta_N \bar{H} + d^{N_q})N_q(t) \\
Df_5(X^*)X &= \beta_N \bar{H} N_q(t) - \delta N_f(t) \\
Df_7(X^*)X &= \delta s_3 N_f(t-\tau_{(N,A)}) - (\beta_A \bar{H} + d^{A_q})A_q(t) \\
Df_8(X^*)X &= \beta_A \bar{H} A_q(t) - \delta A_f(t) \\
Df_9(X^*)X &= \varepsilon \delta A_f(t) - d^{A_{elf}} A_{elf}(t) \\
Df_{12}(X^*)X &= -(\mu + \frac{c}{K}\bar{H})H_{r+}(t)
\end{aligned} \tag{4.33}$$

Using the theory of monotone dynamical systems we can see that system (4.24) is cooperative ([109] Corollary 3.2) and therefore stability of the zero equilibrium of system (4.33) is given by the stability of the corresponding ODE system.

Theorem 4.4. *If $\mathcal{R}_0^v < 1$, then $X = 0$ is the only equilibrium point of the system* (4.24) *and is locally asymptotically stable. When $\mathcal{R}_0^v > 1$, there exists a positive equilibrium point and $X = 0$ is unstable.*

Proof. We use the method of next generation matrix for the ODE system given by $X'(t) = JX(t)$

where the matrix J is obtained from system (4.33):

$$J = \begin{bmatrix} -\beta_L\bar{H} - d^{L_q} & 0 & 0 & 0 & 0 & 0 & ps_1 & 0 \\ \beta_L\bar{H} & -\delta & 0 & 0 & 0 & 0 & 0 & 0 \\ 0 & \delta s_2 & -\beta_N\bar{H} - d^{N_q} & 0 & 0 & 0 & 0 & 0 \\ 0 & 0 & \beta_N\bar{H} & -\delta & 0 & 0 & 0 & 0 \\ 0 & 0 & 0 & \delta s_3 & -\beta_A\bar{H} - d^{A_q} & 0 & 0 & 0 \\ 0 & 0 & 0 & 0 & \beta_A\bar{H} & -\delta & 0 & 0 \\ 0 & 0 & 0 & 0 & 0 & \epsilon\delta & -d^{A_{elf}} & 0 \\ 0 & 0 & 0 & 0 & 0 & 0 & 0 & -b \end{bmatrix}$$

The matrix J can be written as $J = F - V$. The zero equilibrium is locally asymptotically stable if $\rho(FV^{-1}) < 1$ (ρ is the spectral radius of FV^{-1}) and it is unstable if $\rho(FV^{-1}) > 1$. We can see that

$$\rho(FV^{-1}) = \left(\frac{ps_1s_2s_3\epsilon\beta_L\beta_N\beta_A\bar{H}^3}{d^{A_{elf}}(\beta_L\bar{H} + d^{L_q})(\beta_A\bar{H} + d^{A_q})(\beta_N\bar{H} + d^{N_q})}\right)^{1/7}.$$

Finally, we note that $\rho(FV^{-1}) < 1$ is equivalent to $\mathcal{R}_0^v < 1$. This completes the proof.

4.2.3 Numerical Simulations

In this section we study the long-term dynamical behaviour of the system using numerical simulations and perform a sensitivity analysis for different parameters.

Model parametrization and validation

The observation of the dynamical behaviour of each stage of the tick population is demonstrated by applying DDE23 packages in Matlab to System (4.24). The model is parameterized using

parameter values available in mathematical and ecological literature ([57, 79, 95, 103, 104, 132]). Parameter values and initial conditions are given in Tables 4.2-4.1. We note that the grooming behaviour does not impact the initial growth of the tick population, since parameters reflecting the grooming factor do not change the value of the basic reproduction number. We consider three cases to illustrate the dynamics of tick population in the presence of grooming factor. However, in these cases we fix the values for parameters related to the grooming behaviour. In the first case (Figure 4.1) the basic reproduction number is below the threshold value i.e., $\mathcal{R}_0^v < 1$, the tick-free equilibrium is locally asymptotically stable and therefore all stages of ticks go extinct. In case 2 (Figure 4.2) the basic reproduction number is slightly greater than one, the tick-free

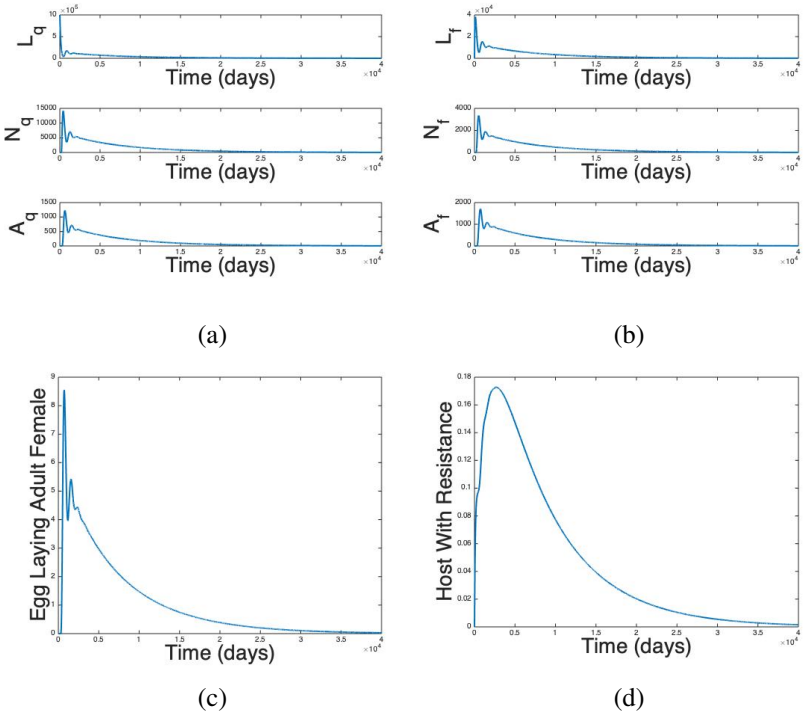

Figure 4.1: Case 1, $\mathcal{R}_0^v < 1$ where $\beta_L = 0.6 \times 10^{-4}$, $\beta_N = 1.8 \times 10^{-4}$ and $p = 200$ yields $\mathcal{R}_0^v = 0.89$.

equilibrium point becomes unstable and the solutions approach the positive equilibrium without any initial oscillatory behaviour. In case 3 (Figure 4.4) the solutions oscillate initially and then approach the positive equilibrium. When the resistance related parameter values are fixed and the rest of the parameters vary, the positive equilibrium becomes unstable and a periodic orbit

appears. Therefore, the solutions oscillate about the equilibrium point. Figure 4.3 shows how a periodic orbit appears as the value of α_A increases from 0 to 1.

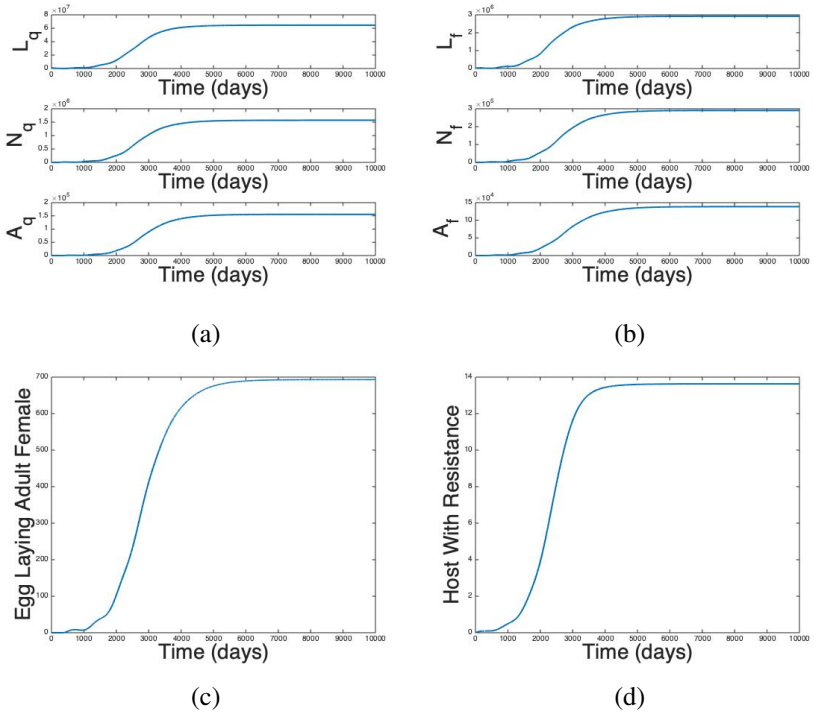

Figure 4.2: In Case 2 the values of p and κ have changed to $p = 1500$ and $\kappa = 0.1 \times 10^{-5}$ and the reproduction number increased to $\mathcal{R}_0^v = 6.71$. The simulations run for a time span of 10000 days. The equilibrium points for each stage of questing, feeding and adult egg laying female tick are as follows: $L_q = 6.5 \times 10^7, N_q = 1.6 \times 10^6, A_q = 1.6 \times 10^5$ $L_f = 2.9 \times 10^6, N_f = 2.9 \times 10^5, A_f = 1.4 \times 10^5, A_{elf} = 693$. In addition, the equilibrium point of the host with resistance is 13.

To study the population behaviour without grooming factor we set $\alpha_L = \alpha_N = \alpha_A = 1$ and $\kappa = 0$ and for intense grooming behaviour the $\alpha_L = \alpha_N = \alpha_A = 0$. In addition, we observe the dynamics for a mild grooming behaviour where $\alpha_L = 0.4, \alpha_N = 0.6, \alpha_A = 0.5$ and $\kappa = 0.1 \times 10^{-5}$. The equilibrium value for all stages are higher when there is no grooming behaviour. In particular, the value of the adult egg laying females at the equilibrium is 693 for a mild resistance behaviour and 1.9×10^3, when there is no resistance (Figure 4.2 and the left side of Figure 4.5). We also see that by decreasing the resistance solutions with non-oscillatory behaviour show damped oscillation. In a maximum intensified grooming behaviour the tick attachment rates to hosts with resistance are reduced to 0, therefore high resistance of hosts affects the tick equilibrium values

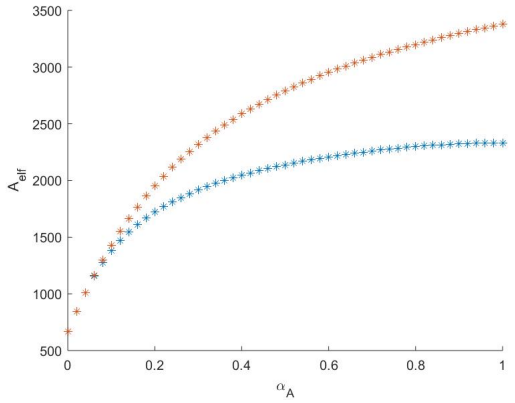

Figure 4.3: The solutions oscillate about the equilibrium point as we change the value of α_A in the interval $[0, 1]$ for parameter values in case 3. The values for α_L and α_N are 0.6 and 0.8. The orange and blue curves represent the highest and lowest value of the oscillatory solutions, respectively.

significantly. For instance, in Figure 4.5 the equilibrium value for A_{elf} reduces from 1.9×10^3, when there is no resistance, to 78 when the resistance is very high. Comparing the right side of Figure 4.4 with 4.6, demonstrates the effect of resistance factors on the dynamical behaviour of the solutions. Reducing the resistance from high to a mild resistance results in an increase in the value of the equilibrium of A_{elf} from 78 to 1600. However, in the absence of host resistance, the tick population at different stages oscillate about a positive equilibrium ($A_{elf} \approx 2.7 \times 10^3$). In other words, by decreasing the grooming behaviour (increasing the value of α_L, α_N and α_A from 0 to 1), there is more available resources for ticks to feed on. Therefore, the dynamical behaviour of tick population at different stages changes from solutions converging to the positive equilibrium to oscillatory solutions. The dynamics of the feeding ticks are similar to those of questing ticks and therefore we exclude the pictures on this paper. When we ignore the resistance behaviour in cases 2 and 3, the host population with resistance H_{r+} is equal to 0 and it reaches a positive equilibrium point when $\alpha_L = \alpha_N = \alpha_A = 0$.

LHS and PRCC

We perform Latin Hypercube Sampling to further analyze the effects of each parameter on the dynamics of each life stage of the ticks [10, 60]. Before we proceed to performing PRCC a

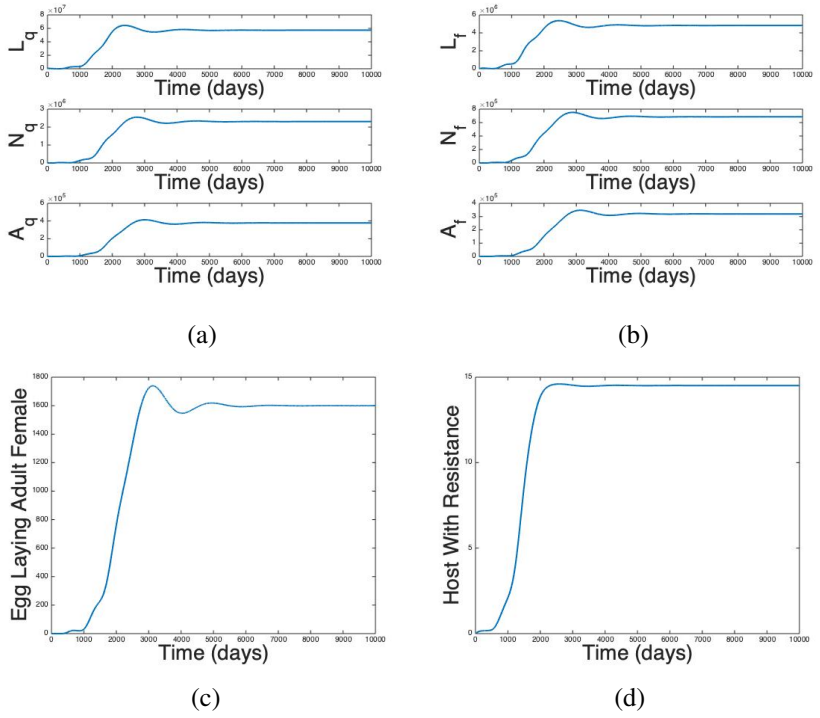

Figure 4.4: In Case 3 the values of β_L and β_N have changed to $\beta_L = 1.2 \times 10^{-4}, \beta_N = 3 \times 10^{-4}$ producing a higher reproduction number, $\mathcal{R}_0^v = 16.9$. The simulation are again running for a time span 10000 days. The equilibrium points for each stage of questing, feeding and adult egg laying female tick are as follows: $L_q = 5.7 \times 10^7, N_q = 2.3 \times 10^6, A_q = 3.8 \times 10^5, L_f = 4.8 \times 10^6, N_f = 6.9 \times 10^5, A_f = 3.2 \times 10^5, A_{elf} = 1600$. In addition, the equilibrium point of the host with resistance is 14.

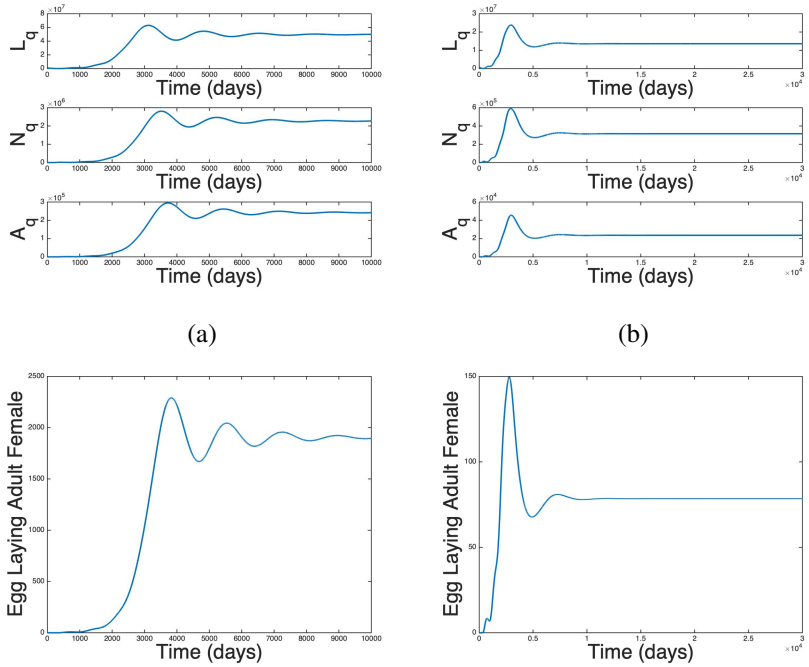

Figure 4.5: The parameter values are the same as in Case 2 except the $\alpha_L = \alpha_N = \alpha_A = 1$ (on the left). The equilibrium points are as follows: $L_q = 5.0 \times 10^7$, $N_q = 2.3 \times 10^6$, $A_q = 2.4 \times 10^5$, $A_{elf} = 1.9 \times 10^3$. There is no resistance and hence $H_r+ = 0$. In case of $\alpha_L = \alpha_N = \alpha_A = 0$ (on the right) the equilibrium points are $L_q = 1.3 \times 10^7$, $N_q = 3.2 \times 10^5$, $A_q = 2.4 \times 10^4$, $A_{elf} = 78$. Since now we introduce resistance, $H_{r+} = 10$.

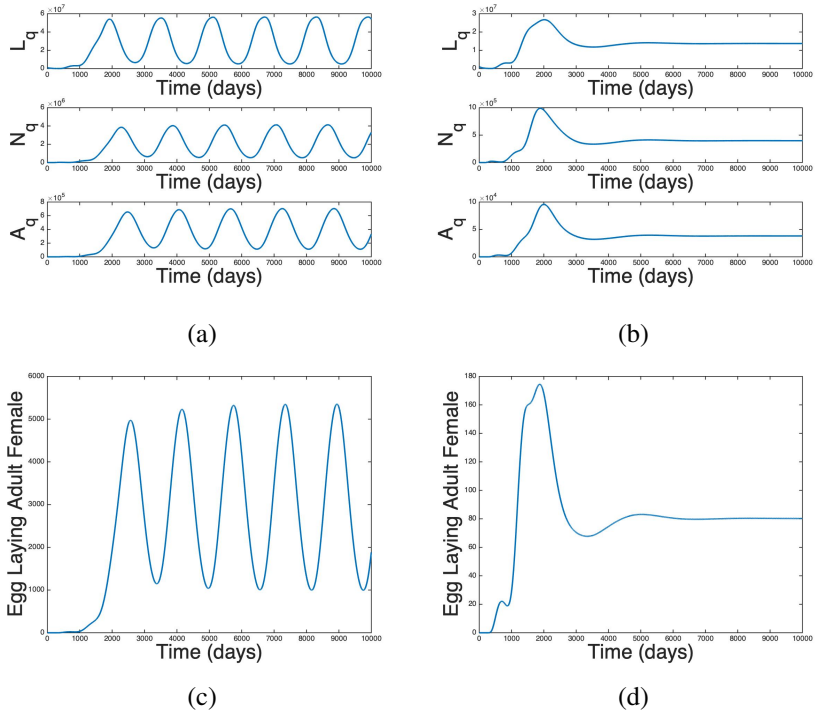

Figure 4.6: The parameter values are the same as in Case 3 except $\alpha_L = \alpha_N = \alpha_A = 1$ (the left). The equilibrium points are as follows: $L_q \approx 2.8 \times 10^7$, $N_q \approx 2.1 \times 10^6$, $A_q \approx 3.5 \times 10^5$, $A_{elf} \approx 2.7 \times 10^3$. Since resistance factor is not introduced the $H_{r+} = 0$. On the right side the $\alpha_L = \alpha_N = \alpha_A = 0$ and the equilibrium points are as follows: $L_q = 1.4 \times 10^7$, $N_q = 4.0 \times 10^5$, $A_q = 3.8 \times 10^4$, $A_{elf} = 80$. The resistance factor increase the population size from zero to $H_{r+} = 11$.

verification of monotonicity is necessary to ensure the correct range of the parameters for PRCC analysis. Next, we calculate the PRCC, which determines the contribution of each parameter to the output variable such the population of larvae questing. A PRCC value significantly greater than 0 indicates a positive correlation and for PRCC significantly less than 0, a negative correlation between the parameter and the output [84]. In Figure 4.7, the PRCC for the larvae questing population demonstrates the negative correlation with the death rates d^{Aelf}, d^{Nm}, d^{Lm}, d^{Nq}, d^{Aq}, d^{Lq}, d^{E} and d^{Lq} having the highest effect on this stage. The detachment rate δ does not have a an impact, however the parameters related to ticks' biological characteristics, p, q, ϵ, have a significant effect. We also observe that the host finding rates β_A, β_N,β_L, have positive correlation with larvae questing dynamics. For the values of most parameters that are taken from the literature, we would expect to see a reasonable correlation between the parameter and the output (in a range where the output is monotonically increasing or decreasing with parameter). For instance the output value of L_q (and therefore L_f) at the equilibrium is supposed to decrease with an increase of the larvae questing death rate (negative correlation).

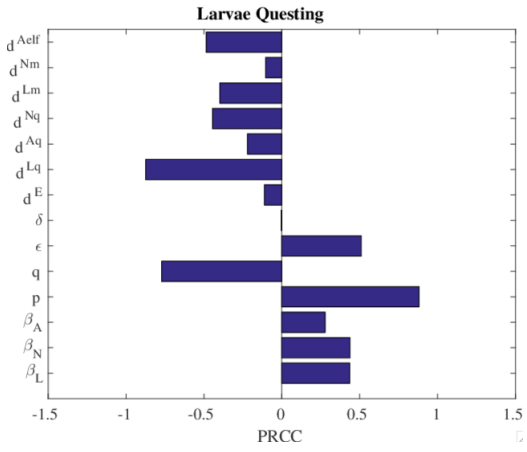

Figure 4.7: PRCC for most of the parameters used in the model at the equilibrium point of L_q. The value of each parameter is taken from 4.2and Case 2 for a range of $(+/-)20\%$

4.2.4 Discussion

In this study, we formulated a delay differential model for black leg ticks, stratified based on stage and activity, with a particular focus on the host grooming behaviour. The basic reproduction

number was calculated and the condition for local stability of tick-free equilibrium, for which the tick populations go extinct, and also for the existence and uniqueness of a positive equilibrium was given. Model parameterization and numerical simulations were carried out to demonstrate the dynamics of tick and host population with and without the grooming behaviour and the effect of the resistance factor on the value of equilibrium points are studied. Parameters related to the grooming and resistance factors, α_L, α_N, α_A, and κ have no effect on the initial growth rate of ticks since these parameters do not change the value of $\mathcal{R}_0^v$. However, with an increase of the intensity of the grooming behaviour from no resistance to a high level of resistance, where either the hosts show intensified grooming behaviour or ticks are withdrawn from feeding or dead, the values of equilibrium points of all tick stages decrease. From the numerical simulations we observed structural changes of the dynamical behaviour of the tick population by changing the parameter values reflecting the effect of the host resistance. Also, the intensified resistance results in higher equilibrium values for H_{r+}.

A sensitivity analysis of the positive equilibrium value to the parameters was carried out by performing LHS and PRCC. From PRCC we observed high positive correlation between the maximum number of eggs per female adult tick (p) and larvae questing; as more eggs are produced the higher the number of larvae questing. The female proportion parameter (ϵ) is also positively correlated to larvae questing. As the female rate proportion increases the higher number of egg production and therefore increasing the value of larvae questing. In contrast, the value of the strength of density dependence (q) and death rate of larvae questing (d^{Lq}) are negatively correlated with the population of larvae questing. As the death rate increases there will be a lower population size of larvae questing. Lastly, as the number of larvae questing increases there will be harder to find resources to survive, hence as q increases the number the L_q decreases.

This study has some limitations. The death rates are assumed to be constants for each stage of the tick and we have ignored the possibility of death during the feeding process resulting from serous exudes which could engulf the tick. Also, interpreting the host resistance as a kind of immunity to ticks we can consider the situation where host resistance decreases in time the hosts lose immunity to ticks. The molting process is demonstrated by constant delay functions. Future

work could incorporate the temperature and humidity on molting process and explore further the effects on tick dynamics.

4.3 Conclusions

Vector-borne diseases have been among the leading causes of deaths, worldwide. According to the 2017 update of the Global Burden of Diseases, Injuries, and Risk Factors Study (GBD) 2016 study [92], malaria was ranked as the 10th, 7th and 10th level 3[1] cause of deaths in 1980, 2007 and 2017, respectively, and one of the communicable diseases largely contributing to global mortality. Reducing the burden of vector-borne diseases such as malaria, Zika, Lyme diseases and so forth requires a thorough understanding of the nature of vector-host interactions as well as the dynamical behaviour of vector population considering seasonal fluctuations due to environmental changes, requiring adaptive control strategies.

In this chapter, we formulated a general model describing the epidemiological dynamics of vector-borne diseases, with and without demographics, using the renewal equation framework. We obtained the threshold condition for an outbreak and the final size of the epidemic. We also established the conditions for the existence and uniqueness of a positive equilibrium in the endemic case and the local stability of this positive equilibrium. We formulated a stage-structured model for the dynamical behaviour of deer tick population in the presence of host resistance. Existence and uniqueness of a positive equilibrium and stability criteria of the tick-free equilibrium were provided. The dynamical behaviour of tick population were illustrated through numerical simulations.

4.4 A remark

The research in this chapter was supported by Natural Sciences and Engineering Research Council of Canada and the Canada Research Chairs Program. The work of Section 4.1 being submitted for publication. The work of Section 4.2 has already been published in [1].

[1]GDB distinguishes causes of deaths at 4 levels. Each level refines the previous level into more specific causes.

5 | Seniors and Long-term Residency Facilities: Disease Prevention and Control in the Most Vulnerable Settings

Estimating and reducing the health and economic burden of infectious diseases are the primary task of the Infection Prevention and Control (IPC) programs. Reliable assessment of the burden of a disease must be based on the outcomes of the disease among individuals which requires a complete understanding of the population susceptible to the disease. Seasonal and pandemic influenza and the COVID-19 pandemic have shown that the probability as well as the outcomes of contracting the disease highly depend on the age and health conditions of individuals. Identifying the risk groups and estimating the burden of the disease in these groups are essential to the effective control of the diseases' health and economic burden. Here we review the disease characteristics, complications, the burden of influenza and COVID-19.

Influenza is a disease caused by the influenza virus. Mutation of the influenza virus to new strains can result in large epidemics and pandemics. Types A and B virus can cause seasonal epidemic, type A can cause global pandemics, while type C can only cause a mild disease. Type A is divided into subtypes based on the two proteins on the surface of the virus, Haemagglutinin (HA) and Neuraminidase (NA), with 16 known HA (H1-H16) and 9 known NA (N1-N9). Systemic symptoms of influenza include fever, chills, headache, myalgia, malaise and anorexia [98]. The virus is specifically more harmful to young children and seniors and it can lead to other respiratory diseases such as pneumonia (among patients hospitalized for influenza, 16%-55% are confirmed with pneumonia). A recent study on the burden of influenza estimated the influenza-related illnesses during influenza seasons in the US to be 9.2-35.9 million, from which 140,000-710,000 are influenza-related hospitalizations [76]. In Canada, Schanzer and colleagues [74] estimated the average annual influenza-related hospitalizations, over eleven influenza seasons (2003-2014), to be 11,000. Many studies have tried to estimate the true burden of influenza from surveillance data using different methods in the US and Canada ([85] and references therein).

The outcomes of contracting influenza vary based on the age groups and clinical conditions. Complication of influenza is beyond respiratory infection in elderly adults, in particular, among those

with chronic diseases. Influenza infection can cause several severe adverse events (SAEs) including cardiac disorder, respiratory, thoracic and mediastinal disorders, nervous system disorders; coronary artery event and pneumonia [108]. The following outcomes are possible: 1) A set of mild disease symptoms possibly resulting in a visit to a physician and use of antiviral drugs; 2) A set of more severe disease symptoms resulting in hospitalization for a few days without further complications; 3) Severe disease experience resulting in hospitalization and followed by more complications (e.g. pneumonia); 4) Severe disease experience resulting in a serious event such as a heart attack or death.

Despite availability of influenza vaccines for 80 years, the control and prevention of influenza is a global challenge. Three classes of vaccines are available today: inactivated virus, live attenuated virus and recombinant haemagglutinin. Effectiveness of the available vaccines for the influenza seasons from 2004-2019 (estimated by CDC [56] in the United States) varies between 10%-60%. The vaccine effectiveness against influenza A virus was highest among children aged 9 months to 8 years (64% with (50,75) 95% confidence interval) and lowest among seniors aged 65 and older (11% with (-28,38) 95% confidence interval), for the 2017-2018 influenza season.

The immunization programs have been implemented to control the incidence of influenza and its consequent SAEs. Since the number of cases, hospitalizations and deaths are particularly high among individuals aged 65 and older, the high dose (HD) trivalent vaccine ($60\mu g$ of hemagglutinin per strain) is recommended for this age group and is suggested to have a better efficacy, compared to standard dose (SD) vaccine ($15\mu g$ of hemagglutinin per strain) with relative efficacy of 24.2%. Clinical and cluster-randomized trials have shown that benefits of the high dose vaccine are not limited to the lower incident of influenza illness. They show that the number of SAEs and all-cause hospitalizations are also lower among individuals vaccinated by HD than those vaccinated by SD vaccine [35, 36, 37, 75]. It is worth mentioning that Influenza vaccines can results in modified infectivity (higher viral shedding) [133] and modified infectious period (quicker recovery) [114]. The effect of these results on disease dynamics have been rigorously studied in [89].

In case of COVID-19, seniors have been most affected during the first wave of the pandemic, in Ontario, Canada. Due to the absence of a vaccine, other control measures have been imple-

mented to reduce the burden of the disease. Major closures (schools, universities, restaurants, entertainment centers and non-essential services), social distancing through working from home and avoiding non-essential activities and mandatory use of PPE for public health settings as well as mandatory use of masks indoors for public are some of the most important control measures implemented in Canada and worldwide during the pandemic. In Canada, during the first wave of the COVID-19 pandemic, seniors aged 65 and older were severely affected. Although the previously mentioned practices had a significant effect on reducing the number of cases (by reducing contact between individuals and reducing the transmission probability) below the health care capacity of the country, these practices did not provide effective protection to the more vulnerable population. A comparison between the rates of COVID-19 among different age groups and the corresponding case fatality rates (CFR) in Ontario shows that both infection rate and CFR are highest among seniors aged 60 and older (see Figure 5.1).

The public health policies need to be revised in order to protect individuals against the disease while recovering the economic losses. Identifying risk groups based on the age, clinical conditions and other conditions will lead to better and efficient IPC policies prioritized to reduce the burden of the disease among these risk groups. Investing on targeted IPC programs will save the countries from both the health and economic losses of the pandemic.

In the next section, we present a study developed to understand the burden of the disease among residents of Long-Term Care Homes in Ontario and to evaluate the effectiveness of the policies implemented. This study is related to the general setting that this thesis has been developing, by considering the sub-population with least immunity against the disease.

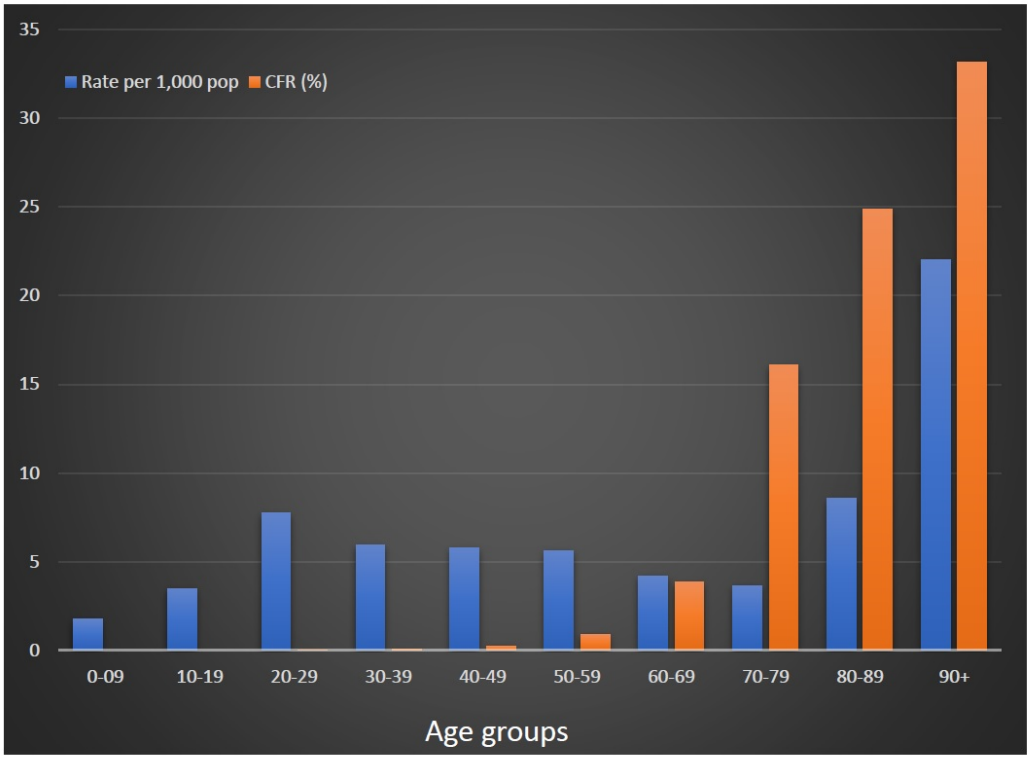

Figure 5.1: Based on the Public Health Ontario's data tool, over the period of Jan 23-Nov 03, case fatality rates and infection rates are higher among seniors aged 60 and above. Individuals aged 20-29 have the highest infection rates per 1000 population among the age group 0-59, with a CFR of 0.025%.

5.1 Markers of community outbreak and facility type for mitigation of COVID-19 in long-term care homes in Ontario, Canada: insights and implications from a time-series analysis

Background and Motivation

In late December 2019, a cluster of pneumonia cases of unknown aetiology was reported in the city of Wuhan, Hubei province, mainland China. The infectious agent responsible for the outbreak was later identified as an emerging coronavirus, termed as "Severe Acute Respiratory Coronavirus Type 2" (SARS-CoV-2). Since then, the virus has quickly spread out into other countries. The World Health Organization (WHO) designated the outbreak initially as a "Public Health Emergency of International Concern" (PHEIC) and then as a global pandemic.

Older adults have been particularly hard hit by the pandemic, dying disproportionately with respect to other age-groups [88, 100]. According to the 2019 United Nations Report [93], there are approximately 703 million people aged 65 years and over globally (about 9 percent of the entire population), with this figure expected to double by 2050 (reaching 16 percent of the population). Nursing homes are residential-oriented healthcare facilities providing long-term care to geriatric populations [107]. During the pandemic, they have become hot-spots, with a high death toll. According to a recent systematic review [105] (up to 26 June 2020), incidence rates of COVID-19 outbreaks in long-term care structures vary between 0 and 72% among residents and between 1.5 and 64% among staff members. Mortality rates among residents range from 0 to 9.5%, whereas case fatality rates vary between 0 and about 34%. While no death of staff has been reported in this survey, the death of residents of long-term care homes represents up to 85% percent of all COVID-19 related deaths

Researchers, worldwide, have studied the burden of COVID-19 among long-term care residents and the association between the severity of the outbreaks and a range of underlying factors ([5, 27, 53, 55, 78, 86, 115, 117, 123]). White and colleagues [123] found that, in the USA, the probability of an outbreak was higher for larger facilities and was also associated with the risk

of COVID-19 in the region surrounding the facility. In the UK, Dutey-Magni and coauthors [53] showed that gender, increasing age, total number of beds, the staff to bed ratio and the resident to bedroom ratio are predictors of an outbreak. In Canada, Fisman and coworkers [55] examined the ratio of death rates in two groups: residents of the LTCH and seniors aged 69 and older outside the LTCH. They found that the disease specific mortality incidence rate ratio among long-term care home residents compared with individuals of age 69 and older living in the community increased from 13.1 to 87.3 over time. They also examined the relative increase in risk of death per staff member with confirmed infection and found that the death of residents lagged by 6 days behind confirmed COVID-19 infection of staff. On the other hand, according to the analysis of Stall and collaborators [110], the total number of COVID-19 confirmed resident cases among homes with outbreaks were associated with the *for-profit management status* of homes whereas the likelihood of outbreaks were associated with the risk of presence of positive COVID-19 cases in the region surrounding the facilities. Older design standards and management type of networks of establishments were the determinants of COVID-19 associated deaths in for-profit long-term care homes. Brown el al. [1] studied the association between severity of COVID-19 and the crowding index, defined as the mean number of residents per bedroom and bathroom (ranging from 0 to 4), and found that homes with crowding index > 2 have larger outbreaks, i.e., higher cases and deaths per 100 residents. None of the above studies, however, have attempted to detect all significant determinants of the high excess COVID-19 mortality among long-term care home residents. In search for the associated determinants, here, we study quantitatively the temporal evolution of COVID-19 outbreaks with fatal outcomes in long-term care homes in Ontario. We aim to answer the following questions:

- How does the size of the LTCH facility (e.g., number of beds), average hours of care per patient-day and type of management (for profit, nonprofit, etc.) affect its COVID-19 patient death outcome?
- Is the evolution of COVID-19 in LTCH linked or affected by COVID-19 epidemic-induced factors such as staff and personal protective equipment (PPE)?
- Did community infection prevention and control (IPC) policies affect measurably the evo-

lution of the outcome of COVID-19 outbreaks in LTCH?

- How does the epidemic evolution in the community in which the LTCH is located affect the evolution of the outcome of COVID-19 outbreak in that facility?

Material and methods: Data source and study design

To address the above questions, we examined several data sources specific to Ontario, Canada. In particular, we obtained data made available to us through the Ontario COVID-19 Modeling Consensus Table, curated by the Ontario Ministry of Long-Term Care. Within this dataset, we utilized time series for number of confirmed COVID-19 positive cases among residents and staff, COVID-19 related deaths, reports of Personal Protective Equipment (PPE) shortage, and reports of staff shortage for all 627 long-term care homes in the province of Ontario. Data from March 29 to June 3 was included and used in our analysis. We also utilized the data on daily number of cases and deaths from Public Health Ontario's data tool stratified by public health unit [97]. In addition, we considered Ontario's census information data divided into Public Health Units from Statistics Canada [29].

We conducted four types of analysis: 1) multivariable linear regression analysis for two models: one examining outbreaks in all homes, and one examining outbreaks summed over health regions; 2) cross-correlation analysis of the daily number of deaths in long term care home residents and in the community; 3) data clustering and feature selection; 4) spatio-temporal analyses using ArcGIS.

5.1.1 Results

We conducted this analysis using the COVID-19 database for 627 long term care homes across Ontario, from March 29 to June 3, 2020. During this period, 194 homes had an outbreak and 106 homes had at least one resident death. A total of 1701 deaths were reported during this period, in 22 health regions. Total number of cases leading to death in Ontario, between March 29 and June 3, 2020 were 2,548, from which 67% were among long term care residents. The focus of this study is on the homes reporting deaths.

Table 5.1: Overview of the characteristics of the 627 homes considered in this study.

	Homes in outbreak	Homes with resident deaths	All homes
Number of homes	194	106	627
Number of confirmed residents	3228 (5202)*		3228 (5202)
Number of resident deaths		1718	1718
Number of confirmed staff			1262 (1865)*
Information based on the home size			
homes with 1-96 beds	50(20%)	21(8.5%)	248
homes with 97-160 beds	70(30%)	37(16%)	234
homes with +160 beds	74(51%)	48(33%)	145
Information based on the home ownership			
Number of for-profit homes	112(31%)	59(16%)	361
Number of not-for-profit homes (non-profit, CHFA, MHFA)**	82(30%)	47(18%)	266
Information based on staff and PPE shortage reports			
Number of homes with staff shortage	65(84%)	59(77%)	77
Number of homes with PPE shortage	49(56%)	38(43%)	88

Characteristics of the homes with respect to their outbreak status, size, ownership and the COVID-19 related staff and PPE shortage reports. Percentages are based on the total numbers within each row. *Cumulative number of cases obtained from the data. These are subject to error due to the lack of information on how the recovered cases are subtracted from the cumulative number of cases. The numbers in brackets are taken from [96]. ** The total number of charitable and Municipal homes are 48 and 93, respectively.

The total number of resident deaths, summed over all homes in the health region, are as low as 1 death in two health regions, Peterborough County-City Health Unit and Sudbury and District Health Unit, and as high as 728 in the Toronto Health Unit. The number of deaths in Toronto accounts for 54.4% of the total deaths in Ontario's LTCHs, while the number of homes in this health unit is only 13.6% of all homes with 19.5% of the total beds in the province.

The most significant policy implemented during this period was the emergency order requiring staff to work in only one long-term care facility, effective on April 22. Figure 5.2a shows that the total number of deaths in the community, including the deaths in LTCH, is the highest during the week of April 19-26 (bottom panel), while the number of deaths in LTCH peaks during the following week (top panel). It is clear that the weekly number of deaths among LTCH residents has slightly increased, before decreasing, and the total number of deaths in Ontario has decreased after the policy was implemented. Therefore this policy could be said to appear to have been effective in slowing the rate of increase of the number of deaths in the community and in a delayed manner in LTCH.

Figure 5.2b shows how the percentage of deaths in long-term care homes evolved with respect to the total number of deaths in Ontario. In this plot we see that the percentage of deaths in long-term care homes continued to grow after the non-staff-sharing policy was implemented and reached its highest value (about 90%). This can be explained by the delay observed between the number of deaths among individuals outside LTCH and the number of deaths in LTCH. We also see in Figure 5.2c that the number of homes reporting a staff shortage is increasing after the date of the policy. According to the Long-Term Care Staffing Study provided by the Ministry of Long-Term Care [94] staff absenteeism has led to a high volume of staff shortages in long-term care facilities. The following were listed among several reasons provided by employers facing staff shortages: fear of contracting COVID-19 in the LTCH, concerns about PPE availability, and the requirement to work in one home.

Although we do not see clear evidence for the effectiveness of the policy on reducing the number of deaths among LTCH residents in these plots, from Figures 5.2a and 5.2c we can infer that a portion of the number of deaths could have been prevented, had the aforementioned policy been

Table 5.2: Characteristics of the homes with respect to the design standard, room occupancy and the quality of care.

Design standard and occupancy*	for-profit (%)	non-profit (%)	municipal (%)
Older design standard	193 (53.6)	30 (18.5)	12 (11.9)
% single occupancy, mean	31.6	49.2	52.8
% double occupancy, mean	38.5	39.9	39.7
% quadruple occupancy, mean	28.3	8.7	6.6
Crowding index**	**Crowding Index < 2 (%)**	**Crowding Index > 2 (%)**	
for-profit	127 (41)	231 (75)	
non-profit	101 (32.6)	58 (18.8)	
municipal	82 (26.5)	19 (6.2)	
$<$ 100 residents	69 (22.3)	175 (56.8)	
$>$ 100 residents	241 (77.7)	133 (43.2)	
Quality of care by management-type and home size***	**Qindex (mean)**	**SD**	
private homes (for-profit)	0.02	0.32	
not-for-profit homes	0.04	0.39	
municipal homes	-0.13	0.32	
1-96 beds	-0.09	0.34	
97-160 beds	0.05	0.33	
$>$160 beds	0.05	0.34	

*The design standards and room occupancy are from [110].** The crowding indices are from [25]. ***The quality of care, as measured by Qindex, by management category and size of the home are from [127]. Percentages in the first row of the design standard and in the first three rows of the crowding index are with respect to all homes in that type of ownership. In the last two rows of the crowding index, the percentages are with respect to the total number of homes with less than or more than 100 residents. 1) The Qindex is a metric for the quality of care in long-term care homes. It is calculated by averaging the z-scores of nine quality indicators, such as number of falls and improved or worsened physical functioning, over a period of 5 years. In this reference, the Qindex values vary between -0.3 and 0.4. 2) From [110], the average number of beds in for-profit, non-profit and municipal homes are 113, 119, and 155, respectively, while the percentage of homes with quadruple occupancy in each sector are 28.3, 8.7 and 6.6, respectively. Note that these inputs do not directly confirm that smaller homes have higher percentage of quadruple occupancy and this requires further confirmation.

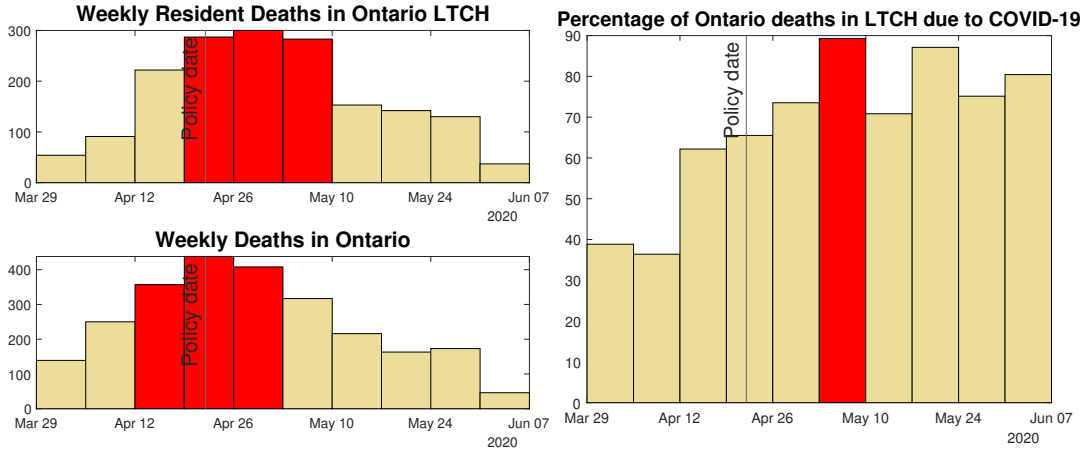

(a) (b)

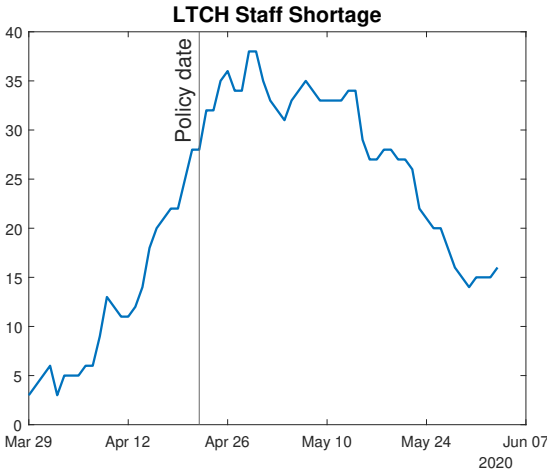

(c) Number of homes reporting a staff shortage in Ontario.

Figure 5.2: (a) Weekly number of total number of deaths among long-term care residents (top panel) and in the community where the LTCH is located (bottom panel), in Ontario, Canada. In red we highlight the three weeks that include the highest number of deaths among long-term care residents (top panel) and in the community (bottom panel) during the period analyzed. (b) Weekly percentage of deaths among residents of LTCH to the total number of deaths in Ontario. In red, here we highlight the week with the highest percentage of COVID-19-induced death in LTCH with respect to COVID-19-induced death in the whole community. (c) Daily number of homes reporting staff shortages. In all these subplots, we have included the first day in which the policy was in effect (April 22) to show its impact on the number of deaths and staff shortage reports.

implemented on an earlier date, prior to the local community epidemic peak, while the number of cases and deaths were lower, while the number of staff available was also higher.

5.1.2 Multi-variable Linear Regression

We used the death-to-bed ratios, defined by

$$100 \times \frac{\text{total number of resident deaths}}{\text{number of beds}}$$

as a measure of the overall extent of COVID-19 severity in long-term care facilities. We examined the association between the death-to-bed ratio and the following factors in our models: facility size (number of beds), facility management (for-profit, non-profit, municipal and charitable), proportion of staff infected, risk of COVID-19 in the community in the surrounding health region, reports of staff shortage and reports of PPE shortage. The first model (Model I) included all homes with an outbreak with a positive death to bed ratio with the death to bed ratio as the primary outcome and type of management (for-profit, non-profit, charitable and municipal), number of beds, staff cases and staff and PPE shortages as the predictive variables (the outcome and predictive vectors have 106 components). In the second model (Model II) , the primary outcome was selected to be the death-to-bed ratios calculated for 34 health regions in Ontario, and for two categories of homes based on the type of management (for-profit homes in one category and non-profit, charitable and municipal homes in another category) and the type of management, risk of the disease in the health region and staff cases as the predictive variables (the outcome and predictive vectors have 68 components)[1]. The results are summarized in Table 5.3.

For-profit homes have been affected the most. The death-to-bed ratio of for-profit and other management types are 2.81% and 1.31%, respectively, in Ontario. Death-to-bed ratios are highest among the following health regions: City of Toronto Health Unit (6.04% and 3.74%), City of Ottawa Health Unit (7.23% and 1.75%), Durham Regional Health Unit (5.97% and 1.53%), Peel Regional Health Unit (4.89% and 2.30%), York Regional Health Unit (4.52% and 3.12%). The ratios are greater than 3% in these regions with a significant difference between for-profit and

[1]More details are given in the supplementary material.

Table 5.3: Correlation coefficients between the death-to-bed ratio and other predictive variables

Model I	Variable	CC	95% CI
	Sector	-0.26	$[-0.43, -0.07]$
	Number of beds	-0.37	$[-0.52, -0.19]$
	Cases per staff	0.42*	$[0.25, 0.56]$
	Number of staff-shortages	0.33	$[0.15, 0.49]$
	Number of PPE-shortages	0.11	$[-0.08, 0.3]$
Model II			
	Sector	-0.37	$[-0.64, -0.026]$
	Risk in the community	0.7	$[0.55, 0.83]$
	Cases per staff	0.89*	$[0.8, 0.95]$

Note: Model I includes all individual homes with a positive deaths to bed ratio (106 homes). In Model II, death-to-bed ratios are averaged over all homes within each health region in two categories. One category includes all for-profit homes and the other category includes all non-profit, municipal and charitable homes.* The value of correlation coefficient can be higher than these values, since the cumulative number of infected staff are lower than the actual number of infected staff.

other types of management.

The negative correlation between death-to-bed ratio and size of the homes surprisingly suggests that smaller homes tend to have higher death-to-bed ratios: The average number of beds among homes with resident deaths was 169, while it was 104 in homes with a death-to-bed ratio greater than 30%. This could be linked to differences in quality of care between the two types of homes. Indeed, this was suggested in Wilkinson et al. (2019) [127] who have shown that the Qindex of the small homes (1-96 beds) have been significantly lower than medium and large sized homes. Qindex is a composite Quality Index (QI) used in Ontario for evaluation of quality of performance, these can include for example, hospitalization and mortality rates as indicators of quality performance. Wilkinson et al. (2019) [127] also discussed that when these small homes start with a low value of Qindex, they show less improvement compared to larger homes, over a period of 5 years [127]. A summary of their findings is given in Table 5.2.

Given the high number of staff involved in direct care to residents (56,000 full time equivalent (FTE) positions in 2018 [94]), we included the proportion of confirmed COVID-19 staff in our models. However, the information on the total number of staff working in each home and the accurate number of staff cases were not available. In the data for the outbreaks in long-term care facilities, the number of recovered staff were subtracted from the cumulative number of staff in the time-series data, and therefore the number of confirmed staff used in this study are lower than the actual number of infected staff, for each home. The total number of infected staff and the number of staff death, summarized in [96], were 1865 and 5, respectively. In order to estimate the number of staff providing direct care to residents, we used the number of hours of care per patient per day, available for for-profit, non-profit and municipal homes [66], assuming that all staff worked 8 hours a day, and using the following formula

$$\frac{1}{8}(\text{average hours of care per resident day} \times \text{number of beds}).$$

Then we used the cumulative number of the infected staff to get a proportion of COVID-19 infected staff to all staff, for each home. Based on these estimates, with the assumptions above,

homes with higher fraction of staff infected have higher death-to-bed ratio (See Table 5.3).

We calculated the risk in the community for each health region, defined by total number of COVID-19 cases over the period from March 29 to June 3, per 1000 population. The lowest calculated risk was 0.185 in the District of Algoma Health Unit, and the highest risk was 4.09 in the City of Toronto Health Unit. We identified 10 health regions with more than 2 case per 1000 population as high-risk regions. All health regions with higher death-to-bed ratio also had higher risk in the community. This is illustrated in Figure 5.10a.

The association between the number of staff and PPE shortage reports and death-to-bed ratios was not significant from the correlation analyses, however the odds of resident deaths among homes with at least one staff shortage report were 35 times higher than homes without staff shortage reports. Moreover, the odds of resident deaths among homes with at least one PPE shortage report were 5 times higher than homes without PPE shortage reports. According to the recent 2020 Long-Term Care Staffing Study [94], provided by the Ministry of Long-Term Care, a large portion of the staff shortages was associated with personal support workers (PSW). PWS provide personal support, such as feeding, dressing, bathing, transferring, meal preparation and light housekeeping. They account for 58% of the long-term care employees. Others include 25% registered nurses and 6% activity and health care assistants. Fear of contracting COVID-19 and the requirement to work in one home were among the reasons for work absenteeism.

5.1.3 Temporal and Spatio-Temporal Analyses: cross-correlation and indoor conditions

We studied the temporal behavior of the spread of COVID-19 among LTCH residents, using the time-series of cumulative number of deaths and the death-to-bed ratio. Among the health regions with average death-to-bed ratio greater than 3%, for-profit homes in Durham Regional Health Unit and the City of Ottawa Health Unit have significantly higher ratios, compared to non-profit homes. The average daily increase of the death-to-bed ratio, calculated for the first three weeks from the day of first resident death, were higher in for-profit homes in most regions (in 14 out of 22 regions with LTCH resident deaths- and in 7 out of 10 high-risk regions). In the Peel Regional,

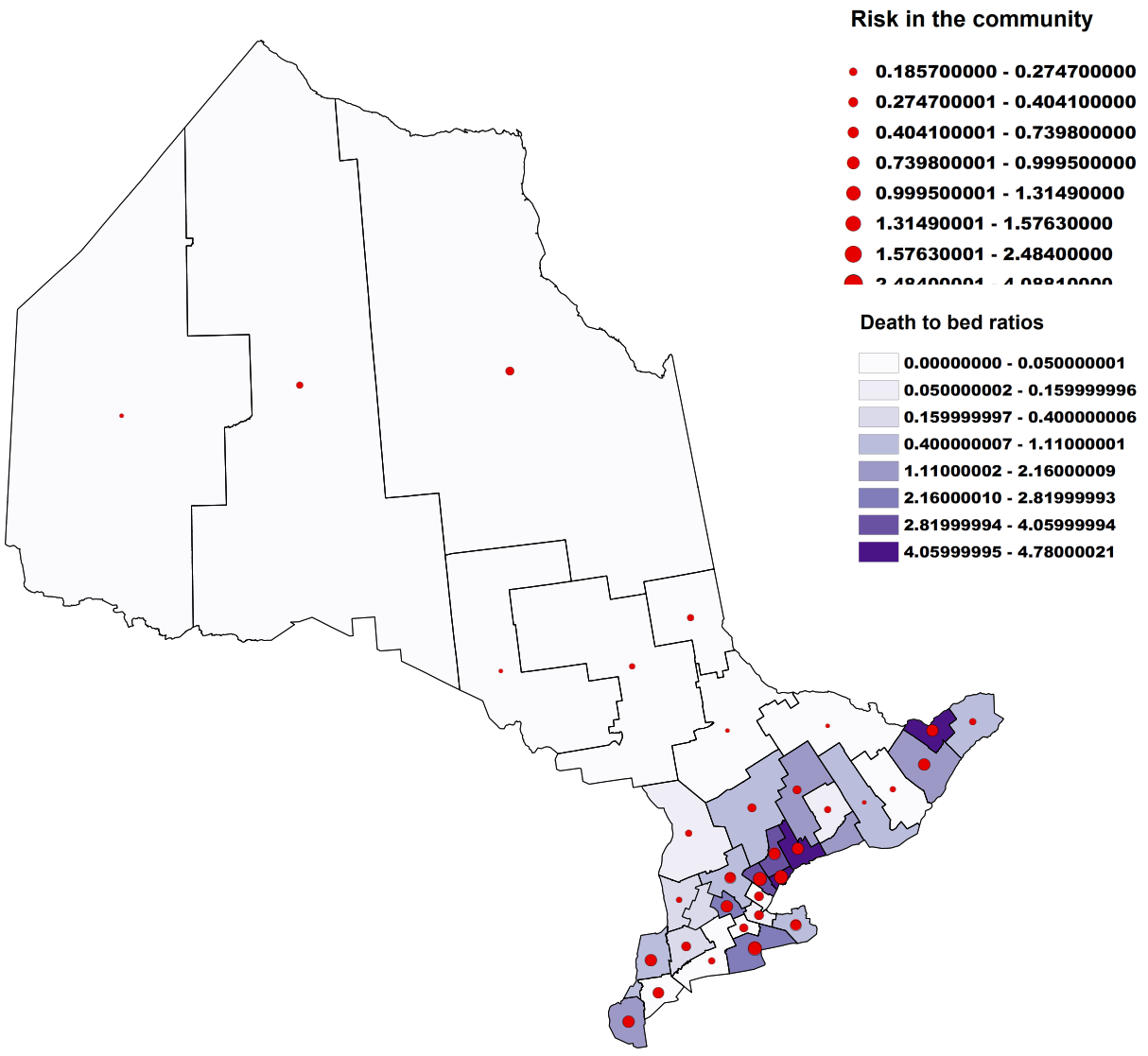

Figure 5.3: Death-to-bed ratio in the long-term care homes compared to the risk in the corresponding community. Health regions with high risk in the community (larger colored circles) also have higher death-to-bed ratios (darker colors).

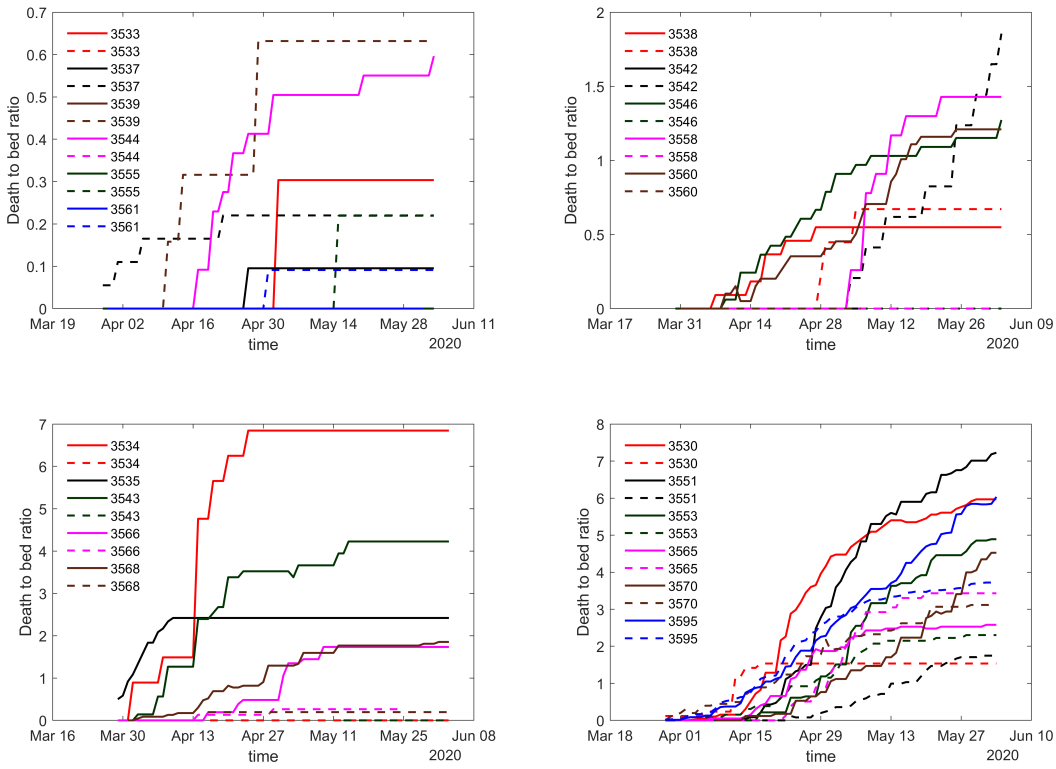

Figure 5.4: Death-to-bed ratios by sector and health region. The four panels include regions with overall death-to-bed ratios of <0.5% (top left), 0.5-1% (top right), 1-3% (bottom left), >3% (bottom right). The solid lines represent the death-to-bed ratio in for-profit homes and the dashed lines represent the ratios in other types of homes. The two sector type in each health region are represented with the same colour. A list of Ontario health regions and the corresponding public health unit code is available in the Appendix.

Durham Regional and the City of Ottawa Health Units the rate of increase in for-profit homes were 2.8, 2.4 and 1.7 times higher than not-for-profit homes, respectively. For-profit homes in Toronto had higher death-to-bed ratio compared to other types of management, but the average daily rate of increase were slightly lower. The differences between for-profit and non-profit homes were significant. In most health regions non-profit homes not only had a lower death-to-bed ratio, but also had a better control in keeping the numbers low over time (Figure 5.4).

The rationale for the significant differences between death-to-bed ratio in for-profit and non-profit LTCH can include the actual physical indoor environment, which includes indoor air quality handling, in addition to occupancy levels in these homes. Indeed, [110] (summarized in Table 2) reported that for-profit homes are more likely to be of older design standard and with quadruple occupancy compared to non-profit and municipal homes. More precisely, 53% of for-profit homes have older building design standard compare to 18.5% in non-profit and 11.9% in municipal homes. Also, [25] reported that for-profit homes account for 75% of homes with a crowding index > 2. On the other hand, for-profit homes have smaller number of beds on average and based on [127] smaller homes (i.e., homes with less than 97 beds) have lower Qindex than larger homes. Combining these facts, the inadequate management of COVID-19 in for-profit homes can be associated with the fact that for-profit homes have lower home standards overall, with more poor indoor environmental conditions combined with higher levels of crowding. These factors are now recognized to enhance risk of transmission indoors [11, 12, 70] and require further investigation for the specifics of the LTCH in question.

Among 22 health regions reporting LTCH residents' deaths, the date corresponding to the first reported deaths in the region ranged between March 29 to May 15 (a window of 48 days). Durham, Haliburton, Hamilton and Toronto were the first regions, followed by York Region, Haldimand, Leeds, Windsor and Peel. It is worth noting that 5 of these regions share geographical borders and have high death-to-bed ratio, as shown in Figures 5.5a and 5.5b. These health regions also have higher density of homes (number of homes per square meter). Maps illustrating the density of homes and the progress of the number of deaths are available in the Appendix. Also, regions with the first death reported prior to April 10 have higher death-to-bed ratio than those reporting

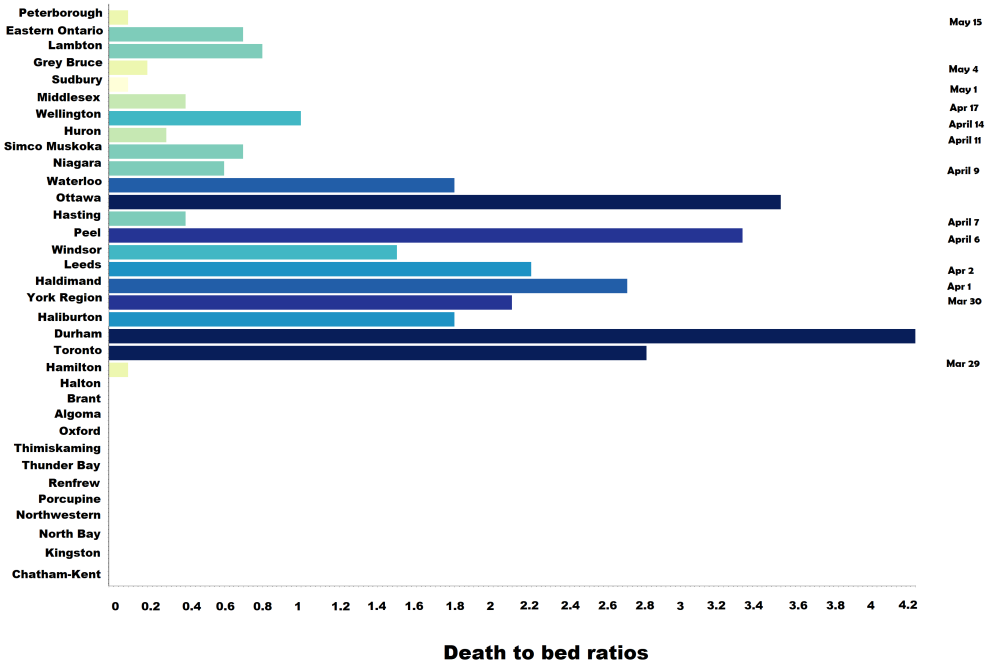

(a)

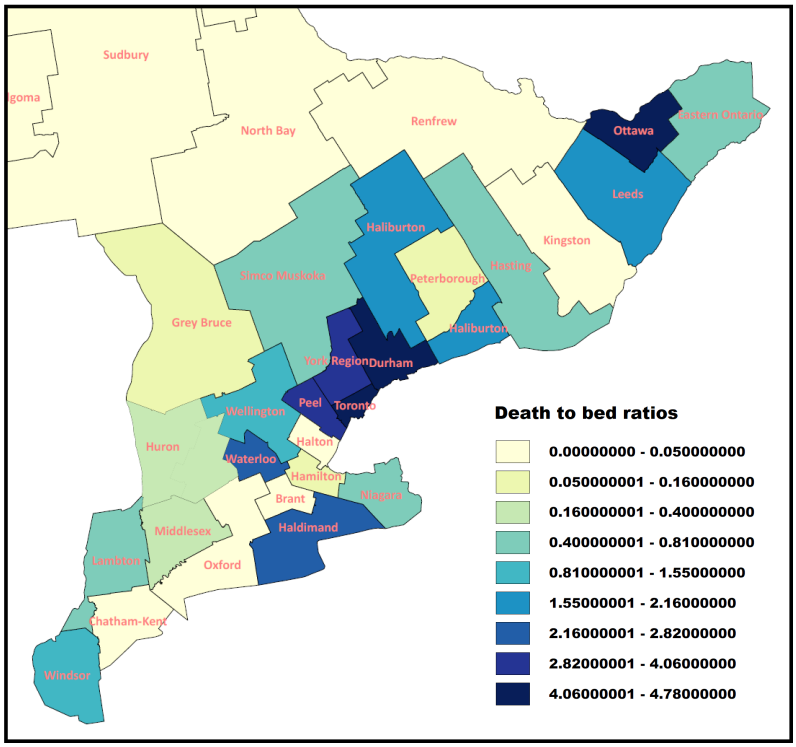

(b)

Figure 5.5: (a) The date of first reported resident death, ordered from bottom to top between March 29, 2020 to May 15, 2020, and the corresponding death-to-bed ratio (x-axis). (b) Geographical location of the Ontario health regions with the colours representing the corresponding death-to-bed ratio. Colours are identical to those in (a).

deaths after April 10. This could be associated with the higher risks in those health regions.

A cross-correlation analysis[2] was performed to determine whether a delay is observable between outbreaks in the community and the deaths among LTCH residents. These analyses show that the outbreaks in the community with fatal cases lead to the outbreak in LTCHs with a delay of up to 11 days, depending on the health region. For instance, there is a delay of 8 days between the outbreak in the community and in the long-term care facilities in the Niagara Regional Area Health Unit depicted in Figure 5.6a. The cross-correlations were performed for the daily number of deaths in the community minus the number of deaths in LTCHs and the daily number of deaths among LTCH residents. For the accuracy of the results regions with less than 10 data points were excluded. The lags with highest significance were collected for the death data in 14 regions and for the aggregated death data in Ontario. Figure 5.6c shows the histogram of the lags, showing the large spread up to 11 days, with a mode however around 2 days.

Data clustering

We performed a clustering analysis on all LTCH in Ontario and singled out the homes that were most relevant regarding the burden of the disease. We studied the burden of Covid-19 in Ontario long term care homes by comparing the homes according to the number of beds, total number of resident deaths, number of staff and PPE shortage reports, number of confirmed residents and number of confirmed staff, between March 29 and June 3, 2020. As explained in the previous sections, the accurate number of confirmed resident and staff were not available from the data and therefore an estimate of the number of cases was used in our analyses. In the clustering analysis, the maximum number of confirmed residents and confirmed staff were selected as an estimate.

The clustering algorithm PART-A was used. This algorithm is the combination of two different clustering techniques: PART and k-means. The former is a neural-network architecture, developed in Cao and Wu [30], to find projective clusters in a high-dimensional space (there are six

[2]The analysis uses the crosscorr package in Matlab to examine the correlation between two time series at a number of lags (e.g., 0 to 40 lags). The positive correlation values show the correlation between time series A and B assuming that A leads to B, i.e., A is highly correlated to B at a given lag when the correlation coefficient is greater that 0.2. Values less than 0.2 (or 0.1) indicate no significant correlation. The same interpretation can be obtained by considering either left or right side of the x-axis.

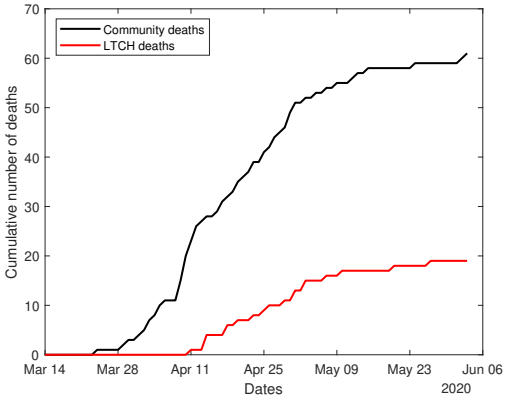

(a)

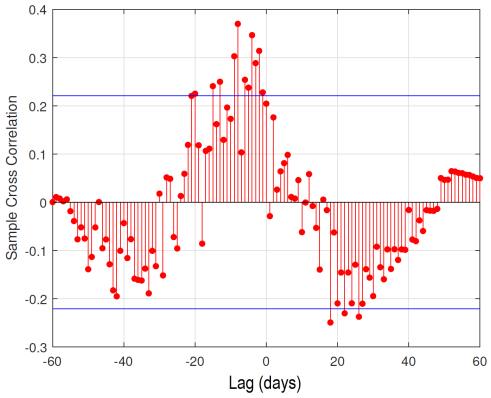

(b)

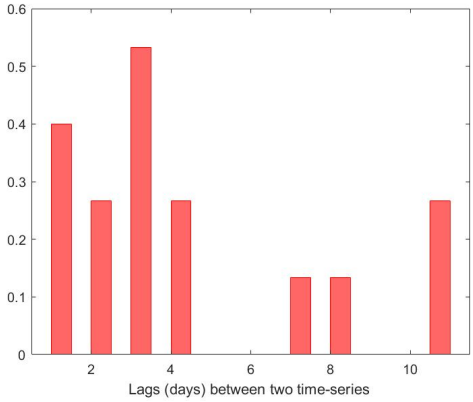

(c)

Figure 5.6: The cross-correlation analysis shows that there is a lag of 8 days between the outbreak in the community resulting in fatal cases and the LTCH resident in the Niagara Regional Area Health Unit, as depicted in (a) and (b). (a) Cumulative number of all deaths in the community vs cumulative number of deaths in LTCH. (b) Correlation coefficients calculated for each lag for a total of 60 lags. (c) Histogram of the delay between pairs of time-series of deaths inside and outside of the LTCH in each health region. The delay varies between 0 to 11 days, with a mode around 2 days.

Home Name	Sector	Public Health Unit	Total # Beds 2020	Residents Deaths	# of Staff Shortages	# of PPE Shortages	Max Resident Cases	Max Staff Cases
T1	NH for-profit	Toronto	247	42	19	41	143	88
T2	NH for-profit	Toronto	252	59	22	3	66	92
T3	NH for-profit	Toronto	269	47	22	0	96	105
T4	NH for-profit	Toronto	159	52	0	0	125	62
T5	NH for-profit	Toronto	169	39	0	0	96	31
O1	NH for-profit	Ottawa	303	61	25	8	132	88
P	NH for-profit	Peel	236	67	6	0	152	57
W	NH for-profit	Waterloo	240	51	26	14	171	69
D	NH for-profit	Durham	233	71	21	15	144	65
T6	Charitable (CHFA)	Toronto	168	48	37	0	84	45
O2	NH for-profit	Ottawa	160	44	31	13	55	50

Figure 5.7: The list of the 11 long-term care homes singled out through clustering analysis. For privacy, we anonymized the relevant homes and denoted by T1-T6 for homes in Toronto, O1 and O2 for homes in Ottawa and D, P, and W for homes in Durham, Peel and Waterloo health regions, respectively.

dimensions in our data). The latter is a well-known center-based algorithm ideated by MacQueen in 1967 [81]. The combination of these two techniques provides an efficient algorithm that merges the benefit of using both a projective and a center-based algorithm. The former allows to work in a reasonable subspace and avoid the so-called curse of dimensionality for which, in a high-dimensional space, all points tend to be far apart and a notion of “distance" loses its relevance. The latter instead is able to associate a point to each cluster which is the “average" and is key in making the algorithm order-independent. There are two main parameters involved in the process: σ which determines whether each dimension of data points is close enough with respect to the cluster average; and ρ which determines the minimum number of similar dimensions needed for points to be in the same cluster. We applied the algorithm by varying the two parameters and chose the values that minimized the distance within a single cluster and maximized the distance between different clusters.

Amongst the different clusters obtained, we chose to analyze the ones that had a relevant amount of cases by checking the average point of each cluster. We then singled out the homes that were affected enough and in a similar way by the epidemic. We ended up with eleven LTCH all around Ontario which are listed in Table 5.7. Analysing all these long-term care facilities, we see that

they all have a high number of resident deaths, staff shortage reports and number of confirmed residents and staff (see Table 5.7). We also note that all but one of these homes are for-profit and this strengthens our previous finding on the association between the extent of outbreaks and the type of home management. All these homes are located in the health regions known to have a high risk of COVID-19. It is also worth noting that 6 out of 11 homes are located in Toronto.

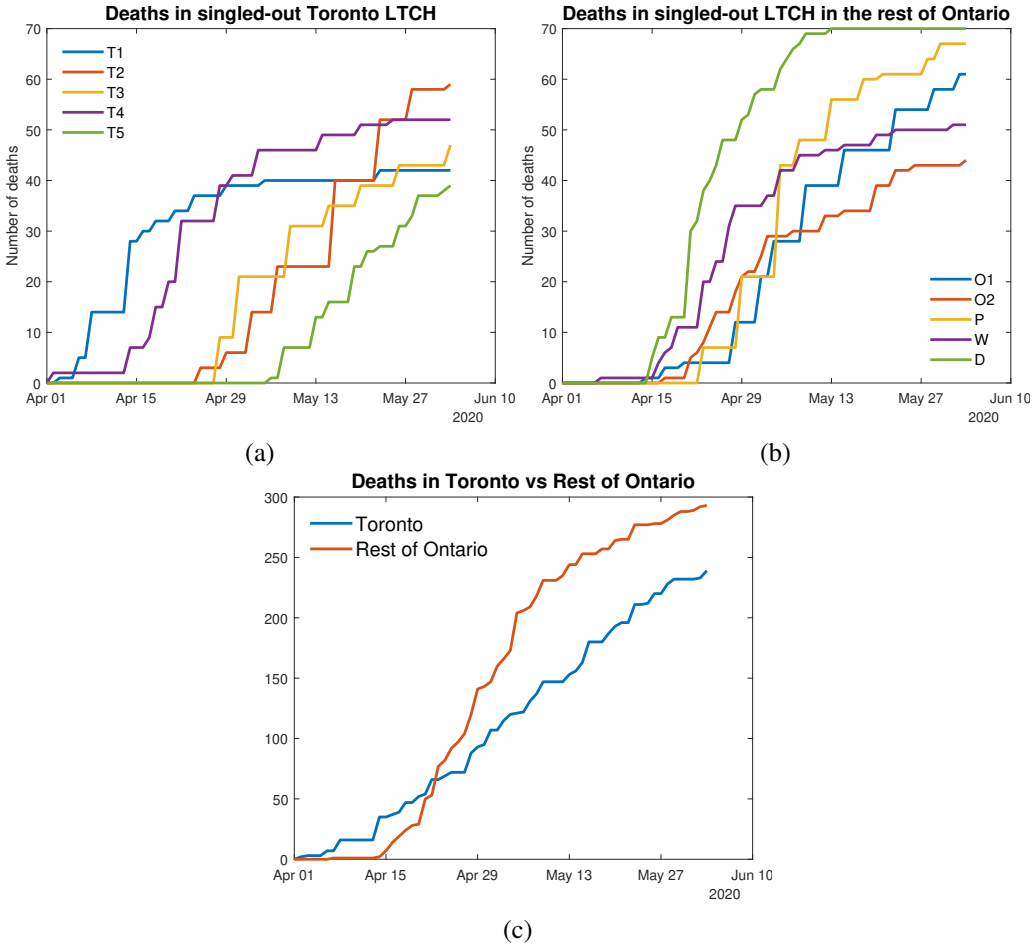

Figure 5.8: (a) Time-series of cumulative number of resident deaths in the singled-out LTCH in Toronto. (b) Time-series of cumulative number of resident deaths in the singled-out LTCH in Ontario excluding Toronto. The Toronto deaths continuously increase in the time analyzed while in the rest of Ontario deaths start occurring in the last 20 days of April as the plot (c) shows.

A time-series analysis of the cumulative number of deaths among the homes in Toronto and outside Toronto, shows that the first outbreak time is different throughout the former (see Figure

5.8a), while it has similar behavior in the latter (see Figure 5.8b), showing that those in Toronto had more of a staggered onset (or at least reporting of detection) compared to those outside of Toronto, which interestingly appear to have a common time of onset. There was no relation between the location of the singled-out LTCH inside versus those outside of Toronto. No geographical proximity was found between these homes. It is also clear from Figure 5.8c that the outbreaks start among the homes located in the Toronto health region and then move to the homes located in the other three health regions. There is a clear difference in the behavior of the two time series shown in Figure 5.8c: the Toronto deaths continuously increase in the time-window analyzed while in the rest of Ontario deaths start occurring in last 20 days of April (Figure 5.8c).

5.1.4 Nuances and limitations

Confirmed COVID-19 positive case counts are subject to several forms of error, including underestimation (combined effects of underreporting and under-ascertainment) [59] and testing protocols in each LTCH. Hence, throughout our analysis, we primarily utilized the time series for number of deaths as a metric for disease severity in each LTCH. Deaths may be subject to a lower degree of uncertainty and may be a more reliable source than confirmed COVID-19 cases; hence, the higher confidence in the analyses presented. Various sources of data were available for the number of cases and deaths in Ontario, stratified by health region, age and gender. These data sources are different in the date of reports and the number of cases and deaths. The raw data, publicly accessible through the Government of Ontario COVID-19 data, has particularly a line list of data with additional information on case acquisition and dates of episode, specimen collection, test report and case report. Results provided by the Government of Ontario based on this data and results provided by Public Health Ontario differ in both date and number of deaths and cases.

5.1.5 Discussion

Several COVID-19 outbreaks have occurred in long-term care homes worldwide, with clusters being reported in the USA [5, 86, 105], UK [27, 123], Italy [53, 78] and other European countries [117], as well as in Canada [55, 115]. In the USA, White and colleagues [123] have found that COVID-19 outbreaks in long-term care homes were associated with the dimension of the struc-

ture (the larger the facility the higher the probability of an outbreak) and its region (characterized by high SARS-CoV-2 prevalence rates). In the UK, Dutey-Magni and coauthors [53] have identified gender (being male) and increasing age, total number of beds, the bed/staff ratio and the occupants/bedrooms ratio as independent predictors of outbreaks.

In this analysis, we found an association between the normalized number of COVID-19 induced death in a given LTCH and the type of management associated with such LTCH (for profit, non-profit, etc). We found that for-profit homes have higher death-to-bed ratio. This is consistent with findings from the study of Stall et. al. [110], where they link this to the considerably higher percentage of for-profit homes with older design standard and rooms with quadruple occupancy. For-profit homes also account for 75% of homes with a crowding index > 2, defined as the average number of residents per bedroom and bathroom in [25] (65% of for-profit, 36% of non-profit and 18% of municipal homes have a crowding index > 2). In addition, we showed that the average rate of increase of the death-to-bed ratio is higher for for-profit homes than other types of management models in most regions in Ontario. This is particularly true in regions where the overall death-to-bed ratios are higher than 1%. This can also be partially explained by the higher percentage of quadruple occupancy and crowding index of for-profit homes [25, 110] resulting in the accelerated increase of the number of deaths in these homes. What remains unknown to decipher this result, is the link between the management type of the facility and the specific age of the building, its building code, in particular ventilation standard and quality, and very importantly, the number of individuals occupying each room as well the staff-to-resident ratio, or time allocated by staff to each resident. These factors will be critical to analyze in more details for the months to come to explain these important differences between LTCH.

Moreover, we identified through cross-correlation analysis a lag of up to 11 day between deaths in the community and deaths in LTCHs, depending on the health region (e.g., Figure 5.6). This finding suggests that circulation of disease in the community disperses into LTCHs and leads to eventual deaths after a period of time. In light of this, deaths in the surrounding community may serve as an early warning for transmission to have already occurred in LTCHs and inform immediate action and proactive measures, such as systematic testing among residents and staff, to

mitigate the burden of disease.

Our analyses showed that the extent of the outbreaks in long-term care facilities are strongly correlated with the proportion of confirmed staff. However, the analyses performed here are subject to high uncertainties due to the lack of information on both number of staff present at work and number of confirmed staff. Both numbers used in the correlation analysis are lower than the actual numbers. It is important to have more accurate information on the number of staff in LTCH, particularly those giving direct care to residents, since there is an association between the total number of staff, the staff shortages and the burden of disease in the LTCH.

We also found that the odds of resident death are 35 times higher in homes with at least one staff shortage report. Note that the number of staff shortage reports provided in the data does not include the number of vacant shifts and it only provides the date on which a staff shortage was reported. Homes experiencing critical staff shortages in Ontario reported as high as 60 vacant shifts related to personal support workers every day [94], during the pandemic. Our results emphasize the importance of staff availability to maintain the quality of care, increase the staff safety and therefore reduce the burden of the disease among LTCH residents and staff.

In sum, older subjects are particularly vulnerable to the COVID-19 pandemic. It is urgent that public health organisations and institutions protect their health and implement measures such as timely and universal testing strategies and enhanced access to personal protective equipment. Foreseeing future epidemics and pandemics and preparedness for such events is essential. Here, we have identified key markers that can guide policy: The LTCH's size, the building design standard, room occupancy. This suggest that a combined strategy of indoor air, occupancy, and decontamination management coupled with overall quality of care and high staff-to-bed ratio are among the key factors that should be revised and improved as a part of the Infection Prevention and Control Plans. Finally, we have shown that policy makers can use the information about the community's cases and death rates, which is a precursor – by up to 11 days – of worsening conditions in LTCH to act in advance on restricting access to LTCH or implement changes in care protocols, so as to minimize catastrophic effects among the LTCH vulnerable population.

5.2 Conclusions

Two respiratory diseases were discussed in this chapter: Influenza and COVID-19. Both diseases have a large mortality and morbidity rates among specific age groups with underlying clinical conditions. The main goal of this chapter was to emphasize the key role of timely identification of the risk groups (prior to or during the early stages of an epidemic) in successful control of the epidemic and protecting these risk groups. A review of the influenza complications among seniors and the available immunization programs in the US and Canada was given. A rigorous analysis of the burden of COVID-19 was provided for the residents of long-term care homes in Ontario, Canada.

5.3 A remark

A major part of this chapter was partially supported by the Canadian Institute of Health Research (CIHR) 2019 Novel Coronavirus (COVID-19) rapid research program; Esri Canada through the partnership with the York University ESRI License managed and funded by the York University ESRI License Partners: Faculty of Environmental Studies, Lassonde School of Engineering, Faculty of Arts and Professional Studies, and York Universities Libraries.

5.4 Supplementary Material

A: Multi Variable Linear Regression

For both Model I and Model II the correlation coefficients were calculated using the corrcoef package in Matlab testing the hypothesis that there is no correlation between the primary outcome and the explanatory variables.

In Model I, the primary outcome is a vector of death to bed ratios for 106 LTCH ($Y = (y_i)$, $i = 1, \cdots 106$ and $y_i \in (0, 1)$). Each explanatory variable is also a vector of 106 values ($X = (x_i)$, $i = 1, \cdots 106$). For example for the number of staff shortages $0 \leq x_i \leq 40$. For the sector corresponding to each home we have a categorical variable and this variable was converted to a numer-

ical variable by assigning the following numbers: 1 =for-profit, 2 =non-profit, 3 =municipal and 4 =charitable and therefore $x_i = 1, \cdots, 4$. The negative correlation means that for-profit homes have higher death to bed ratios. A linear relationship $Y = cX$ is considered between Y and each explanatory variable X.

In Model II, the primary outcome is a vector of 68 entries (death to bed ratios for two types of ownership, for-profit and not-for-profit, for each public health unit). The explanatory variables are also vectors of the same size calculated for each public health unit in two types of ownership.

B: Maps

In this section, the spatial data of the LTCH death to bed ratios and the density of the home, for two types of ownership, and the number of deaths evolving in time are visualized.

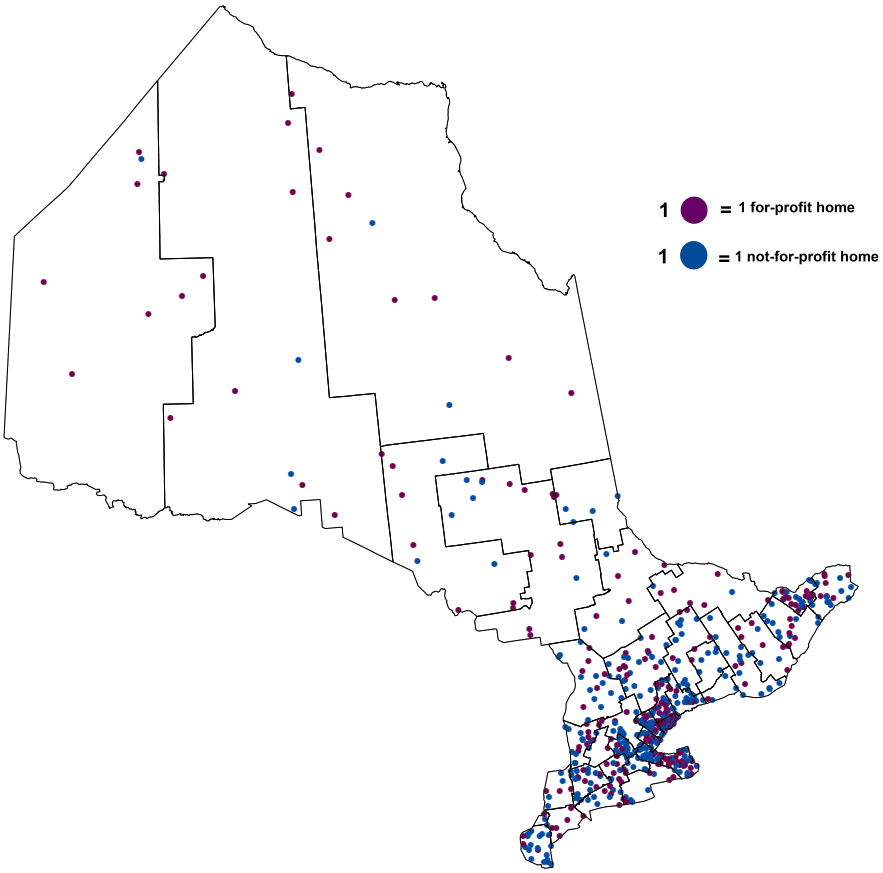

Figure 5.9: Density of long-term care facilities by the type of ownership: one dot represents one home. Note that the dots do not represent the precise location of the homes on the map.

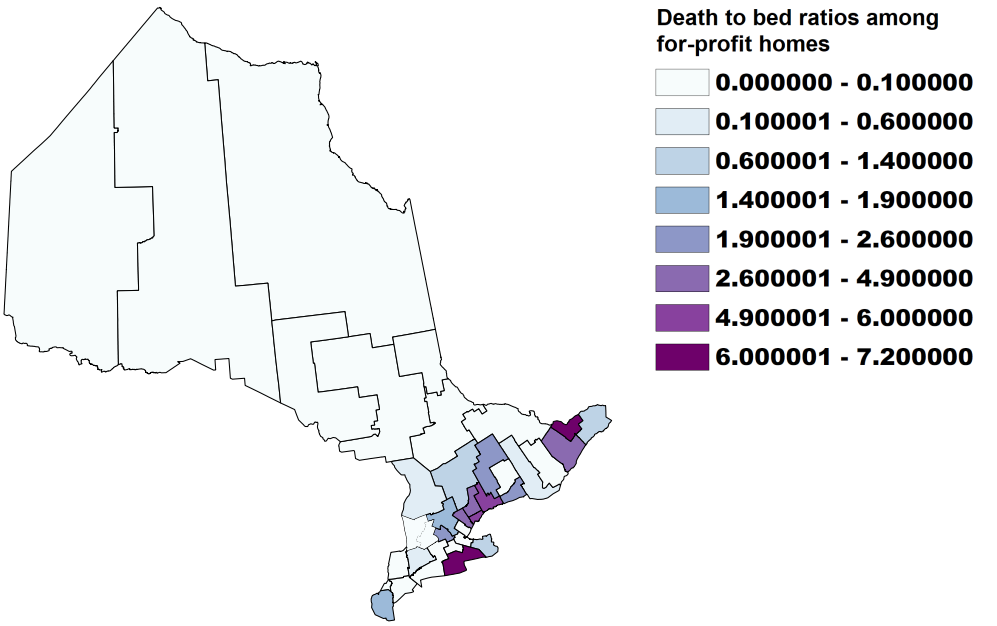

(a)

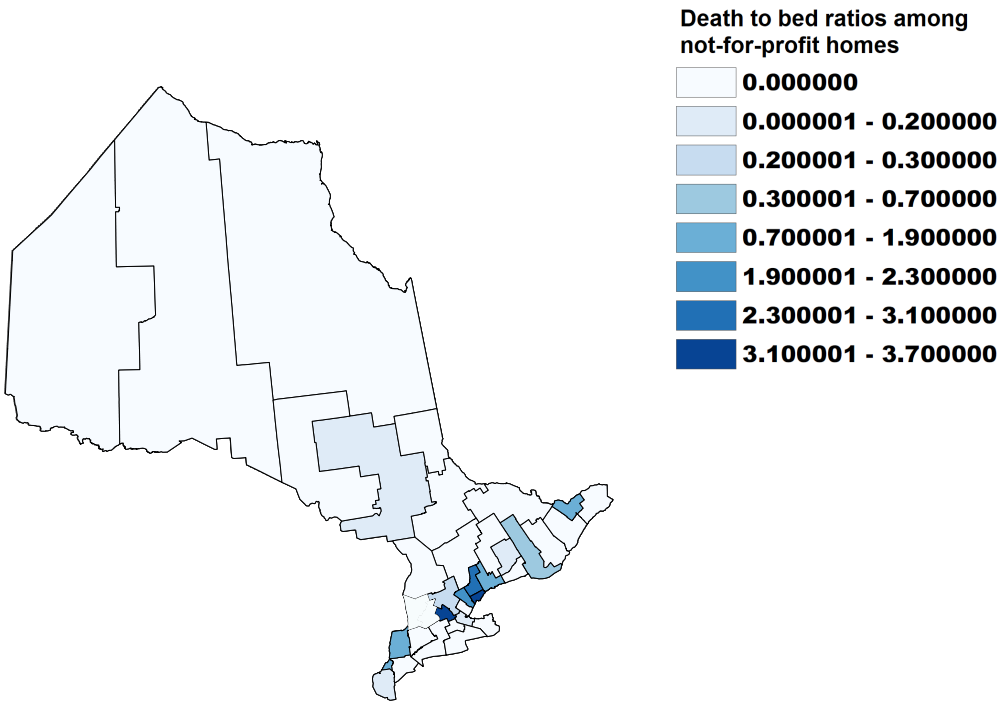

(b)

Figure 5.10: (a) Death to bed ratios in for-profit homes. (b) Death to bed ratios in not-for-profit homes.

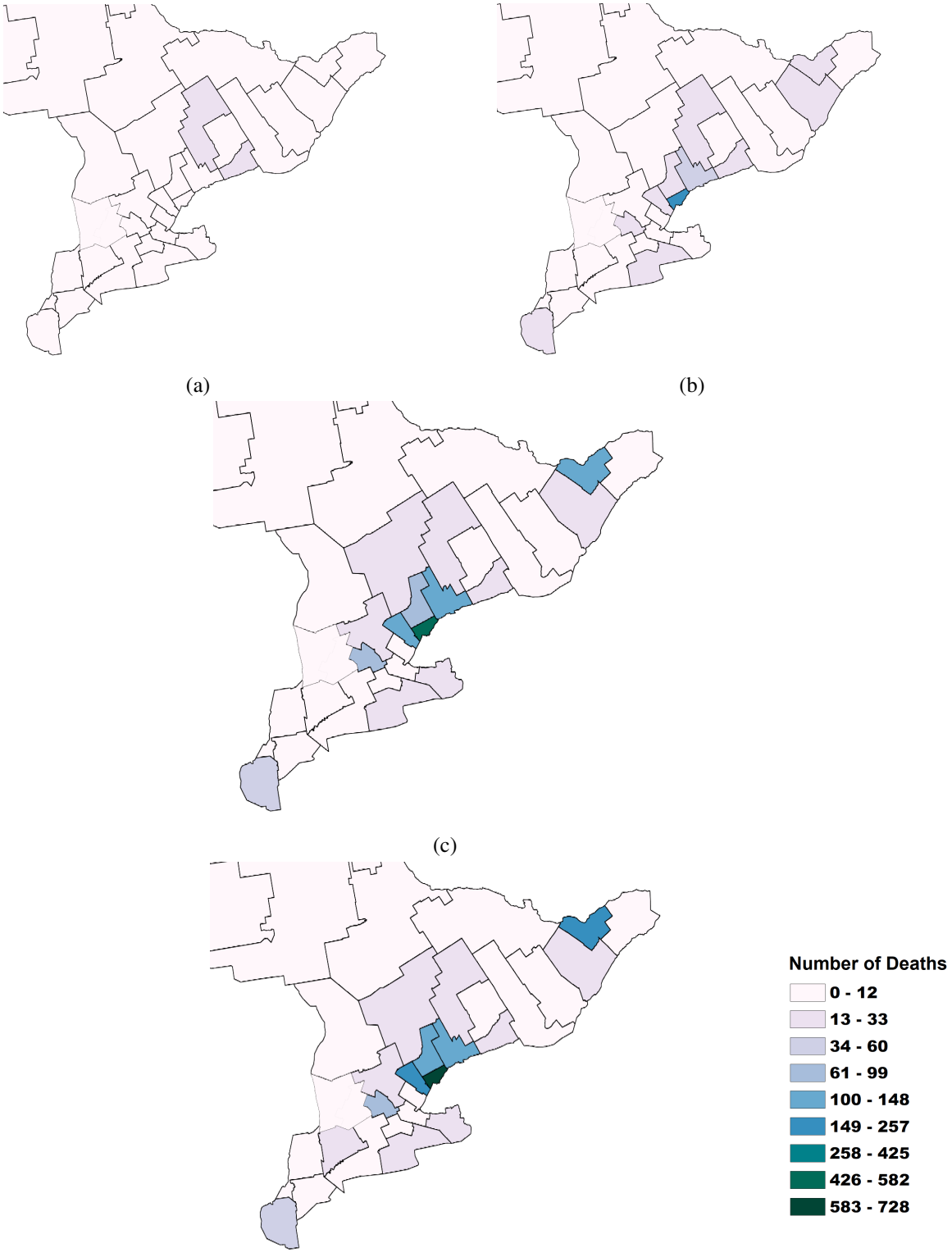

Figure 5.11: The evolution of the number of deaths among long-term care home residents between March 29 and June 3. (a) April 1st. (b) April 22nd (c) May 13th. (d) June 3rd

Table 5.4: Name and code of Ontario public health units.

Public Health Unit (PHU)	PHU Code
The District of Algoma Health Unit	3526
Brant County Health Unit	3527
Durham Regional Health Unit	3530
Grey Bruce Health Unit	3533
Haldimand-Norfolk Health Unit	3534
Haliburton, Kawartha, Pine Ridge District Health Unit	3535
Halton Regional Health Unit	3536
City of Hamilton Health Unit	3537
Hastings and Prince Edward Counties	3538
Huron county Health Unit	3539
Chatham-Kent Health Unit	3540
Kingston, Frontenac and Lennox and Addington Health Unit	3541
Lambton Health Unit	3542
Leeds, Grenvile and Lanark District Health Unit	3543
Middlesex-London Health Unit	3544
Niagara Regional Area Health Unit	3546
North Bay Parry Sound District Health Unit	3547
Northwestern Health Unit	3549
City of Ottawa Health Unit	3551
Peel Regional Health Unit	3553
Peterborough County-City Health Unit	3555
Porcupine Health Unit	3556
Renfrew County and District Health Unit	3557
The Eastern Ontario Health Unit	3558
Simcoe Muskoka District Health Unit	3560
Sudbury and District Health Unit	3561
Thunder Bay District Health Unit	3562
Thimiskaming Health Unit	3563
Waterloo Health Unit	3565
Wellington-Dufferin-Guelph Health Unit	3566
Windsor-Essex County Health Unit	3568
York Regional Health Unit	3570
Oxford Elgin St. Thomas Health Unit	3575
City of Toronto Health Unit	3595

6 | Conclusions

Mathematical models have been long used to describe biological, ecological and epidemiological phenomena underpinning the transmission dynamics of infectious diseases. The benefits of using mathematical models in understanding these phenomena, foreseeing future risks and advising preventive measures are evident. The highly disruptive COVID-19 pandemic has in particular highlighted the significant contribution of these models to the establishment of effective infection prevention and control measures.

Mathematical models are strong tools which help governments and the public health professionals and authorities to develop evidence based prevention and control strategies. The contribution of mathematical models to the disease prevention and control is multifold: understanding the dynamics; forecasting the disease spread; understanding the impact of public health interventions; optimizing the allocation of available resources; evaluating the effectiveness of the implemented interventions; identifying the critical outcomes and the key causes; and adjusting the interventions for better results.

This thesis was primarily devoted to the development of a framework using renewal equations, developed and furthered in earlier studies [71, 38, 15, 16, 18], in an extended setting where we allow a general function to describe the contribution of infected individuals to the force of infection which depends on the time since infection as well as the immunity status of the individual before acquiring the infection. This was done in Chapter 2 with a detailed analysis of a special case where we consider n constant values for the immunity status of individuals in the population.

In Chapter 3, we developed an age-structured model for the dynamics of vertically transmitted diseases using renewal equations in a single population with a constant birth function and a general survival function where the probability of producing an infected new borne by an infected mother depends on time since infection. Existence and uniqueness of a positive steady state and the local stability of the disease free equilibrium was given in the general form. Sensitivity of the positive equilibrium and the basic reproduction number on some of the key model parameters were illustrated through numerical simulations.

Dynamical models of vector-borne diseases and a stage-structured model for tick population were developed and analyzed in Chapter 4. We developed models using renewal equations to study vector-borne epidemics with one type of host population (with and without host-to-host transmissions), epidemics with multiple types of host population (without host-to-host transmission) and the endemic disease dynamics. The second part of this chapter was dedicated to a system of delay differential equations to study the impact of host resistance on tick population dynamics.

Finally, we examined the infection prevention and control interventions for two respiratory diseases, influenza and COVID-19, among individuals aged 65 and older, with a detailed investigation of COVID-19 deaths among long-term care home residents in Ontario, Canada. The results are given in Chapter 5, and these studies set the age why a renewal equation with immunity as a state-variable of the individuals is essential to describe the transmission patterns and disease burdens.

Limitations and Future Work

The models developed in Chapters 2 and 3 have not been analyzed in full details. The disease dynamics and the final size of the epidemic in the general form with varying level of immunity, developed in Section 2.1, can be explored to optimize targeted immunization programs.

In Chapter 3, the stability analysis of the positive equilibrium and bifurcation analysis of the system are not provided. Various and more realistic forms of the fertility function and the probability of producing an infected newborn can help us evaluate the interventions aiming to reduce/eliminate vertical transmission.

None of the theories provided in Chapters 2, 3 and the first part of 4 have been implemented to a specific disease. Diseases of interest, where these theories can be utilized as a case study, include respiratory diseases such as influenza and COVID-19, HIV/AIDS and malaria.

Bibliography

[1] M. Alavinejad, J. Sadiku, and J. Wu. Modeling the impact of host resistance on structured tick population dynamics. *Mathematics in Applied Sciences and Engineering*, 1(1):65–84, 2020.

[2] M. Alavinejad and J. Wu. Coupled systems of renewal equations for forces of infection through a contact network. *Canadian Mathematical Bulletin*, 63(3):624–632, 2020.

[3] A. Andò, D. Breda, and F. Scarabel. Numerical continuation and delay equations: A novel approach for complex models of structured populations. *Discrete & Continuous Dynamical Systems -S*, 13(9):2619–2640, 2020.

[4] O. O. Apenteng, P. P. Osei, B. Oduro, M. P. Kwabla, and N. A. Ismail. The impact of implementing hiv prevention policies therapy and control strategy among hiv and aids incidence cases in malaysia. *Infectious Disease Modelling*, 5:755–765, 2020.

[5] M. M. Arons, K. M. Hatfield, S. C. Reddy, A. Kimball, A. James, J. R. Jacobs, J. Taylor, K. Spicer, A. C. Bardossy, L. P. Oakley, S. Tanwar, J. W. Dyal, J. Harney, Z. Chisty, J. M. Bell, M. Methner, P. Paul, C. M. Carlson, H. P. McLaughlin, N. Thornburg, S. Tong, A. Tamin, Y. Tao, A. Uehara, J. Harcourt, S. Clark, C. Brostrom-Smith, L. C. Page, M. Kay, J. Lewis, P. Montgomery, N. D. Stone, T. A. Clark, M. A. Honein, J. S. Duchin, J. A. Jernigan, Public Health–Seattle, King County, and CDC COVID-19 Investigation Team. Presymptomatic sars-cov-2 infections and transmission in a skilled nursing facility. *The New England Journal of Medicine*, 22(382):2081–2090, 2020.

[6] N. Arora, Y. Sadovsky, T. S. Dermody, and C. B. Coyne. Microbial vertical transmission during human pregnancy. *Cell Host Microbe*, 21(5):561–567, 2017.

[7] M. V. Barbarossa, M. Polner, and G. Röst. Stability switches induced by immune system boosting in an sirs model with discrete and distributed delays. *SIAM Journal on Applied Math*, 77(3):905–923, 2017.

[8] M. V. Barbarossa and G. Röst. Immuno-epidemiology of a population structured by immune status: a mathematical study of waning immunity and immune system boosting. *Journal of Mathematical Biology*, 71(6-7):1737–1770, 2015.

[9] S. Bhattacharyya and S. Ghosh. Optimal control of vertically transmitted disease: an integrated approach. *Computational and Mathematical Methods in Medicine*, 11(4):369–387, 2010.

[10] S. M Blower and H. Dowlatabadi. Sensitivity and uncertainty analysis of complex models of disease transmission: an hiv model, as an example. *International Statistical Review/Revue Internationale de Statistique*, 62(2):229–243, 1994.

[11] L. Bourouiba. Turbulent gas clouds and respiratory pathogen emissions: Potential implications for reducing transmission of COVID-19. *JAMA*, 323(18):1837–1838, 2020.

[12] L. Bourouiba. The fluid dynamics of disease transmission. *Annual Review of Fluid Mechanics*, 53:473–508, 2021.

[13] J. Bowessidjaou. Effects and duration of resistance acquired by rabbits on feeding and egg laying in ixodes ricinius. *L. Experientia*, 33(4):528–530, 1977.

[14] F. Brauer. On a nonlinear integral equation for population growth problems. *SIAM Journal on Mathematical Analysis*, 6(2):312–317, 1975.

[15] F. Brauer. Age-of-infection and the final size relation. *Mathematical Biosciences and Engineering*, 5(4):681–690, 2008.

[16] F. Brauer. Heterogeneous mixing in epidemic models. *Canadian Applied Mathematics Quarterly*, 20(1), 2012.

[17] F. Brauer. A singular perturbation approach to epidemics of vector-transmitted diseases. *Infectious Disease Modelling*, 4:115–123, 2019.

[18] D. Breda, O. Diekmann, W. F. de Graaf, A Pugliese, and R. Vermiglio. On the formulation of epidemic models (an appraisal of kermack and mckendrick). *Journal of Biological Dynamics*, 6(supp2):103–117, 2012.

[19] D. Breda, O. Diekmann, M. Gyllenberg, F. Scarabel, and R. Vermiglio. Pseudospectral discretization of nonlinear delay equations: New prospects for numerical bifurcation analysis. *SIAM Journal on Applied Dynamical Systems*, 15(1):1–23, 2016.

[20] D. Breda, O. Diekmann, D. Liessi, and F. Scarabel. Numerical bifurcation analysis of a class of nonlinear renewal equations. *Electronic Journal of Qualitative Theory of Differential Equations*, (65):1–24, 2016.

[21] D. Breda, O. Diekmann, Maset S., and R. Vermiglio. A numerical approach for investigating the stability of equilibria for structured population models. *Journal of Biological Dynamics*, 7 Suppl 1(Suppl 1):4–20, 2013.

[22] D. Breda, P. Getto, J. Sánchez Sanz, and R. Vermiglio. Computing the eigenvalues of realistic daphnia models by pseudospectral methods. *SIAM Journal on Scientific Computing*, 37(6):A2607–A2629, 2015.

[23] D. Breda and D. Liessi. Approximation of eigenvalues of evolution operators for linear renewal equations. *SIAM Journal on Numerical Analysis*, 56(3):1456–1481.

[24] D. Breda and D. Liessi. Floquet theory and stability of periodic solutions of renewal equations. *Journal of Dynamics and Differential Equations*, 2020.

[25] K. A. Brown, A. Jones, N. Daneman, K. A. Chan, K. L. Schwartz, G. E. Garber, A. P. Costa, and N. M. Stall. Association Between Nursing Home Crowding and COVID-19 Infection and Mortality in Ontario, Canada. *JAMA Internal Medicine*, Nov 2020.

[26] S. J. Brown and P. W. Askenase. Rejection of ticks from guinea pigs by anti-hapten-antibody-mediated degranulation of basophils at cutaneous basophil hypersensitivity sites: role of mediators other than histamine. *The Journal of Immunology*, 134(2):1160–1165, 1985.

[27] T. Burki. England and wales see 20000 excess deaths in care homes. *The Lancet*, 395(10237):1602, May 2020.

[28] S. Busenberg and K. Cooke. *Vertically Transmitted Diseases*. Springer-Verlag, 1993.

[29] Statistics Canada. Census profile, 2016 canada.

[30] Y. Cao and J. Wu. Projective art for clustering data sets in high dimensional spaces. *Neural Networks*, 15(1):105–120, 2002.

[31] P. Clement, O. Diekmann, M. Gyllenberg, H. J. A. M. Heijmans, and H. R. Thieme. Perturbation theory for dual semigroups. i. the sun-reflexive case. *Mathematische Annalen*, 277(4):709–725, 1987.

[32] J. Cui, Y. Zhang, and Z. Feng. Influence of non-homogeneous mixing on final epidemic size in a meta-population model. *Journal of Biological Dynamics*, 13(sup1):31–46, 2019.

[33] A. M. de Roos, O. Diekmann, P. Getto, and M. A. Kirkilionis. Numerical equilibrium analysis for structured consumer resource models. *Bulletin of Mathematical Biology*, 72(2):259–297, 2010.

[34] A. M. de Roos, O. Diekmann, P. Getto, and M. A. Kirkilionis. Erratum to: Numerical equilibrium analysis for structured consumer resource models. *Bulletin of Mathematical Biology*, 78(2):350–351, 2016.

[35] C. A. DiazGranados, A. J. Dunning, E. Jordanov, V. Landolfi, M. Denis, and H. K. Talbot. High-dose trivalent influenza vaccine compared to standard dose vaccine in elderly adults: Safety, immunogenicity and relative efficacy during the 2009-2010 season. *Vaccine*, 31(6):861–866, 2013.

[36] C. A. DiazGranados, A. J. Dunning, M. Kimmel, D. Kirby, J. Treanor, A. Collins, R. Pollak, J. Christoff, J. Earl, V. Landolfi, E. Martin, S. Gurunathan, R. Nathan, D. P. Greenberg, N. G. Tornieporth, M. D. Decker, and H. K. Talbot. Efficacy of high-dose versus standard-dose influenza vaccine in older adults. *The new England Journal of Medicine*, 371(7):635–45, 2014.

[37] C. A. DiazGranados, C. A. Robertson, H. K. Talbot, V. Landolfi, A. J. Dunning, and D. P. Greenberg. Prevention of serious events in adults 65 years of age or older:a comparison be-

tween high-dose and standard-dose inactivated influenza vaccines. *Vaccine*, 33(38):4988–4993, 2015.

[38] O. Diekmann. Limiting behaviour in an epidemic model. *Nonlinear Anallysis*, 1(5):459–470, 1977.

[39] O. Diekmann. *Renewal Equations in Population Biology. Lecture Notes.IRC, LIAM and Fields-CQAM MfPH Distinguished Lecture Series*. 2019.

[40] O. Diekmann, P. Getto, and G. Mats. Stability and bifurcation analysis of volterra functional equations in the light of suns and stars. *SIAM Journal on Mathematical Analysis*, 39(4):1023–1069, 2007.

[41] O. Diekmann, P. Getto, and Y. Nakata. On the characteristic equation the context of a cell population model. *Journal of Mathematical Biology*, 72:877–908, 2016.

[42] O. Diekmann, S.A. van Gils, S.M.V. Lunel, and H.-O. Walther. *Delay Equations Functional-, Complex-, and nonlinear Analysis*. Springer-Verlag, 1995.

[43] O. Diekmann and M. Gyllenberg. The second halfłwith a quarter of a century delay. *Mathematical Modelling of Natural Phenomena*, 3(7):36–48, 2008.

[44] O. Diekmann and M. Gyllenberg. Equations with infinite delay: Blending the abstract and the concrete. *Journal of Differential Equations*, 252(2):819–851, 2012.

[45] O. Diekmann, M. Gyllenberg, and J. Metz. Finite dimensional state representation of linear and nonlinear delay systems. *Journal of Dynamics and Differential Equatations*, 30:1439–1467, 2018.

[46] O. Diekmann, M. Gyllenberg, and J. A. J. Metz. Steady-state analysis of structured population models. *Theoretical Population Biology*, 63(4):309–338, 2003.

[47] O. Diekmann, M. Gyllenberg, J. A. J. Metz, S. Nakaoka, and A. M. de Roos. Daphnia revisited: local stability and bifurcation theory for physiologically structured population models explained by way of an example. *Journal of Mathematical Biology*, 61(2):227–318, 2010.

[48] O. Diekmann, J. A. Heesterbeek, and J. A. Metz. On the definition and the computation of the basic reproduction ratio r0 in models for infectious diseases in heterogeneous populations. *Journal of Mathematical Biology*, 28(4):365–82, 1990.

[49] O. Diekmann and S. A. Van Gils. Invariant manifolds for volterra integral equations of convolution type. *Journal of differential equations*, 54:139–180, 1984.

[50] O. Diekmann, R. Vermiglio, and F. Scarabel. Pseudospectral discretization of delay equations: Results and conjectures. *Discrete & Continuous Dynamical Systems -S*, 13, 2018.

[51] P. van den Driessche and J. Watmough. Reproduction numbers and sub-threshold endemic equilibria for compartmental models of disease transmission. *Mathematical Biosciences*, 180(1):29 – 48, 2002.

[52] S. J. Dumler. Molecular diagnosis of lyme disease: review and meta-analysis. *Molecular Diagnosis*, 6(1):1–11, 2001.

[53] P. F. Dutey-Magni, H. Williams, A. Jhass, G. Rait, H. Hemingway, A. C. Hayward, and L. Shallcross. Covid-19 infection and attributable mortality in uk long term care facilities: Cohort study using active surveillance and electronic records (march-june 2020). *medRxiv*, 2020.

[54] G. Fan, H. R Thieme, and H. Zhu. Delay differential systems for tick population dynamics. *Journal of Mathematical Biology*, 71(5):1017–1048, 2015.

[55] D. Fisman, I. Bogoch, L. Lapointe-Shaw, J. McCready, and A. Tuite. Risk factors associated with mortality among residents with coronavirus disease 2019 (COVID-19) in long-term care facilities in ontario, canada. *JAMA Network Open*, 3(7), 2020.

[56] Centers for Disease Control and Prevention. Past seasons vaccine effectiveness estimates, 2020.

[57] H. D. Gaff and L. J. Gross. Modeling tick-borne disease: A metapopulation model. *Bulletin of Mathematical Biology*, 69(1):265–288, 2007.

[58] P. Getto, M. Gyllenberg, Y. Nakata, and F. Scarabel. Stability analysis of a state-dependent delay differential equation for cell maturation: analytical and numerical methods. *Journal of Mathematical Biology*, 79(1):281–328, 2019.

[59] C. L. Gibbons, M. J. Mangen, D. Plass, A. H. Havelaar, R. J. Brooke, P. Kramarz, K. L. Peterson, A. L. Stuurman, A. Cassini, E. M. Fèvre, and M. E. E. Kretzschmar. Measuring underreporting and under-ascertainment in infectious disease datasets: a comparison of methods. *BMC Public Health*, 14(1):147, 2014.

[60] B. Gomero. Latin hypercube sampling and partial rank correlation coefficient analysis applied to an optimal control problem. *University of Tennessee, Knoxville. Masters Thesis*, 2012.

[61] G. Gripenberg, S. O. Londen, and O. Staffans. *Volterra Integral and Functional Equations*. Cambridge University Press, 1990.

[62] M. Gyllenberg, F. Scarabel, and R. Vermiglio. Equations with infinite delay: Numerical bifurcation analysis via pseudospectral discretization. *Applied Mathematics and Computation*, 333:490–505, 2018.

[63] J. K. Hale. Asymptotic behavior of dissipative systems. *Mathematical Surveys and Monographs 25, American Mathematical Society*, 1988.

[64] J. M. Heffernan, R. J. Smith, and L. M. Wahl. Perspectives on the basic reproductive ratio. *Journal of The Royal Society Interface*, 2:281–293, 2005.

[65] R. A. Horn and C. R. Johnson. *Matrix Analysis, Second Edition*. Cambridge University Press, 2013.

[66] A. T. Hsu, W. Berta, P. C. Coyte, and A. Laporte. Staffing in ontario's long-term care homes: Differences by profit status and chain ownership. *Canadian Journal on Aging*, 35(2):175–189, 2016.

[67] S. J. Brown. Highlights of contemporary research on host immune response to ticks. *Veterinary Parasitology*, 28:321–334, 1988.

[68] R. Jennings, Y. Kuang, H. R. Thieme, J. Wu, and X. Wu. How ticks keep ticking in the adversity of host immune reactions. *Journal of Mathematical Biology*, 78(5):1331–1364, 2019.

[69] R. C. Johnson, G. P. Schmid, F. W. Hyde, A. G. Steigerwalt, and D. J. Brenner. Borrelia burgdorferi sp. nov.: etiologic agent of lyme disease. *International Journal of Systematic and Evolutionary Microbiology*, 34(4):496–497, 1984.

[70] N. R. Jones, Z.U. Qureshi, R. J. Temple, J. P. J. Larwood, T. Greenhalgh, and L. Bourouiba. Two metres or one: what is the evidence for physical distancing in COVID-19? *BMJ*, 370, 2020.

[71] W. O. Kermack and A. G. McKendrick. A contribution to the mathematical theory of epidemics. *Proceedings of the Royal Society*, 105A(700), 1927.

[72] M. A. Kirkilionis, O. Diekmann, B. Lisser, M. Nool, B. Sommeijer, and A. M. de Roos. Numerical continuation of equilibria of physiologically structured population models. i. theory. *Mathematical Models and Methods in Applied Sciences.*, 6(S. 11):1101–1127., 2011.

[73] O. Krylova and D. J. Earn. Effects of the infectious period distribution on predicted transitions in childhood disease dynamics. *Journal of The Royal Society Interface*, 10(84), 2013.

[74] D. L. Schanzer, M. Saboui, L. Lee, A. Nwosu, and C. Bancej. Burden of influenza, respiratory syncytial virus, and other respiratory viruses and the completeness of respiratory viral identification among respiratory inpatients, canada, 2003-2014. *Influenza and Other Respiratory Viruses*, 12(1):113–121, 2018.

[75] J. K. H. Lee, G. K. L. Lam, T. Shin, J. Kim, A. Krishnan, D. P. Greenberg, and A. Chit. Efficacy and effectiveness of high-dose versus standard-dose influenza vaccination for older adults: a systematic review and meta-analysis. *Expert Review of Vaccines*, 17(5):435–443, 2018.

[76] V. J. Lee, Z. J. M. Ho, E. H. Goh, H. Campbell, C. Cohen, V. Cozza, J. Fitzner, J. Jara, A. Krishnan, J. Bresee, and WHO Working Group on Influenza Burden of Disease. Advances in measuring influenza burden of disease. *Influenza and Other Respiratory Viruses*, 12(1):3–9, 2018.

[77] A. L Lloyd. Realistic distributions of infectious periods in epidemic models: Changing patterns of persistence and dynamics. *Theoretical Population Biology*, 60(1):59–71, 2001.

[78] S. Logar. Care home facilities as new covid-19 hotspots: Lombardy region (italy) case study. *Archives of Gerontology and Geriatrics*, 89:104087, 2020.

[79] Y. Lou and J. Wu. Tick seeking assumptions and their implications for lyme disease predictions. *Ecological Complexity*, 17:99–106, 2014.

[80] W. H. R. Lumsden. *Advances in Parasitology, Volume 18*. Academic Press, 1980.

[81] J. MacQueen. Some methods for classification and analysis of multivariate observations. *Proceedings of the Fifth Berkeley Symposium on Mathematical Statistics and Probability, Volume 1: Statistics*, 1:281–297, 1967.

[82] N. K. Madhav, J. S. Brownstein, J. I. Tsao, and D. Fish. A dispersal model for the range expansion of blacklegged tick (acari: Ixodidae). *Journal of Medical Entomology*, 41(5):842–852, 2004.

[83] P. Magal and S. Ruan. *Theory and Applications of Abstract Semilinear Cauchy Problems*. Cham, Switzerland: Springer, 2018.

[84] S. Marino, I. B. Hogue, C. J. Ray, and D. E. Kirschner. A methodology for performing global uncertainty and sensitivity analysis in systems biology. *Journal of Theoretical Biology*, 254(1):178–196, 2008.

[85] Z. McCarthy, S. Athar, M. Alavinejad, C. Chow, I. Moyles, K. Nah, J. D. Kong, N. Agrawal, A. Jaber, L. Keane, S. Liu, M. Nahirniak, R. Jean, D. S. Romanescu, J. Stockdale, L. Seet, B. T. Coudeville, E. Thommes, A. F. Taurel, J. Lee, T. Shin, J. Arino, J. Heffernan, A. Chit,

and J. Wu. Quantifying the annual incidence and underestimation of seasonal influenza: A modelling approach. *Theoretical Biology and Medical Modeling*, 17(1):11, 2020.

[86] T. M. McMichael, D. W. Currie, S. Clark, S. Pogosjans, M. Kay, N. G. Schwartz, J. Lewis, A. Baer, V. Kawakami, M. D. Lukoff, J. Ferro, C. Brostrom-Smith, T. D. Rea, M. R. Sayre, F. X. Riedo, D. Russell, B. Hiatt, P. Montgomery, A. K. Rao, E. J. Chow, F. Tobolowsky, M. J. Hughes, A. C. Bardossy, L. P. Oakley, J. R. Jacobs, N. D. Stone, S. C. Reddy, J. A Jernigan, M. A. Honein, T. A. Clark, J. S. Duchin, Public Health–Seattle, King County, EvergreenHealth, and CDC COVID-19 Investigation Team. Epidemiology of covid-19 in a long-term care facility in king county, washington. *The New England Journal of Medicine*, 21(382):2005–2011, 2020.

[87] J. A. J. Metz and O. Diekmann. *Lecture Notes in Biomathematics: The Dynamics of Physiologically Structured Populations a Systematic Exposition*, volume 68. Springer-Verlag Berlin Heidelberg GmbH, 1986.

[88] E. A. Miller. Protecting and improving the lives of older adults in the covid-19 era. *Journal of Aging & Social Policy.*, 4-5(32):297–309, 2020.

[89] K. Nah, M. Alavinejad, A. Rahman, J. M. Heffernan, and J. Wu. Impact of influenza vaccine-modified infectivity on attack rate, case fatality ratio and mortality. *J Theor Biol*, 492:110190, 2020.

[90] A. Nzokem and N. Madras. Epidemic dynamics and adaptive vaccination strategy: Renewal equation approach. *Bulletin of Mathematical Biology*, 82(122), 2020.

[91] Government of Canada. Surveillance of lyme disease, 2020.

[92] GBD 2017 Causes of Death Collaborators. Global, regional, and national age-sex-specific mortality for 282 causes of death in 195 countries and territories, 1980–2017: a systematic analysis for the global burden of disease study 2017. *The Lancet*, 392(10159):1736–88, 2018.

[93] United Nations, Department of Economic and Social Affairs, Population Division. World population ageing 2019: Highlights, 2019.

[94] Long-Term Care Staffing Study Advisory Group, Ministry of Long-Term Care. Long-term care staffing study, 2020.

[95] N. H. Ogden, M. Bigras-Poulin, C. J. O'callaghan, I. K. Barker, L. R. Lindsay, A. Maarouf, K. E. Smoyer-Tomic, D. Waltner-Toews, and D. Charron. A dynamic population model to investigate effects of climate on geographic range and seasonality of the tick ixodes scapularis. *International Journal for Parasitology*, 35(4):375–389, 2005.

[96] Public Health Ontario. Covid-19 in ontario: January 15, 2020 to june 3, 2020.

[97] Public Health Ontario. Ontario covid-19 data tool, 2020.

[98] C. Paules and K. Subbarao. Influenz. *The Lancet*, 390(10095):697–708, 2017.

[99] J. Piesman, T. N Mather, R. Sinsky, and A. Spielman. Duration of tick attachment and borrelia burgdorferi transmission. *Journal of Clinical Microbiology*, 25(3):557–558, 1987.

[100] T. Powell, E. Bellin, and A. R. Ehrlich. Older adults and covid-19: The most vulnerable, the hardest hit. *Hastings Center Report*, 3(50):61–63, 2020.

[101] S. Randolph. Tick ecology: processes and patterns behind the epidemiological risk posed by ixodid ticks as vectors. *Parasitology*, 129(S1):S37–S65, 2004.

[102] R. Rosà and A. Pugliese. Effects of tick population dynamics and host densities on the persistence of tick-borne infections. *Mathematical Biosciences*, 208(1):216–240, 2007.

[103] R. Rosà, A. Pugliese, R. Norman, and P. J Hudson. Thresholds for disease persistence in models for tick-borne infections including non-viraemic transmission, extended feeding and tick aggregation. *Journal of Theoretical Biology*, 224(3):359–376, 2003.

[104] R. Rosà and A. Pugliese. Effects of tick population dynamics and host densities on the persistence of tick-borne infections. *Mathematical Biosciences*, 208(1):216–240, 2007.

[105] M. Salcher-Konrad, A. Jhass, H. Naci, M. Tan, Y. El-Tawil, and A. Comas-Herrera. Covid-19 related mortality and spread of disease in long-term care: a living systematic review of emerging evidence. *medRxiv*, 2020.

[106] F. Scarabel, L. Pellis, N. H. Ogden, and J. Wu. A renewal equation model to assess roles and limitations of contact tracing for disease outbreak control. *medArxive*, 2021.

[107] M. Scopetti, A. Santurro, R. Tartaglia, P. Frati, and V. Fineschi. Expanding frontiers of risk management: care safety in nursing home during covid-19 pandemic. *International Journal for Quality in Health Care*, 2020.

[108] S. A. Sellers, M. S. Hagan, F. G. Hayden, and W. A. Fischer II. The hidden burden of influenza: A review of the extra-pulmonary complications of influenza infection. *Influenza and Other Respiratory Viruses*, 11(5):372–393, 2017.

[109] H. L. Smith. Monotone semiflows generated by functional differential equations . *Journal Of Differential Equations*, 66:420–442, 1987.

[110] N. M. Stall, A. Jones, K. A. Brown, P. A. Rochon, and A. P. Costa. For-profit long-term care homes and the risk of covid-19 outbreaks and resident deaths. *Canadian Medical Association Journal*, 192(33):E946–E955, 2020.

[111] A. C. Steere, J. Coburn, and L. Glickstein. The emergence of lyme disease. *The Journal of Clinical Investigation*, 113(8):1093–1101, 2004.

[112] A. C. Steere, R. L. Grodzicki, A. L. Kornblatt, J. E. Craft, A. G. Barbour, W. Burgdorfer, G. P. Schmid, E. Johnson, and S. E. Malawista. The spirochetal etiology of lyme disease. *New England Journal of Medicine*, 308(13):733–740, 1983.

[113] J. F. Strauß, M. Chauvet, and A. Telschow. The infection dynamics of vertically transmitted viruses in a two-population model. *BioRxiv*, 2018.

[114] T. R. Talbot, D. D. Crocker, J. Peters, J. K. Doersam, M. R. Ikizler, E. Sannella, P. F. Wright, and K. M. Edwards. Duration of virus shedding after trivalent intranasal live attenuated in-

fluenza vaccination in adults. *Infection Control & Hospital Epidemiology*, 26(5):494–500, 2005.

[115] ECDC Public Health Emergency Team, K. Danis, L. Fonteneau, S. Georges, C. Daniau, S. Bernard-Stoecklin, L. Domegan, J. O'Donnell, S. H. Hauge, S. Dequeker, E. Vandael, J. Van der Heyden, F. Renard, N. B. Sierra, E. Ricchizzi, B. Schweickert, N. Schmidt, M. Abu Sin, T. Eckmanns, J. A. Paiva, and E. Schneider. High impact of covid-19 in long-term care facilities, suggestion for monitoring in the eu/eea, may 2020. *Eurosurveillance*, 25(22), 2020.

[116] H. R. Thieme. Renewal theorems for linear periodic volterra integral equations. *Journal of Integral Equations*, 7(3):253–277, 1984.

[117] E. M. Trecarichi, M. Mazzitelli, F. Serapide, M. C. Pelle, B. Tassone, E. Arrighi, G. Perri, P. Fusco, V. Scaglione, C. Davoli, R. Lionello, V. La Gamba, G. Marrazzo, M. T. Busceti, A. Giudice, M. Ricchio, A. Cancelliere, E. Lio, G. Procopio, F. S. Costanzo, D. Foti, G. Matera, and C. Torti. Characteristics, outcome and predictors of in-hospital mortality in an elderly population from a sars-cov-2 outbreak in a long-term care facility. *medRxiv.*, 2020.

[118] P. van den Driessche. Reproduction numbers of infectious disease models. *Infectious Disease Modeling*, 2(3):288–303, 2017.

[119] B. M Wagland. Host resistance to cattle tick (boophilus microplus) in brahman (bos indicus) cattle. ii. the dynamics of resistance in previously unexposed and exposed cattle. *Australian Journal of Agricultural Research*, 29:395–400, 1978.

[120] X. Wang and X. Zhao. Dynamics of a time-delayed lyme disease model with seasonality. *SIAM. Applied Dynamical Systems*, 16:853–881, 2017.

[121] G. F. Webb. *Theory of Nonlinear Age-Dependent Population Dynamics*. New York: M. Dekker, 1985.

[122] J. P. Webster, A. Borlase, and J. W. Rudge. Who acquires infection from whom and how? disentangling multi-host and multi-mode transmission dynamics in the 'elimination' era. *Phil. Trans. R. Soc. B*, 372(1719), 2017.

[123] E. M. White, C. M. Kosar, R. A. Feifer, C. Blackman, S. Gravenstein, J. Ouslander, and V. Mor. Variation in sars-cov-2 prevalence in us skilled nursing facilities (published online ahead of print, 2020 jul 16). *Journal of the American Geriatrics Society*, 68(10):2167–2173, 2020.

[124] World Health Organization (WHO). Hiv/aids, 2020.

[125] World Health Organization (WHO). Vector-borne diseases, 2020.

[126] World Health Organization (WHO). The world bank in malaysia-data, 2021.

[127] A. Wilkinson, V. Haroun, T. Wong, N. Cooper, and M. Chignell. Overall quality performance of long-term care homes in ontario. *Healthcare Quarterly*, 22(2):55–62, 2019.

[128] A. L. Wilson, O. Courtenay, L. A. Kelly-Hope, T. W. Scott, W. Takken, S. J. Torr, and S. W. Lindsay. The importance of vector control for the control and elimination of vector-borne diseases. *PLOS Neglected Tropical Diseases*, 14(1), 2020.

[129] J. Wu and X Zhang. *Transmission Dynamics of Tick-Borne Diseases with Co-Feeding, Developmental and Behavioural Diapause*. Springer Nature, 2020.

[130] X. Wu. Modeling the impact of climate change on tick population dynamics and tick-borne disease spread. *York University. PhD thesis*, 2013.

[131] X. Wu, F. M Magpantay, J. Wu, and X. Zou. Stage-structured population systems with temporally periodic delay. *Mathematical Methods in the Applied Sciences*, 38(16):3464–3481, 2015.

[132] X. Wu, V. RSK Duvvuri, and J. Wu. Modeling dynamical temperature influence on tick ixodes scapularis population. *International Congress on Environmental Modelling and Software*, (223), 2010.

[133] J. Yan, M. Grantham, J. Pantelic, P. J. Bueno de Mesquita, B. Albert, Fengjie Liu, Sheryl Ehrman, and Donald K. Milton. Infectious virus in exhaled breath of symptomatic seasonal influenza cases from a college community. *Proceedings of the National Academy of Sciences*, 115(5):1081–1086, 2018.

[134] H. Yuan, M. Baguelin, K. O. Kwok, N. Arinaminpathy, E. van Leeuwen, and S. Riley. The impact of stratified immunity on the transmission dynamics of influenza. *Epidemics*, 20:84–93, 2017.

[135] X. Zhao. *Dynamical Systems in Population Biology*. Springer, 2003.